Addis Ababa University

Addis Ababa Institute of Technology

School of Electrical and Computer Engineering

Fractional Order Sliding Mode Controller Design for Fixed-wing Unmanned Aerial Vehicles Trajectory Tracking

A Thesis Submitted to the School of Graduate Studies of Addis Ababa University in Partial Fulfillment of the Requirements for the Degree of Master of Science in Control Engineering

By

Enanwo Wondem

Advisor

Dr. Lebsework Negash

January, 2024

Addis Ababa, Ethiopia

Addis Ababa University

Addis Ababa Institute of Technology

School of Electrical and Computer Engineering

This document confirms that the thesis authored by Enanwo Wondem, titled "**Fractional Order Sliding Mode Controller Design For Fixed-wing Unmanned Aerial Vehicle Trajectory Tracking,**" submitted as part of the requirements for the Master of Sciences degree in Control Engineering, adheres to university regulations and upholds recognized standards regarding its originality and caliber.

Approved by the Board of Examiners

Name	Signature	Date
Dr. Bisrat Derebssa		
(School dean)		
Dr. Lebsework Negash		
(Control Chairman)		
Dr. Lebsework Negash		
(Advisor)		
Dr. Challa Merga		
(External Examiner)		
Mr. Teshome Hambissa		
(Internal Examiner)		

Declaration

I hereby affirm that the research study titled "**Fractional Order Sliding Mode Controller Design For Fixed-wing Unmanned Aerial Vehicle Trajectory Tracking**" is solely the product of my own effort and intellect. This research has not been presented for any academic degree at this institution or elsewhere. I have diligently acknowledged all sources and references utilized throughout this thesis.

Enanwo Wondem		January , 2024
Name of Student	**Signature**	**Submission Date**

This thesis has been submitted for examination with my approval as a university advisor.

Name of Advisors	**Signature**
Dr. Lebsework Negash	

Acknowledgment

I express deep gratitude to God, whose consistent guidance and blessings have illuminated my path and given me the strength to overcome challenges throughout my thesis journey. I extend heartfelt thanks to my esteemed thesis advisor, Dr. Lebsework Negash, for his invaluable guidance, unwavering support, and expert insights that have played a crucial role in shaping the trajectory of this research. Appreciation is also extended to the dedicated instructors in control engineering at Addis Ababa Institute of Technology (AAiT) for their exceptional teaching, mentorship, and contributions to my academic development. To my family, your unconditional love, encouragement, and belief in my potential have served as the foundational pillars of my success. Your steadfast support has inspired me to strive for excellence. To my classmates, I appreciate the camaraderie, shared experiences, and intellectual discussions that have enriched my academic journey and made it truly memorable. I am indebted to all those who have contributed to my educational pursuits. The collective impact of your influence has left an enduring mark on my life, and I am privileged to have your support and guidance.

Enanwo Wondem

Abstract

This thesis focuses on the tracking of trajectories for fixed-wing unmanned aerial vehicles. (FWUAVs) using Fractional Order Sliding Mode Controller (FOSMC) . FWUAVs are widely utilized in both military and civilian sectors due to their ability to perform risky or inaccessible operations. However, controlling FWUAVs is challenging due to their nonlinear and coupled nature. The mathematical model of FWUAVs is complex, incorporating physical laws, Newton and Euler formulations, and coordinate systems with transformation matrices. To solve this complexity, a FOSMC ,which combines the robustness of conventional Sliding Mode Controller (SMC) with flexible fractional calculus, is applied. Particle Swarm Optimization (PSO) is used for tuning the control gains of FOSMC. The Integral Time Absolute Error (ITAE) is employed as a performance metric, aiming to minimize both settling time and overshoot. External disturbances and parameter variation is added to evaluate the performance of the controller. Comparison is done between Linear Quadratic Regulator (LQR), Fractional Order PID (FOPID), SMC and FOSMC for pitch angle using step input. FOSMC performs better than LQR, FOPID and SMC in terms of tracking accuracy, speed of response and overshoot. Open loop model verification and overall control system of FWUAV is done by MATLAB/Simulink software.

Keywords: fixed-wing, MATLAB, FOSMC, UAV, trajectory tracking, PSO, LQR, FOPID

Contents

List of Figures

List of Tables

List of Acronyms

FOC	Fractional-Order Controller
FNN	Fuzzy Neural Network
FOMCON	Fractional Order Modeling and Control
FOPID	Fractional Order PID
FOPID	Fractional-Order Proportional-Integral-Derivative
FOSMC	Fractional Order Sliding Mode Controller
FWUAV	Fixed Wing Unmanned Aerial Vehicle
IAE	Integral Absolute Error
ISE	Integral Square Error
ITAE	Integral Time Absolute Error
ITSE	Integral Time Square Error
PSO	Particle Swarm Optimization
SMC	Sliding Mode Controller
STW-SMC	Sliding Mode Control with Second-Order Terminal Sliding Surface

Chapter 1

Introduction

1.1 Background of the Thesis

Unmanned aerial vehicles (UAVs) have experienced a surge in popularity and find extensive utilization in both military and civilian sectors, providing unparalleled benefits in executing hazardous or hard-to-reach missions. There are two main categories of UAVs: multi-rotor UAVs and fixed-wing UAVs, each possessing unique attributes and serving specific applications. A FWUAV is an unmanned aircraft that is designed to fly with fixed wings, similar to traditional airplanes. Unlike rotary-wing UAVs (such as helicopters or quadcopters), fixed-wing UAVs generate lift through the shape of their wings and rely on forward motion for flight. They typically have a more efficient endurance and range compared to their rotary-wing counterparts [1].

FWUAVs excel in missions requiring high speed endurance and altitude, possessing features such as rapid flight, the ability to operate at high altitudes, and adaptability in attitude control. However, controlling FWUAVs can be challenging due to their complex model, which entails numerous state variables, strong coupling, nonlinearity, and various interference factors. Properly modeling fixed-wing UAVs is a demanding and time-consuming task, as it necessitates addressing the intricate design and behavior of these UAVs. Developing an accurate model is crucial for designing effective control systems and ensuring the safe and efficient operation of fixed-wing UAVs. Researchers and engineers in the UAV field devote significant effort to modeling and control development to overcome these challenges. The process requires a multidisciplinary approach, combining knowledge from fields such as aerodynamics, control theory, and robotics. Ongoing research and development endeavors aim to optimize the performance and capabilities of FWUAVs, expanding their applications

across various disciplines and driving advancements in unmanned aerial technology [1].

In recent years, there has been notable interest in the application of nonlinear control theory to UAVs. This is mainly due to the nonlinear characteristics exhibited by UAV systems and the wide range of applications they offer. These applications include monitoring disaster areas, localizing victims, inspecting inaccessible infrastructure, and conducting surveillance and photography. To enable these applications, various control strategies are employed, such as UAV formation control, path following, and trajectory tracking. By leveraging nonlinear control theory, researchers and engineers strive to develop robust control algorithms capable of managing the complex dynamics and uncertainties inherent in UAV operations. This, in turn, enables safe and reliable autonomous flight, even in challenging conditions characterized by low visibility or adverse weather. Overall, the integration of UAV technology with advanced control techniques paves the way for a broad spectrum of applications that can enhance efficiency, safety, and accessibility across various industries and sectors[2].

FWUAVs, propelled by aerodynamic forces acting on a fixed surface, are commonly utilized for tasks demanding high altitude and speed due to their rapid flight capability, extensive range, and robust payload capacity. Despite their advantageous features, devising control systems ensuring optimal performance poses significant challenges. This is primarily attributed to the intricate nature of fixed-wing UAV models, characterized by uncertainty, nonlinearity, and the interplay of multiple state variables. In this thesis, an analysis of a fixed-wing UAV is conducted under numerous assumptions, including treating the UAV as a rigid body and assuming constant ground acceleration. These assumptions highlight the disparity between the actual and ideal models, contributing to the uncertainty in system parameters. [3].

In this thesis, the mathematical modeling of FWUAV is analyzed based on different assumptions. The control surfaces of the FWUAV, such as the elevator, rudder, and two ailerons, are considered in controlling the UAV to achieve the desired flight trajectory. Flight control systems are essential to ensure accurate tracking of the designated flight path. In this study, FOSMC is developed as the chosen control strategy. FOSMC is recognized for its best and powerful control capabilities, making it well-suited for tracking the desired trajectories of both the positions and attitudes of the FWUAV. This control technique combines the principles of sliding mode control and fractional calculus.Through the implementation of FOSMC, the control system endeavors to govern the positions and attitudes of the FWUAV, allowing it to precisely adhere to the desired trajectories. [14].

1.2 Problem Statement

Fixed-Wing Unmanned Aerial Vehicles (FWUAVs) are frequently employed for tasks requiring high-speed endurance and altitude due to their characteristics such as rapid flying speed, high altitude capabilities, and flexible attitude. The mathematical model of FWUAVs is intricate owing to the system's nonlinearity, coupled dynamics, and uncertainty stemming from numerous internal and external interference factors [3]. Consequently, devising a control law to achieve desired performance poses a significant challenge. To tackle these complexities, various control strategies have been proposed and explored in the realm of FWUAV control, including the Linear Quadratic Regulator (LQR) [5], Proportional-Integral-Derivative (PID) Control [6], Model Predictive Control (MPC) [12], and Sliding Mode Control (SMC) [9]. In this thesis, a FOSMC scheme is used for stabilizing and tracking references in FWUAVs. FOSMC combines the robustness of SMC with the flexibility of fractional calculus. By utilizing fractional order differentiation and integration, this control scheme can handle the complex dynamics, uncertainties, and disturbances encountered in FWUAVs.

1.3 Objectives

1.3.1 General objectives

Enhancing the trajectory tracking performance of fixed-wing UAVs through the design of a fractional order sliding mode controller(FOSMC).

1.3.2 Specific Objectives

The particular aims of the thesis include:

- To derive the mathematical representation of a FWUAV.
- To develop a fractional order sliding mode controller for trajectory tracking of FWUAVs.
- To assess the effectiveness of the designed controller in terms of trajectory tracking and stabilization amid disturbances.
- To contrast the tracking performance of FOSMC with traditional SMC methods.
- To conduct simulations of the mathematical models utilizing the proposed controller through MATLAB.

1.4 Methodology

To fulfill the outlined objectives, the study progresses through the following procedures:

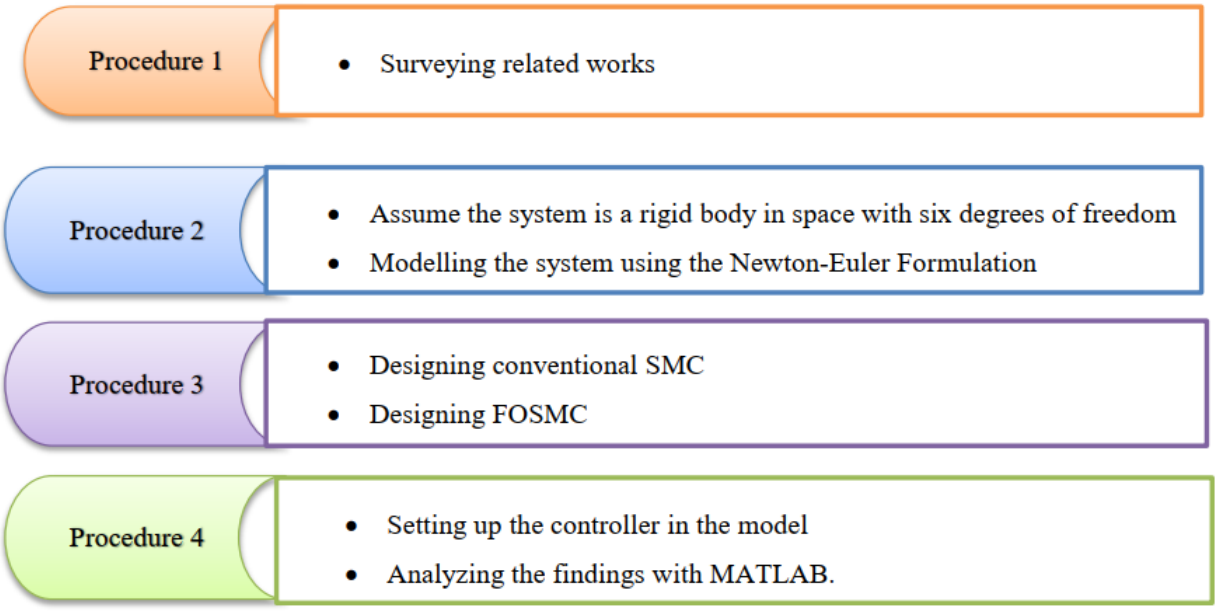

1.5 Significance of the Thesis

There is a huge significant of this thesis especially for our country in countless areas of applications and create motivation on this field of study. FWUAVs have many useful applications such as for agricultural sector, in air missions that are dangerous and impractical for a human pilot, surveillance, border patrol monitoring and materials delivery. Generally, the main significant of this thesis is to create awareness about FWUAVs through modelling, designing a controller providing better tracking accuracy, which is crucial for FWUAVs to perform different tasks with reduced chattering. As a result, companies, governments, and whole societies may benefit from more dependable, efficient, and safe operations in a variety of applications.

1.6 Thesis Scope

This thesis concentrates on the comprehensive procedure of formulating a mathematical model for a FWUAV, devising a Fractional Order Sliding Mode Controller (FOSMC) for it, and conducting simulations utilizing MATLAB/Simulink software. The entirety of the investigation is executed within a simulated setting, omitting practical implementation of the developed system.

1.7 Thesis Outline

The thesis comprises six chapters, which are structured in the following manner: **chapter 1:** The introduction provides an overview of FWUAVs, detailing their operational principles, applications, and significance. Furthermore, it outlines the focus of this thesis, highlighting its emphasis on specific aspects related to FWUAVs. **chapter 2:** Describes the work of others witch is review of literature's(past work done by others)about Overview of FWUAV trajectory tracking, the basic structure and flight principles of FWUAV and different controllers used for trajectory tracking of FWUAV . **chapter 3:** Describes the mathematical modelling of FWUAV with different assumptions and coordinate frames and the model is verified using different scenarios. **chapter 4:** Describes Decoupling the model of FWUAV and FOSMC design and the parameters are tuned using PSO. **chapter 5:** Describes the results obtained using the model with its designed controller for trajectory tracking and discussions are done for each results. **chapter 6:** The conclusion drawn from the research conducted in this thesis incorporates recommendations and suggestions for future endeavors.

Chapter 2

Overview of Fixed-wing UAVs

2.1 Review of Existing Literature

The term "Unmanned Aerial Vehicles" (UAVs) has indeed sparked significant curiosity and interest in recent decades. Initially, UAVs emerged primarily in the military sector, where they found important applications for reconnaissance, surveillance, and combat operations. However, as electronic components became smaller and more affordable, there was a significant shift that allowed UAVs to be utilized in civilian settings as well. This transition created opportunity for a variety of parties, including corporations, research organizations, and hobbyists, to investigate and identify civic applications for UAV technology. The word "UAVs" refers to a vast range of vehicle kinds and sizes that cater to a variety of applications and requirements. Fixed-wing and multi-rotor UAVs are the two most common forms of UAVs. FWUAVs, as the name implies, have a fixed-wing configuration comparable to regular airplanes. They are distinguished by their capacity to fly effectively over longer distances, at higher speeds, and at higher altitudes. Fixed-wing UAVs are frequently selected for applications requiring quick and long-range flights, such as aerial mapping, surveillance, freight delivery, and environmental monitoring [4].

In [5] the studied work on the trajectory control system for a FWUAV, the LQR method is used. LQR is a control methodology that entails designing the controller by linearizing the nonlinear dynamic models of the system. However, due to assumptions and approximations made during the linearization process, the linearized model may not precisely represent the actual system. Therefore, LQR may not be suitable for highly nonlinear systems, as its efficacy depends on the precision of the linearized model. In cases where the system exhibits strong nonlinearities, uncertainties, or disturbances, alternative control methods

that can handle these complexities may be more appropriate. The FOSMC is designed as an alternative to LQR in this thesis. The FOSMC is well-known for its resistance to uncertainties and shocks, making it an excellent choice for nonlinear systems.

In [6], This study introduces the deployment of a PID controller for flight path regulation in a FWUAV with 3-DOF. The controller comprises three PID loops, each dedicated to altitude control, turn and turn-rate control, and airspeed control, These control loops are designed to stabilize and control the UAV's flight path. The system is characterized using the 6-DOF fixed-wing equations of motion, which effectively capture the dynamics of the aircraft. Layered PID loops are utilized within the flight controller to address longitudinal and lateral instabilities. Simulations are carried out to evaluate the system's performance. The findings indicate that the PID controller adeptly follows the desired flight path, even when subjected to minor wind disturbances. This underscores the controller's capability to stabilize and regulate the UAV's flight. However, the authors acknowledge that there is room for further development and improvement of the system. One potential area for enhancement is the incorporation of adaptive approaches for controller parameter tuning. By utilizing FOSMC techniques, parameter tuning is introduced, enhancing the controller's capability to handle various operating conditions, disturbances, and uncertainties. This improvement can ultimately lead to better flight path tracking and stability for the UAV.

In [7] the Newton-Euler method is utilized to develop a comprehensive 6-DOF nonlinear dynamic model for the UAV. This model captures the complex dynamics and kinematics of the UAV system. A proposed method for regulating the altitude of the UAV involves employing an adaptive PID control technique. This control approach employs parameter optimization techniques and a system of fuzzy inference to adaptively alter the settings of the PID controller depending on the UAV's performance and feedback.The suggested adaptive PID control is compared with fuzzy logic control and genetically-tuned PID control in terms of efficiency, performance, and robustness. The performance evaluation considers various factors such as tracking accuracy, stability, response time, and disturbance rejection. But the paper focuses on height control only, it should also explore how the suggested control algorithms might be used to regulate other UAV states or trajectories. The approach's flexibility to various control goals should be addressed.

In [8], a new control method is introduced for a FWUAV, which utilizes a learning-based approach grounded in Sliding Mode Control (SMC) theory to effectively manage wind disturbances. The suggested control system comprises a P-controller and a Fuzzy Neural Network (FNN) that can adapt and learn the opposite dynamics of the UAV's system model

in real-time. The research highlights that the suggested approach offers both reliability and simplicity. By combining SMC theory with the adaptive capabilities of the FNN, the control system effectively manages the uncertainties and disturbances caused by wind. The simplicity of this approach makes it straightforward to implement and practical for real-world applications. The control system's ability to learn and adapt to the UAV's dynamics in real-time enhances its reliability and effectiveness, particularly when dealing with wind disturbances.

In [9], focuses on developing an observer-based control system for a fixed-wing UAV (FWUAV) aimed at precisely following desired trajectories. The control system incorporates an extended observer, which is responsible for estimating crucial information about the UAV's state vector and external disturbances affecting its performance. The extended observer plays a vital role in estimating the UAV's state vector, which includes variables such as attitude (orientation) and airspeed. By accurately estimating these states, the controller can make informed decisions and adjust the control inputs to ensure the UAV closely adheres to the intended trajectory. The adaptive Second-Order Sliding Mode (SOSM) control law is employed to steer the UAV along specified trajectories. This control law is designed to adapt and adjust its parameters in response to varying conditions, enabling the control system to robustly handle external disturbances. By counteracting the effects of disturbances, the control system maintains accurate trajectory tracking performance.

In [10], the author intends to simulate and compare a linear PID control approach with a non-linear SMC technique known as STW-SMC for stabilizing a UAV's attitude and height. The purpose of this comparison is to demonstrate that, in certain situations, a linear control method like PID is deemed adequate for stabilizing the UAV, and the energy demand for control is comparable for both approaches.

The linear PID control method is widely utilized for its ability to ensure stability and enhance performance through adjustments in control inputs based on the disparity between desired and actual system states. It is commonly employed in various applications, including UAV control. On the other hand, the non-linear STW-SMC technique, which stands for Sliding Mode Control with Second-Order Terminal Sliding Surface, is a more advanced control approach that is capable of dealing with non-linearities and uncertainties in the system. It achieves stability by driving the system state onto a predefined sliding surface. By simulating both control techniques, the author aims to compare their performance in stabilizing the UAV's attitude and height.

In [11], researchers employ a Nonlinear Model Predictive Controller (NMPC) enhanced

by Particle Swarm Optimization (PSO) to track the trajectory of a Fixed-Wing Unmanned Aerial Vehicle (FWUAV). The primary objective is to evaluate the controller's performance with and without wind adjustment. The NMPC strategy entails forecasting the future actions of the UAV using a nonlinear model and optimizing control inputs to minimize a predefined cost function associated with trajectory tracking. The control inputs of the NMPC are tuned to increase trajectory tracking performance by adding PSO, which is inspired by the behavior of a swarm of particles. The research is particularly dedicated to evaluating how well the NMPC with PSO performs when wind compensation is applied. Wind adjustment involves a method for considering the influence of wind on the course of the UAV trajectory. By considering wind disturbances and compensating for them, the controller aims to enhance trajectory tracking accuracy and stability. By comparing the controller's performance in the presence and absence of wind compensation, the study aims to evaluate its effectiveness, limitations, and potential for real-world applications in fixed-wing UAV systems.

[12] This research introduces a novel approach for creating a guidance controller specifically tailored for small UAVs to achieve accurate path following when there are wind disruptions. Traditional guidance controllers for UAVs often rely on predefined trajectories or way points to guide the aircraft along a desired path. However, these controllers may struggle to maintain precise path following when wind disturbances are present, as wind can significantly impact the UAV's dynamics and trajectory. To overcome this challenge, the study proposes an alternative method of designing a guidance controller that can effectively handle wind disturbances and ensure accurate path following. The specific details and techniques utilized in this alternative approach should be provided for a more comprehensive understanding. The suggested guidance controller's performance under wind disturbances would most likely be compared to that of standard controllers. Path tracking accuracy, stability, resilience to wind disturbances, energy efficiency, and reaction time are likely to be utilized to analyze and compare the proposed controller's efficacy to previous systems.

Research [13], this study describes a control system for trajectory tracking that was created primarily to give FWUAVs with crucial spatial-temporal feedback control capabilities. The main aim of this control design is to ensure that UAVs can carry out time-sensitive missions with dependability. In time-critical missions, it is crucial for UAVs to accurately track desired trajectories while considering both spatial and temporal aspects. The study's trajectory tracking control approach meets these objectives by adding spatial-temporal feedback control capabilities. The effectiveness of the control design is probably assessed using different measures, such as trajectory tracking precision, resilience to disturbances, and adherence

to time constraints.

In [14], this work provides a tracking control method that is fault-tolerant for a FWUAV with specified performance, with the goal of allowing the UAV to track desired trajectories even in the presence of an actuator defects. The control scheme incorporates several key components and techniques. Firstly, the outer-loop position dynamics of the UAV are transformed into a second-order nonlinear model. This transformation allows for the application of control techniques suitable for handling nonlinear systems. Neural networks play a crucial role in the control scheme by identifying unknown nonlinear functions that may contain information about actuator faults. The neural networks learn and approximate these functions, enabling the detection and compensation of actuator faults during the control process. Notably, the paper offers a minimal learning parameter for neural networks, which reduces computing cost and improves the control method's practicability and efficiency. The proposed control strategy attempts to offer robust trajectory tracking capabilities for the FWUAV, even in the face of actuator defects, by integrating FOSMC, fault detection and compensation, and neural network approximation. The study focuses on achieving prescribed performance, ensuring that the UAV maintains accurate trajectory tracking and satisfies specific performance criteria.

Chapter 3

Mathematical Modelling of FWUAV

Developing a mathematical model of an FWUAV is an important step in understanding its kinematics and dynamic motion. The mathematical model represents the FWUAV's behavior mathematically, allowing for analysis, simulation, and controller design. The mathematical model typically involves formulating equations that describe the FWUAV's kinematics (motion description) and dynamics (forces and torques acting on the FWUAV). The kinematic equations define the connection between the location, velocity, and orientation of the UAV.The dynamic equations consider the forces and torques acting on the FWUAV, which encompass aerodynamic forces, gravity, and control inputs [14].

3.1 Modelling Assumptions

Certain assumptions are typically used while constructing a mathematical model for a FWUAV to simplify the modeling process and make it more tractable. These assumptions aid in capturing the UAV's core dynamics and behaviors while decreasing complexity. This thesis makes the following assumptions:

- The UAV is represented in the model as a rigid body, with aerodynamic forces generated by both the propeller and wing.
- It is assumed that the center of mass aligns with the origin of the body-fixed frame.
- The UAV's mass is considered constant during flight, without accounting for changes due to fuel consumption or variations in payload.
- Wind is seen as an external disturbance.

3.1.1 FWUAV Coordinate Frames

Before driving the FWUAV mathematical model, it is vital to grasp distinct coordinate frames and transformations between them.There are two fundamental operations: rotation and translation convert one coordinate frame into another coordinate frame [15]. A FWUAV uses a rotation matrix to transform from one coordinate to another, how these rotation matrices are generated is presented in appendix (A). Here are some instants of coordinate frames summarized using block diagrams in figure 3.1 [16]:

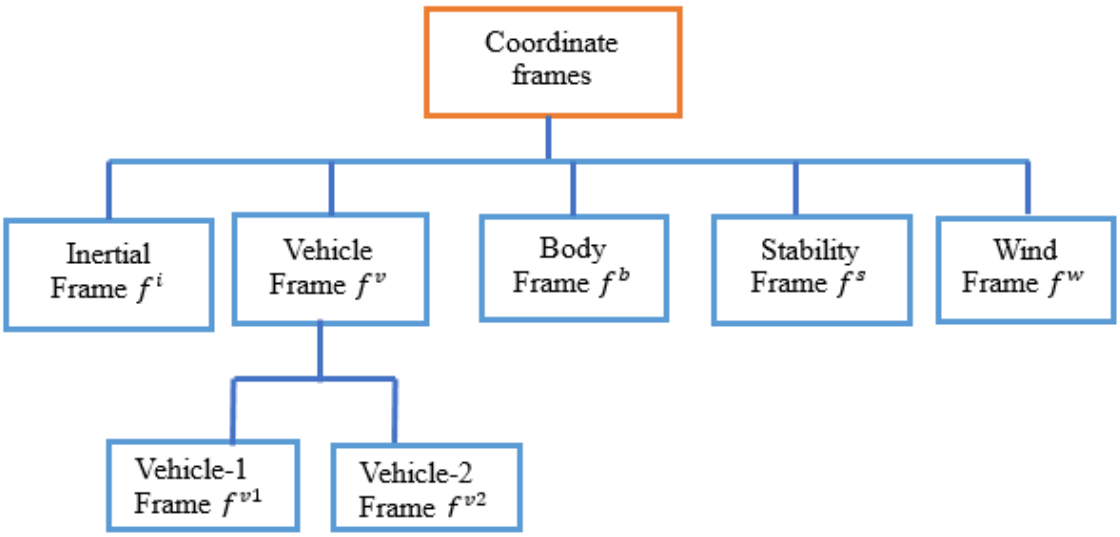

Figure 3.1: Tree Illustrating the Links Between Coordinate Systems

3.1.1.1 Inertial Frame (f^i)

The inertial coordinate system is a frame fixed to the Earth, with its origin positioned at the designated home location. The unit vectors i^i, j^i, and k^i point north, east, and downward, respectively, toward the center of the Earth, as illustrated in figure 3.2. This frame is commonly known as the NED (North-East-Down) frame.

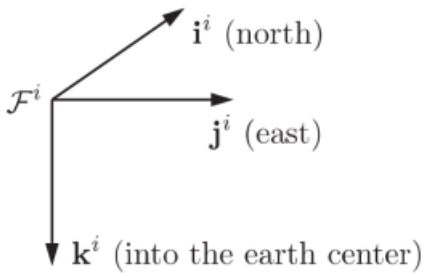

Figure 3.2: The Inertial Frame f^i [16]

3.1.1.2 Vehicle Frame (f^v)

f^v denotes the f^i translated onto the center of mass of the vehicle. The axes of f^v align with those of f^i as depicted in figure 3.3.

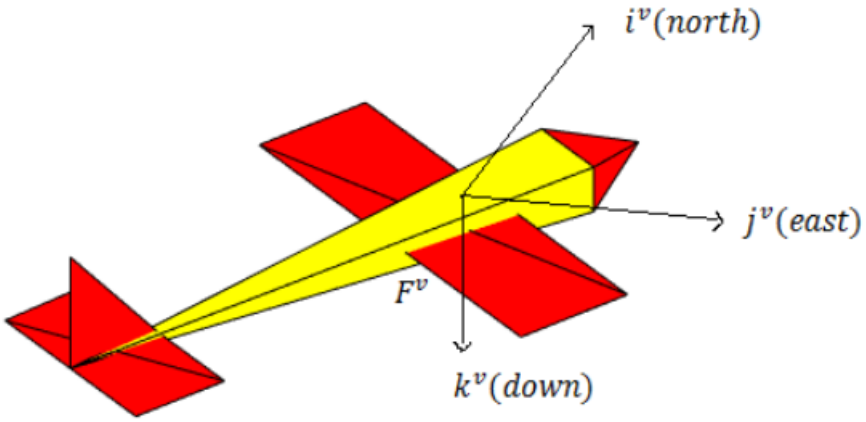

Figure 3.3: f^v Located at Center of Mass of the UAV.
[16]

3.1.1.3 Vehicle-1 Frame (f^v)

f^{v1} is obtained from f^v by rotating the i^v axis until it aligns with the aircraft's heading (ψ), ensuring that i^{v1} points forward from the aircraft's nose, and j^{v1} extends out from the starboard wing, as depicted in figure 3.4.

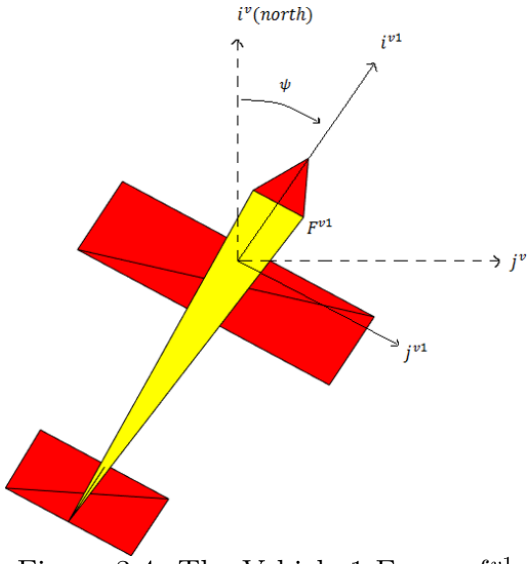

Figure 3.4: The Vehicle-1 Frame f^{v1}
[16]

k^{v1} remains unchanged from k^v except for its label because the rotation occurs around the vertical axis. The rotation matrix R_v^{v1} is used for this transformation. The rotation angle is

denoted by ψ.The derivation of the rotation matrix R_v^{v1} an be performed in equation (3.1):

$$R_v^{v1}(\psi) = \begin{bmatrix} cos\psi & sin\psi & 0 \\ -sin\psi & cos\psi & 0 \\ 0 & 0 & 1 \end{bmatrix} \tag{3.1}$$

3.1.1.4 Vehicle-2 Frame (f^{v2})

Similarly, f^{v2} is derived from f^{v1} by rotating j^{v1} by (θ) as shown in figure 3.5.

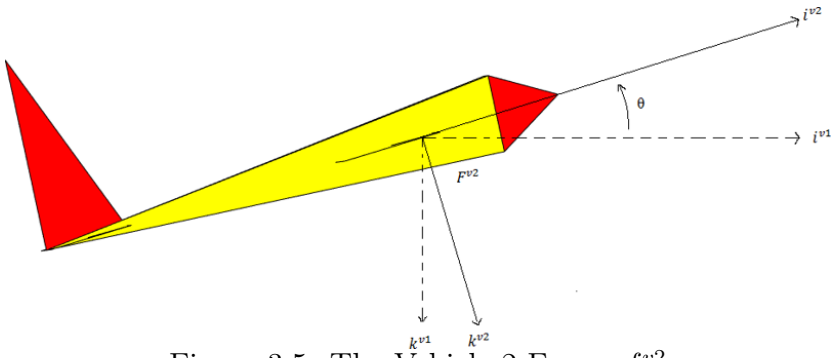

Figure 3.5: The Vehicle-2 Frame f^{v2} [16]

In this rotation, j^{v1} axis serves as the axis, ensuring that j^{v2} aligns with j^{v1} a post-rotation, maintaining its orientation outward from the starboard wing. The same methodology as previously described is applied, utilizing the rotation matrix R_{v1}^{v2} in equation (3.2):

$$R_{v1}^{v2}(\theta) = \begin{bmatrix} cos\theta & 0 & -sin\theta \\ 0 & 1 & 0 \\ sin\theta & 0 & cos\theta \end{bmatrix} \tag{3.2}$$

3.1.1.5 The Body Frame (f^b)

f^b is derived from the f^{v2} through a right-hand rotation by the roll angle (ϕ), as demonstrated in figure 3.6.

The rotation reorients j^b to pass through the starboard wing and k^b to be perpendicular to that (directed downward), all while preserving the origin at the center of mass/center of gravity. This transformation can be represented using the rotation matrix R_{v2}^b is defined in equation (3.3):

$$R_{v2}^b(\phi) = \begin{bmatrix} 1 & 0 & 0 \\ 0 & cos\phi & sin\phi \\ 0 & -sin\phi & cos\phi \end{bmatrix} \tag{3.3}$$

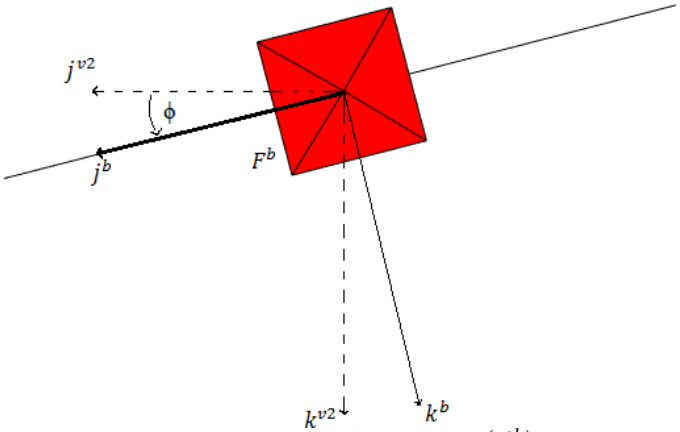

Figure 3.6: Body Frame (f^b) [16]

The intermediate frames f^{v1} and f^{v2} facilitate the rotation from the vehicle frame to the body frame. Initially, the right-handed rotation matrix about the k^v axis by ψ (R_v^{v1}) is established. Subsequently, a rotation about j^{v1} by θ (R_{v1}^{v2}) is conducted. Finally, the body frame f^b is achieved by the last rotation around the i^{v2} axis by ϕ (R_{v2}^b) as shown in figure 3.7:

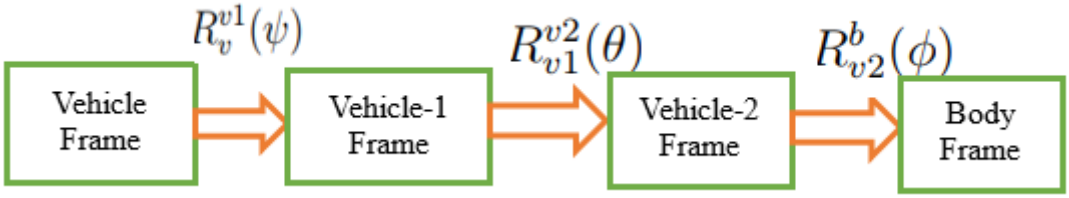

Figure 3.7: Using Rotation Matrices, Vehicle to Body Frame Transformation

The composite rotation matrix from the vehicle frame to the body frame results from the multiplication of the three rotation matrices: $R_{v2}^b(\phi)$, $R_{v1}^{v2}(\theta)$ and $R_v^{v1}(\psi)$ as shown in equation (3.4):

$$R_v^b(\phi,\theta,\psi) = R_{v2}^b(\phi)R_{v1}^{v2}(\theta)R_v^{v1}(\psi)$$

$$R_v^b(\phi,\theta,\psi) = \begin{bmatrix} C\psi C\theta & S\psi C\theta & -S\theta \\ C\psi S\theta S\phi - S\psi C\phi & S\psi S\theta S\phi + C\psi C\phi & C\theta S\phi \\ C\psi S\theta C\phi + S\psi S\phi & S\psi S\theta C\phi - C\psi S\phi & C\theta C\phi \end{bmatrix} \tag{3.4}$$

In this context, C and S represent the cosine and sine trigonometric functions, respectively. The set of three angles (ϕ,θ,ψ) is commonly known as Euler angles, as they provide a straightforward method of describing the orientation of the body relative to the inertial frame.

3.1.2 Stability Frame(f^s)

f^s is created by rotating f^b around the j^b axis. The UAV's velocity relative to the surrounding air is indicated as V_a. Lift necessary for flight is generated by maintaining the wings at a positive angle to the airspeed vector, known as the angle of attack α. Therefore, introducing the stability frame involves a left-handed rotation around j^b at α from f^b. For the right-handed rotation from the stability frame to the body frame, a positive angle of attack necessitates a left-handed rotation. This rotation configuration is illustrated in the figure. This circumstance is represented in figure figure 3.8. The rotation matrix from f^b to f^s is

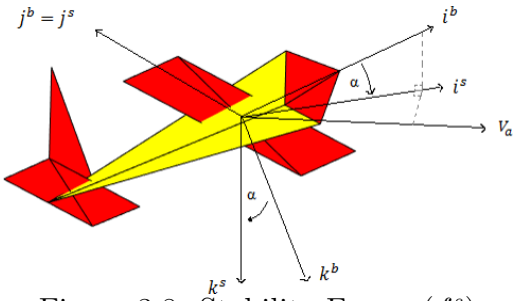

Figure 3.8: Stability Frame (f^s)
[16]

expressed by Equation 3.5, employing a left-handed convention.

$$R_b^s(\alpha) = \begin{bmatrix} cos\alpha & 0 & sin\alpha \\ 0 & 1 & 0 \\ -sin\alpha & 0 & cos\alpha \end{bmatrix} \tag{3.5}$$

3.1.2.1 Wind frame(f^w)

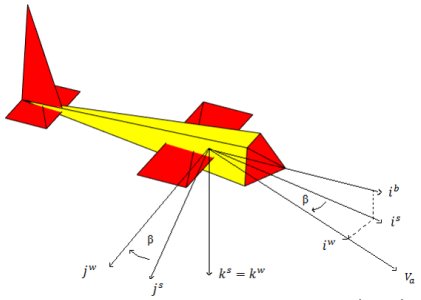

Figure 3.9: Wind Frame (f^w)
[16]

In cases where the airspeed vector does not lie on the (i^b, k^b) plane, it becomes necessary to specify another angle known as the side-slip angle (β). A new coordinate system, termed the wind frame (f^w), is established by rotating the stability frame by an angle of β about k^s in the right-handed direction, as depicted in Figure 3.9. In this configuration, the airspeed

direction V_a and the unit vector i^w are aligned within the wind frame. The rotation matrix from f^s to f^w about side-slip angle β is given by equation (3.6).

$$R_s^w(\beta) = \begin{bmatrix} cos\beta & sin\beta & 0 \\ -sin\beta & cos\beta & 0 \\ 0 & 0 & 1 \end{bmatrix} \tag{3.6}$$

The complete transformation from the body frame to the wind frame involves both the rotation matrix around the side slip angle and the rotation matrix around the angle of attack, as illustrated in figure 3.10.

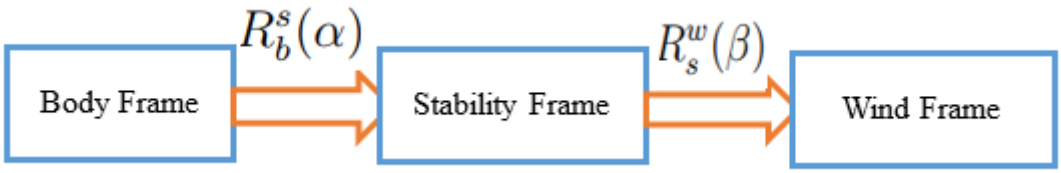

Figure 3.10: Using rotation matrices, the body is transformed to the wind frame

Equation 3.7 provides the rotation matrix that transforms from the body frame to the wind frame.

$$R_b^w(\alpha,\beta) = R_s^w(\beta)R_b^s(\alpha)$$

$$R_b^w(\alpha,\beta) = \begin{bmatrix} cos\beta cos\alpha & sin\beta & cos\beta sin\alpha \\ -sin\beta cos\alpha & cos\beta & -sin\beta sin\alpha \\ -sin\alpha & 0 & cos\alpha \end{bmatrix} \tag{3.7}$$

3.1.2.2 The Wind Triangle

When considering UAV dynamics, wind significantly influences flight mechanics, especially since aerodynamic forces are contingent on the relative speed relative to the surrounding air. Therefore, accurate modeling necessitates proper consideration of wind effects. To formulate the equations of motion for a UAV, it's imperative to derive key expressions. The wind velocity relative to the inertial frame is denoted as V_w, while the airspeed relative to the same frame is represented by V_a. To account for the impact of wind, defining ground speed as V_g is essential, indicating the UAV velocity relative to the inertial frame. The vectors representing airspeed, ground speed, and wind speed are interconnected by equation 3.8.

$$V_a = V_g - V_w \tag{3.8}$$

In this thesis, wind velocity is not taken as a design consideration, but it can be treated as an external disturbance to evaluate the performance of the controller. Therefore, air speed equals to ground speed.

$$V_a = V_g = \begin{bmatrix} u \\ v \\ w \end{bmatrix} \tag{3.9}$$

Equation 3.10 describes the relationship between the airspeed components of V_a resolved in the body frame and the airspeed, as well as the angles of attack and sideslip.

$$\begin{bmatrix} u \\ v \\ w \end{bmatrix} = R_w^b(\alpha, \beta) \begin{bmatrix} V_a \\ 0 \\ 0 \end{bmatrix} = \begin{bmatrix} cos\beta cos\alpha & -sin\beta cos\alpha & -sin\alpha \\ sin\beta & cos\beta & 0 \\ cos\beta sin\alpha & -sin\beta sin\alpha & cos\alpha \end{bmatrix} \begin{bmatrix} V_a \\ 0 \\ 0 \end{bmatrix}$$

$$\begin{bmatrix} u \\ v \\ w \end{bmatrix} = V_a \begin{bmatrix} cos\beta cos\alpha \\ sin\beta \\ cos\beta sin\alpha \end{bmatrix} \tag{3.10}$$

By inverting Equation 3.10, one can compute the airspeed V_a along with the angles α and β, resulting in Equation 3.11.

$$\begin{aligned} V_a &= \sqrt{u^2 + v^2 + w^2} \\ \alpha &= \arctan \frac{w}{u} \\ \beta &= \arcsin \frac{v}{V_a} \end{aligned} \tag{3.11}$$

3.2 Kinematics and Flight Dynamics

In the process of formulating equations of motion for a FWUAV,t is standard practice to incorporate twelve state variables. These state variables represent various aspects of the FWUAV's motion and orientation. These are position variables (x, y, z), velocity variables (u, v, w), attitude variables (ϕ, θ, ψ) and angular velocity variables (p, q, r) as summarized in table 3.1. These twelve state variables together provide a comprehensive representation of the FWUAV's motion and dynamics. These variables enable the development of equations of motion, which articulate the evolution of these parameters over time and elucidate the forces and torques exerted on the FWUAV.

The movement of a FWUAV can be described in terms of three primary axes, which are commonly referred to as the body-fixed coordinate axes which are depicted in figure 3.11.

Table 3.1: State Variables of the Equations of Motion

Name of states	Description
x, y, z	Inertial NED positions along i^i, j^i, k^i axes
u, v, w	Body frame velocities i^b, j^b, k^b axes
ϕ, θ, ψ	Attitude angles defined with respect to f^{v2}, f^{v1}, f^v frames
p, q, r	Body frame angular rate measured along i^b, j^b, k^b axes

These axes are aligned with the vehicle's physical structure and are essential for understanding and analyzing its dynamics.

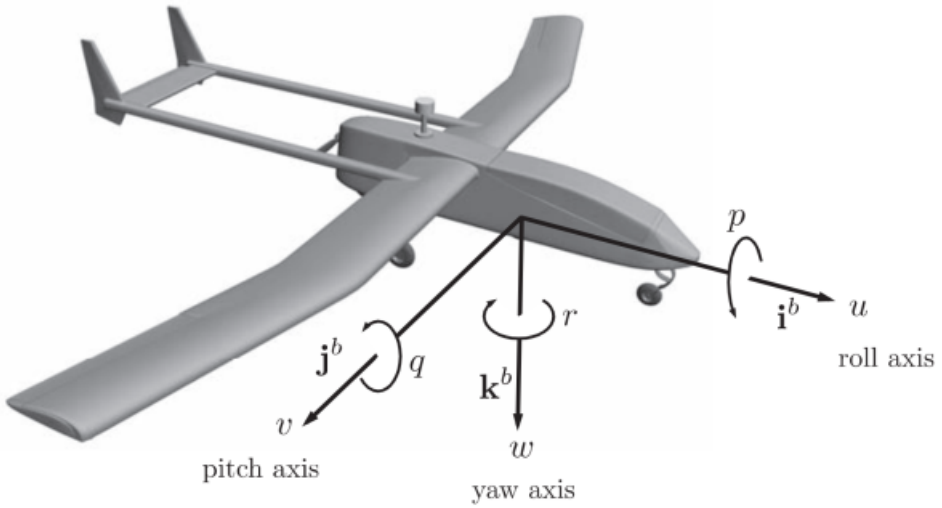

Figure 3.11: Definition of Axes of Rotation of FWUAV [17]

Irrespective of the aircraft type, there exist three axes along which it can maneuver: side-to-side (lateral or pitch) axis, front-to-back (longitudinal or roll) axis, and up-and-down (vertical or yaw) axis.

The lateral (pitch) axis: extends from one wing tip to the other, and the aircraft pitches around this axis.

The longitudinal (roll) axis: runs from the nose to the tail of the aircraft, and it is the axis about which the aircraft rolls.

The vertical (yaw) axis: runs vertically through the center of the aircraft, and the aircraft yaws around this axis.

3.2.1 Kinematics of FWUAV

Differentiation and rotation are required for the relationship between translational velocity and position which is given in equation (3.12)

$$\begin{bmatrix} \dot{x} \\ \dot{y} \\ \dot{z} \end{bmatrix} = R_b^v(\phi, \theta, \psi) \begin{bmatrix} u \\ v \\ w \end{bmatrix} \tag{3.12}$$

Describing roll, pitch, and yaw angles concerning their relative intermediate frames can add intricacies when calculating angular measurements. Through proper angular rotations, the body-frame angular rates can be represented in relation to the derivatives of the Euler angles, and this process is executed as follows:

$$\begin{bmatrix} p \\ q \\ r \end{bmatrix} = \begin{bmatrix} \dot{\phi} \\ 0 \\ 0 \end{bmatrix} + R_{v2}^b(\phi) \begin{bmatrix} 0 \\ \dot{\theta} \\ 0 \end{bmatrix} + R_{v2}^b(\phi) R_{v1}^{v2}(\theta) \begin{bmatrix} 0 \\ 0 \\ \dot{\psi} \end{bmatrix} \tag{3.13}$$

which gives:

$$\begin{bmatrix} p \\ q \\ r \end{bmatrix} = \begin{bmatrix} 1 & 0 & -sin\theta \\ 0 & cos\phi & sin\phi cos\theta \\ 0 & -sin\phi & cos\phi cos\theta \end{bmatrix} \begin{bmatrix} \dot{\phi} \\ \dot{\theta} \\ \dot{\psi} \end{bmatrix} \tag{3.14}$$

Inverting this expression yields

$$\begin{bmatrix} \dot{\phi} \\ \dot{\theta} \\ \dot{\psi} \end{bmatrix} = \begin{bmatrix} 1 & sin\phi tan\theta & cos\phi tan\theta \\ 0 & cos\phi & -sin\phi \\ 0 & \frac{sin\phi}{cos\theta} & \frac{cos\psi}{cos\theta} \end{bmatrix} \begin{bmatrix} p \\ q \\ r \end{bmatrix} \tag{3.15}$$

3.2.2 Rigid-Body Dynamics

Newton's second law is employed to derive the dynamic equations of motion for both translational and rotational degrees of freedom. The inertial frame serves as a necessary reference for expressing forces and moments, although components from other frames, like the body frame, can also be utilized for this purpose. The flat earth model, which is suitable for small UAVs, is employed.

3.2.2.1 Translational Motion

Newton's second law of motion states that the rate of change of momentum of an object is equal to the net force acting on it. In the context of translational motion of a UAV, expressed in terms of vectors, it can be represented as:

$$m\frac{d\boldsymbol{V}_g}{dt_i} = f \tag{3.16}$$

Here, m represents the mass of the UAV, $\frac{d}{dt_i}$ denotes the time derivative in the inertial frame, and f is the sum of all external forces acting on the UAV, such as gravity, aerodynamic forces, and propulsion forces. To simplify the application of Newton's law, we express the derivative of the velocity vector $\boldsymbol{V}_g$ in terms of the body frame components. This leads us to:

$$m(\frac{d\boldsymbol{V}_g^b}{dt_i^b} + \omega_{b/i}^b \times \boldsymbol{V_g^b}) = f^b \tag{3.17}$$

here $\omega_{b/i}$ represents the angular velocity of the body frame f^b in the inertial frame f^i. Breaking down the velocity and angular velocity components as $\boldsymbol{V_g^b}$ and $\omega_{b/i}^b$ respectively, and organizing the forces f^b into components, we arrive at the expression for translational motion:

$$\begin{bmatrix} \dot{u} \\ \dot{v} \\ \dot{w} \end{bmatrix} = \begin{bmatrix} rv - qw \\ pw - ru \\ qu - pv \end{bmatrix} + \frac{1}{m}\begin{bmatrix} f_x \\ f_y \\ f_z \end{bmatrix} \tag{3.18}$$

This equation describes the rates of change of the UAV's velocities in the body frame (u, v, w) concerning the angular velocities (p, q, r), and the external forces acting on the UAV.

3.2.2.2 Rotational Motion

Newton's law for rotational motion asserts that the rate of change of angular momentum, denoted by H in vector form, is equal to the sum of all externally applied moments, represented by M. Expanding the derivative of angular momentum in the inertial frame using the vector derivative rule yields:

$$\frac{d\boldsymbol{H}}{dt_i} = \frac{d\boldsymbol{H}}{dt_b} + \omega_{b/i} \times \boldsymbol{H}) = M \tag{3.19}$$

Expressing equation (3.19) in the body frame results in:

$$\frac{d\boldsymbol{H^b}}{dt_b} + \omega^b_{b/i} \times \boldsymbol{H^b}) = M^b \tag{3.20}$$

For a rigid body, the formula for angular momentum is given by $\boldsymbol{H}^b = J\omega^b_{b/i}$, where J represents the inertia tensor which is given in appendix (A). In the context of aircraft, which are commonly symmetric about the plane spanned by i^b and k^b, certain components of J become zero. Consequently, the derivative of J in the body frame is zero. Thus, the equation simplifies to:

$$\frac{d\boldsymbol{H^b}}{dt_b} + \omega^b_{b/i} \times \boldsymbol{H^b}) = M^b \tag{3.21}$$

Solving for $\frac{d\omega^b_{b/i}}{dt_b}$ leads to:

$$\frac{d\omega^b_{b/i}}{dt_b} = \dot{\omega}^b_{b/i} = J^{-1}(-\omega^b_{b/i} \times (J\omega^b_{b/i}) + M^b) \tag{3.22}$$

Given that the angular rates in the body frame are denoted by p, q, and r, the equation can be represented as:

$$\omega^b_{b/i} = \begin{bmatrix} p & q & r \end{bmatrix}^T \implies \dot{\omega}^b_{b/i} = \begin{bmatrix} \dot{p} & \dot{q} & \dot{r} \end{bmatrix}^T$$

By performing the inverse matrix of J and the cross product in the equation, and defining the moment vector M, the rotational dynamics equations are derived as:

$$\begin{pmatrix} \dot{p} \\ \dot{q} \\ \dot{r} \end{pmatrix} = \begin{bmatrix} \Gamma_1 pq - \Gamma_2 qr \\ \Gamma_5 pr - \Gamma_6(p^2 - r^2) \\ \Gamma_7 pq - \Gamma_1 qr \end{bmatrix} + \begin{bmatrix} \Gamma_3 L + \Gamma_4 N \\ \frac{1}{\Gamma_y} M \\ \Gamma_4 L + \Gamma_8 N \end{bmatrix} \tag{3.23}$$

Here Γ_1.....Γ_8 represent constants derived from the formula given in the appendix(A).
he six-degree-of-freedom, 12-state model for fixed-wing UAV kinematics and dynamics are summarized in the provided equations below. These equations describe the translational and rotational motion dynamics of the UAV in terms of its position, velocity, orientation, angular rates, and the forces and moments acting upon it.

$$\begin{bmatrix} \dot{x} \\ \dot{y} \\ \dot{z} \end{bmatrix} = \begin{bmatrix} C\psi C\theta & C\psi S\theta S\phi - S\psi C\phi & C\phi S\theta C\psi + S\phi S\psi \\ C\theta S\psi & S\phi S\theta S\psi + C\phi C\psi & C\phi S\theta S\psi - S\phi c\psi \\ -S\theta & S\phi C\theta & C\phi C\theta \end{bmatrix} \begin{bmatrix} u \\ v \\ w \end{bmatrix} \tag{3.24}$$

$$\begin{bmatrix} \dot{u} \\ \dot{v} \\ \dot{w} \end{bmatrix} = \begin{bmatrix} rv - qw \\ pw - ru \\ qu - pv \end{bmatrix} + \frac{1}{m} \begin{bmatrix} f_x \\ f^y \\ f_z \end{bmatrix} \tag{3.25}$$

$$\begin{bmatrix} \dot{\phi} \\ \dot{\theta} \\ \dot{\psi} \end{bmatrix} = \begin{bmatrix} 1 & sin\phi tan\theta & cos\phi tan\theta \\ 0 & cos\phi & -sin\phi \\ 0 & sin\phi sec\theta & cos\psi sec\theta \end{bmatrix} \begin{bmatrix} p \\ q \\ r \end{bmatrix} \tag{3.26}$$

$$\begin{pmatrix} \dot{p} \\ \dot{q} \\ \dot{r} \end{pmatrix} = \begin{bmatrix} \Gamma_1 pq - \Gamma_2 qr \\ \Gamma_5 pr - \Gamma_6 (p^2 - r^2) \\ \Gamma_7 pq - \Gamma_1 qr \end{bmatrix} + \begin{bmatrix} \Gamma_3 L + \Gamma_4 N \\ \frac{1}{\Gamma_y} M \\ \Gamma_4 L + \Gamma_8 N \end{bmatrix} \tag{3.27}$$

3.3 External forces and moments

The aggregate of all external forces and moments acting upon the fixed-wing Unmanned Aerial Vehicle (FWUAV) is described as:

$$F = f_g + f_a + f_p$$

$$M = M_a + M_p$$

Here, F represents the overall force exerted on the air frame, while M signifies the total moment applied to the air frame. The symbols g, a, and p denote the gravitational, aerodynamic, and propulsion components, respectively, of these forces and moments.

3.3.0.1 Gravitational Force

The impact of the gravitational field is expressed as a force operating in the k^v direction, specifically at the center of mass of the aircraft. This force doesn't generate any moments. In the vehicle frame f^v, the gravity force can be defined as:

$$f_g^v = \begin{bmatrix} 0 \\ 0 \\ mg \end{bmatrix}$$

In the body frame, the gravitational force can be described as:

$$f_g^b = R_v^b \begin{bmatrix} 0 \\ 0 \\ mg \end{bmatrix} = \begin{bmatrix} -mgsin\theta \\ mgcos\theta sin\phi \\ mgcos\theta cos\phi \end{bmatrix} \tag{3.28}$$

3.3.0.2 Aerodynamic Forces and Moments

The distribution of pressure is a significant contributor to the generation of aerodynamic forces and moments. As a UAV travels through the air, it encounters varying pressure distributions around its body, as shown in figure 3.12

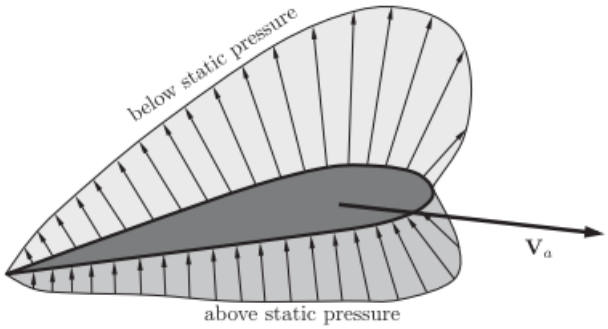

Figure 3.12: Pressure Distribution Around an Airfoil
[17]

The impact of pressure distribution can be represented by a blend of forces and moments. For example, when focusing on the longitudinal $(i^b - k^b)$ plane, the influence of pressure on the UAV body can be simulated through a lift force, a drag force, and a moment, as depicted in figure 3.13.

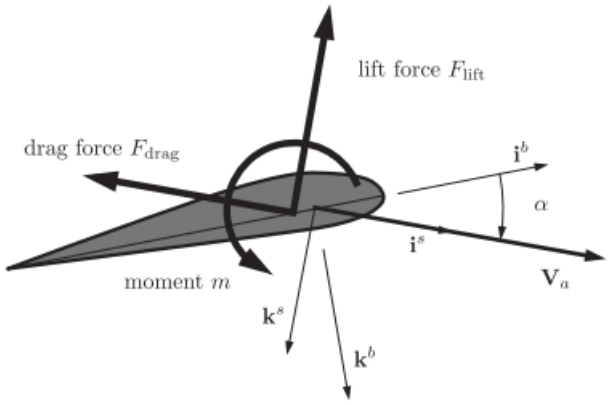

Figure 3.13: Impact of Pressure Distribution
[17]

Before discussing the forces and moments acting on the body, it's essential to introduce the control surfaces. The standard configuration, illustrated in figure 3.14, includes the

aileron deflection denoted as δ_a, the elevator deflection denoted as δ_e, the rudder deflection denoted as δ_r, and the throttle denoted as δ_t. Except for the throttle, these deflections are measured in radians rather than percentages. The positive deflection of the control surfaces is determined by applying the right-hand rule to the hinge axis.

The deflection of the ailerons can be articulated as follows:

$$\delta_a = \frac{1}{2}(\delta_{aleft} - \delta_{aright}) \tag{3.29}$$

Here, δ_{aleft} and δ_{aright} are the left and right ailerons deflection respectively. Thus, a positive δ_a will generate, as will be observed, a positive rolling moment about i^b, thereby adhering to the convention. It is a standard practice to partition aerodynamic forces and moments into

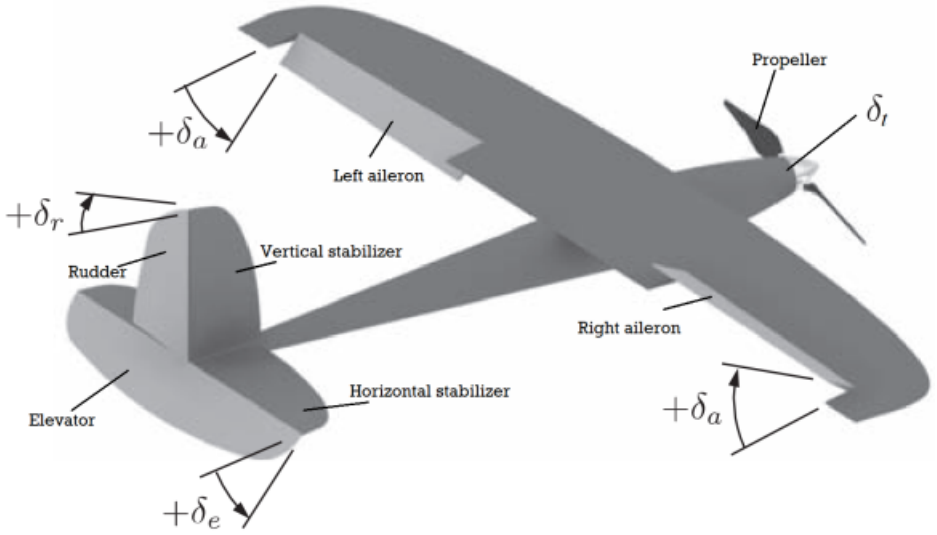

Figure 3.14: Representation of Aircraft Control Surfaces and Propellers [17]

two categories: longitudinal and lateral.

Longitudinal Aerodynamics

The lift force, drag force, and pitch moment are the forces and moments responsible for inducing motion in the (i^b, k^b) plane of the body. These definitions are provided in equations equation (3.30), equation (3.31), and equation (3.32), respectively.

$$f_{lift} = \frac{1}{2}\rho {V_a}^2 S C_L(\alpha, q, \delta_e) \tag{3.30}$$

$$f_{drag} = \frac{1}{2}\rho {V_a}^2 S C_D(\alpha, q, \delta_e) \tag{3.31}$$

$$M = \frac{1}{2}\rho {V_a}^2 S c C_M(\alpha, q, \delta_e) \tag{3.32}$$

Here, ρ represents air density, S denotes the area of a single wing, and c is the main chord of the wing. Va corresponds to the airspeed as defined in equation (3.11). C_L, C_D, and C_M are the dimensionless coefficients of lift force, drag force and pitch moment, which rely on parameters such as angle of attack α, pitch rate q, and elevator deflection δ_e. This nonlinear relationship can be estimated using a first-order Taylor series expansion of equation (3.33)

$$C_L(\alpha, q, \delta_e) = [C_{L0} + C_{L\alpha}\alpha + C_{Lq}\frac{c}{2V_a}q + C_{L\delta_e}\delta_e] \tag{3.33}$$

The coefficients C_{L0}, $C_{L\alpha} = \frac{\partial C_L}{\partial \alpha}$, $C_{Lq} = \frac{\partial C_L}{\partial \frac{qc}{2V_a}}$, and $C_{L\delta_e} = \frac{\partial C_L}{\partial \delta_e}$ are dimensionless parameters. Similarly, the first-order approximations for the aerodynamic drag force and pitching moment are formulated in a comparable fashion.

$$C_D(\alpha, q, \delta_e) = [C_{D0} + C_{D\alpha}\alpha + C_{Dq}\frac{c}{2V_a}q + C_{D\delta_e}\delta_e] \tag{3.34}$$

$$C_M(\alpha, q, \delta_e) = [C_{M0} + C_{M\alpha}\alpha + C_{Mq}\frac{c}{2V_a}q + C_{M\delta_e}\delta_e] \tag{3.35}$$

f_{lift} and f_{drag} are represented in the stability frame, as depicted in figure 3.13. To transform them into the body frame, equation (3.33) applies:

$$\begin{bmatrix} f_x \\ 0 \\ f_z \end{bmatrix} = R_s^b(\alpha) \begin{bmatrix} -f_{drag} \\ 0 \\ -f_{lift} \end{bmatrix} \tag{3.36}$$

But, from the property of rotation matrix and using the rotation matrix from the body frame to the stability frame in equation (3.5), $R_s^b(\alpha) = (R_b^s(\alpha))^T$

$$\begin{bmatrix} f_x \\ 0 \\ f_z \end{bmatrix} = \begin{bmatrix} cos\alpha & 0 & -sin\alpha \\ 0 & 1 & 0 \\ sin\alpha & 0 & cos\alpha \end{bmatrix} \begin{bmatrix} -f_{drag} \\ 0 \\ -f_{lift} \end{bmatrix}$$

$$f_x = -f_{drag}cos\alpha + f_{lift}sin\alpha \tag{3.37}$$

$$f_z = -f_{drag}sin\alpha - f_{lift}cos\alpha \tag{3.38}$$

Lateral Aerodynamics

The lateral aerodynamic factors that directly affect the lateral direction along j^b are the side force (f_y), the rolling moment (L), and the yawing moment (N). They are significantly influenced by β, as illustrated in equation (3.39), equation (3.40), and equation (3.41) respectively:

$$f_y = \frac{1}{2}\rho {V_a}^2 S C_y(\beta, p, r, \delta_a, \delta_r) \tag{3.39}$$

$$L = \frac{1}{2}\rho {V_a}^2 S b C_l(\beta, p, r, \delta_a, \delta_r) \tag{3.40}$$

$$N = \frac{1}{2}\rho {V_a}^2 S b C_n(\beta, p, r, \delta_a, \delta_r) \tag{3.41}$$

Where, C_y, C_l, and C_n are dimensionless coefficients lateral force , roll moment and yaw moment respectively and b represents the wingspan of the UAV. The first-order Taylor series expansions of the coefficients C_y, C_l, and C_n are given by:

$$C_y(\beta, p, r, \delta_a, \delta_r) = [C_{y0} + C_{Y\beta}\beta + C_{yp}\frac{b}{2V_a}p + C_{yr}\frac{b}{2V_a}r + C_{y\delta_a}\delta_a + C_{y\delta_r}\delta_r] \tag{3.42}$$

$$C_l(\beta, p, r, \delta_a, \delta_r) = [C_{l0} + C_{l\beta}\beta + C_{lp}\frac{b}{2V_a}p + C_{lr}\frac{b}{2V_a}r + C_{l\delta_a}\delta_a + C_{l\delta_r}\delta_r] \tag{3.43}$$

$$C_n(\beta, p, r, \delta_a, \delta_r) = [C_{n0} + C_{n\beta}\beta + C_{np}\frac{b}{2V_a}p + C_{nr}\frac{b}{2V_a}r + C_{n\delta_a}\delta_a + C_{n\delta_r}\delta_r] \tag{3.44}$$

For aircraft symmetric about (i^b, k^b), C_{y0}, C_{l0}, and C_{n0} are zero. Coefficients related to α, β, p, q, and r are commonly termed stability derivatives, while those related to δ_a, δ_e, and δ_r are referred to as control derivatives.

3.3.0.3 Propulsion Force

Numerous propeller models can be found in the literature. The Bernoulli principle can be used to develop a simple model that is appropriate for modeling UAVs. The thrust generated by the propeller, denoted as f_p, is determined by the area swept out by the propeller, S_{prop}, and the pressure difference, ΔP, given by the equation:

$$F_p = S_p \Delta P \tag{3.45}$$

The pressures before and after the propeller, P_{in} and P_{out} respectively, are calculated using Bernoulli's principle as follows:

$$P_{in} = P_0 + \frac{1}{2}\rho {V_a}^2$$
$$P_{out} = P_0 + \frac{1}{2}\rho {V_{out}}^2$$

Where V_{out} represents the air velocity at the exit of the propeller, and P_0 denotes the ambient pressure.

$$V_{out} = k_{motor}\delta_t \tag{3.46}$$

Therefore, the thrust produced by the motor can be given by:

$$f_p = S_p C_{prop}(P_{out} - P_{in}) = \frac{1}{2}\rho S_p C_{prop}((k_{motor}\delta_t)^2 - {V_a}^2) \tag{3.47}$$

Where C_{prop} is a dimensionless coefficient known as the rotor thrust coefficient. For most UAV designs, the thrust acts directly along the i^b body-axis, resulting in no moments about the center of mass. Thus, the total forces and moments acting on the fixed-wing UAV can be expressed as shown in equations equation (3.48) and equation (3.49) respectively:

$$\begin{bmatrix} f_x \\ f_y \\ f_z \end{bmatrix} = \begin{bmatrix} -mgsin\theta \\ mgcos\theta sin\phi \\ mgcos\theta cos\phi \end{bmatrix} + \frac{1}{2}\rho {V_a}^2 S \begin{bmatrix} -C_D(\alpha, q, \delta_e)cos\alpha + C_L(\alpha, q, \delta_e)sin\alpha \\ C_y(\beta, p, r, \delta_a, \delta_r) \\ -C_D(\alpha, q, \delta_e)sin\alpha - C_L(\alpha, q, \delta_e)cos\alpha \end{bmatrix} + \begin{bmatrix} f_p \\ 0 \\ 0 \end{bmatrix} \tag{3.48}$$

$$\begin{bmatrix} L \\ M \\ N \end{bmatrix} = \frac{1}{2}\rho {V_a}^2 S \begin{bmatrix} b[C_{l0} + C_{l\beta}\beta + C_{lp}\frac{b}{2V_a}p + C_{lr}\frac{b}{2V_a}r + C_{l\delta_a}\delta_a + C_{l\delta_r}\delta_r] \\ c[C_{m0} + C_{m\alpha}\alpha + C_{mq}\frac{c}{2V_a}q + C_{m\delta_e}\delta_e] \\ b[C_{n0} + C_{n\beta}\beta + C_{np}\frac{b}{2V_a}p + C_{nr}\frac{b}{2V_a}r + C_{n\delta_a}\delta_a + C_{n\delta_r}\delta_r] \end{bmatrix} \tag{3.49}$$

3.3.1 Summary of Nonlinear Equations of Motion

The 6-DOF equations of motion for FWUAV describe the aircraft's motion in three position and three orientation. The equations are typically nonlinear and can be quite complex. Below is a general representation of the 12-state nonlinear equations of motion for a FWUAV.

Translational Equations

$$
\begin{aligned}
\dot{x} &= \cos\theta\cos\psi u + (\sin\phi\sin\theta\cos\psi - \cos\phi\sin\psi)v + (\cos\phi\sin\theta\cos\psi + \sin\phi\sin\psi)w \\
\dot{y} &= \cos\theta\sin\psi u + (\sin\phi\sin\theta\sin\psi + \cos\phi\cos\psi)v + (\cos\phi\sin\theta\sin\psi - \sin\phi\cos\psi)w \\
\dot{z} &= -\sin\theta u + \sin\phi\cos\theta v + \cos\phi\cos\theta w \\
\dot{u} &= rv - qw - g\sin\theta + \frac{\rho V a^2 S}{2m}[C_X(\alpha) + C_{Xq}(\alpha)\frac{cq}{2Va} + C_{X\delta_e}\delta_e] + \\
&\qquad \frac{\rho S_{\mathrm{p}} C_{\mathrm{p}}}{2m}[(k_{\mathrm{m}}\delta_t)^2 - Va^2] \\
\dot{v} &= pw - ru + g\cos\theta\sin\theta + \frac{\rho V a^2 S}{2m}[C_{y0} + C_{y\beta}\beta + C_{y_p}\frac{bp}{2Va} + \\
&\qquad C_{yr}\frac{br}{2Va} + C_{y\delta_a}\delta_a + C_{y\delta r}\delta_r] \\
\dot{w} &= qu - pv + g\cos\theta\cos\phi + \frac{\rho V a^2 S}{2m}[C_Z(\alpha) + C_{Zq}(\alpha)\frac{cq}{2Va} + C_{Z\delta_e}\delta_e]
\end{aligned}
\tag{3.50}
$$

Rotational Equations

$$
\begin{aligned}
\dot{\phi} &= p + q\sin\phi\tan\theta + r\cos\phi\tan\theta \\
\dot{\theta} &= q\cos\phi - r\sin\phi \\
\dot{\psi} &= q\sin\phi\sec\theta + r\cos\phi\sec\theta \\
\dot{p} &= \Gamma_1 pq - \Gamma_2 qr + \frac{\rho V a^2 Sb}{2}[C_{P0} + C_{P\beta}\beta + C_{P_p}\frac{b_p}{2Va} + C_{P_r}\frac{b_r}{2Va} + C_{P\delta_a}\delta_a + C_{P\delta r}\delta_r] \\
\dot{q} &= \Gamma_5 pr - \Gamma_6(p^2 - r^2) + \frac{\rho V a^2 Sc}{2J_y}[C_{m0} + C_{m\alpha}\alpha + C_{mq}\frac{cq}{2Va} + C_{m\delta_e}\delta_e] \\
\dot{r} &= \Gamma_7 pq - \Gamma_1 qr + \frac{\rho V a^2 Sb}{2}[C_{r_0} + C_{r\beta}\beta + C_{r_p}\frac{bp}{2Va} + C_{r_r}\frac{br}{2Va} + C_{r_{\delta a}}\delta_a + C_{r\delta r}\delta_r]
\end{aligned}
\tag{3.51}
$$

Where

$$
\begin{aligned}
C_{P_0} &= \Gamma_3 C_{l0} + \Gamma_4 C_{n0}, & C_{P_\beta} &= \Gamma_3 C_{l\beta\beta} + \Gamma_4 C_{n_\beta} \\
C_{Pp} &= \Gamma_3 C_{lp} + \Gamma_4 C_{np}, & C_{Pr} &= \Gamma_3 C_{lr} + \Gamma_4 C_{nr} \\
C_{P\delta_a} &= \Gamma_3 C_{l\delta_a} + \Gamma_4 C_{n\delta_a}, & C_{P\delta_r} &= \Gamma_3 C_{l\delta_r} + \Gamma_4 C_{n\delta_r} \\
C_{r0} &= \Gamma_4 C_{l0} + \Gamma_8 C_{n0}, & C_{r\beta} &= \Gamma_4 C_{l\beta} + \Gamma_8 C_{n\beta} \\
C_{rp} &= \Gamma_4 C_{lp} + \Gamma_8 C_{np}, & C_{rr} &= \Gamma_4 C_{lr} + \Gamma_8 C_{nr} \\
C_{r\delta_a} &= \Gamma_4 C_{l\delta_a} + \Gamma_8 C_{n\delta_a}, & C_{r\delta_r} &= \Gamma_4 C_{l\delta_r} + \Gamma_8 C_{n\delta_r}
\end{aligned}
\tag{3.52}
$$

$$C_X(\alpha) = [C_{D0} + C_{D\alpha}\alpha]\cos\alpha + [C_{L0} + C_{L\alpha}\alpha]\sin\alpha, \qquad C_{Xq}(\alpha) = -C_{Dq}\cos\alpha + C_{Lq}\sin\alpha$$

$$C_{X\delta_e}(\alpha) = -C_{D\delta_e}\cos\alpha + C_{L\delta_e}\sin\alpha, \qquad C_{Zq}(\alpha) = -C_{Dq}\sin\alpha - C_{Lq}\cos\alpha$$

$$C_Z(\alpha) = -[C_{D0} + C_{D\alpha}\alpha]\sin\alpha - [C_{L0} + C_{L\alpha}\alpha]\cos\alpha, \qquad C_{Z\delta_e}(\alpha) = -C_{D\delta_e}\sin\alpha - C_{L\delta_e}\cos\alpha$$

The overall block diagram containing all the equations of motion of FWUAV is shown in figure 3.15. The sideslip angle (β), angle of attack (α), body angular rates (p, q, r), and

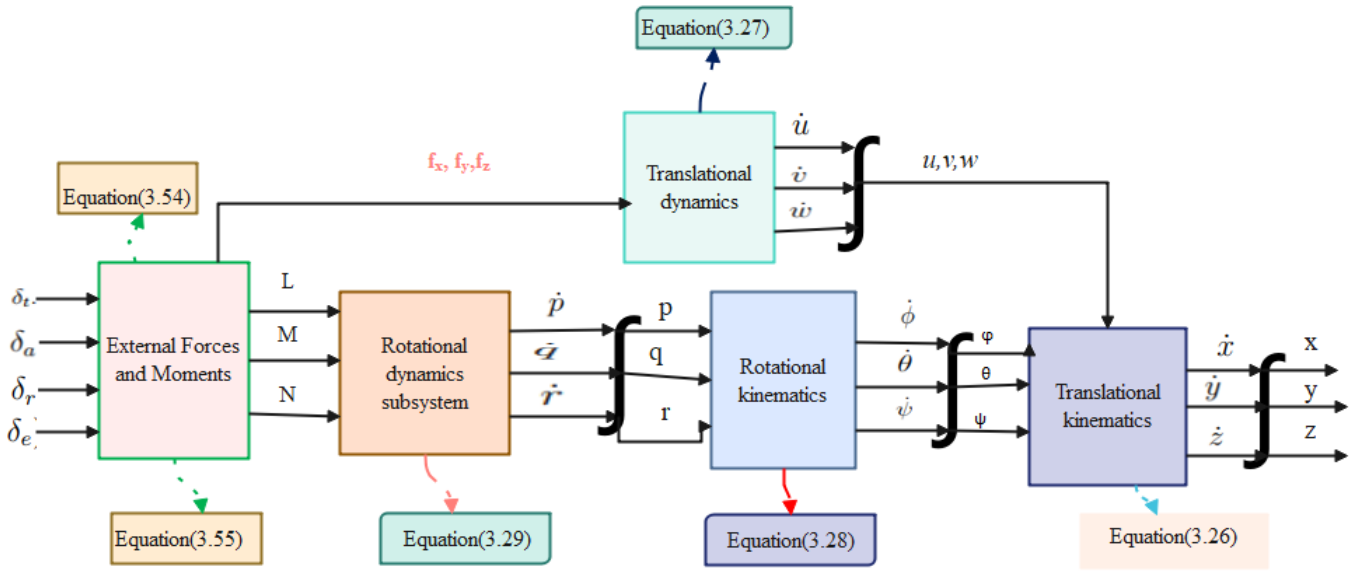

Figure 3.15: Overall Model of FWUAV

Table 3.2: Parameter Values[17]

Parameter symbol	Value	Unit	Description
m	13.5	kg	mass of FWUAV
J_x	0.8244	kgm^2	Moment of inertia around x-axis
J_y	1.135	kgm^2	Moment of inertia around y-axis
J_z	1.759	kgm^2	Moment of inertia around z-axis
J_{xz}	0.1204	kgm^2	Product of inertia about x-axis and z-axis
S	0.55	m^2	Wing area of FWUAV
b	2.8956	m	Wing span
c	0.18994	m	Mean aerodynamic chord
S_{prop}	0.2027	m^2	Area of the propeller
ρ	1.2682	kgm^2	Air density
K_{motor}	80		Motor constant

control surface deflections (δ_a, δ_e, δ_r) are associated with dimensionless aerodynamic coefficients that influence lateral and longitudinal forces as well as moments. To determine the specific values of these aerodynamic coefficients and their relationships to the mentioned variables, experimental methods such as wind tunnel testing or numerical techniques like Computational Fluid Dynamics (CFD) simulations are commonly employed. These meth-

ods help characterize the aerodynamic behavior of the FWUAV and provide the necessary coefficients for accurate modeling and analysis. In this study, a comprehensive review of the literature was undertaken to identify suitable parameter values and aerodynamic coefficients for the selected Fixed-Wing Unmanned Aerial Vehicle (FWUAV), as presented in table 3.2 and table 3.3. The obtained coefficients and values are essential inputs for modeling and analysis efforts. The given Parameter values and aerodynamic coefficients are taken from [17].

Table 3.3: Aerodynamic Coefficients Governing Forces and Moments[17]

Longitudinal coefficients	Value	Lateral coefficients	Value
C_{L_0}	0.28	C_{Y_0}	0
C_{D_0}	0.03	C_{l_0}	0
C_{m_0}	-0.02338	C_{n_0}	0
C_{L_α}	3.45	C_{Y_β}	-0.98
C_{D_α}	0.30	C_{l_β}	-0.12
C_{m_α}	-0.38	C_{n_β}	0.25
C_{L_q}	0	C_{Y_p}	0
C_{D_q}	0	C_{l_p}	-0.26
C_{m_q}	-3.6	C_{n_p}	0.022
$C_{L_{\delta_e}}$	-0.36	C_{Y_r}	0
$C_{D_{\delta_e}}$	0	C_{l_r}	0.14
$C_{m_{\delta_e}}$	-0.5	C_{n_r}	-0.35
C_{prop}	1	$C_{Y_{\delta_a}}$	0
$C_{n_{\delta_a}}$	0.06	$C_{l_{\delta_a}}$	0.08
$C_{l_{\delta_r}}$	0.105	$C_{Y_{\delta_r}}$	-0.17
		$C_{n_{\delta_r}}$	-0.032

3.4 Model Verification

MATLAB Simulink software is used to create a model that includes all of the kinematics and dynamics of a FWUAV. MATLAB Simulink is well-suited for FWUAV modeling because it provides a graphical interface for modeling, simulating, and evaluating dynamic systems. The FWUAV's equations of motion are a somewhat sophisticated set of 12-state non-linear, coupled, first-order ordinary differential equations, as illustrated in figure 3.15. Because the states in the equation of motion are coupled, changing one parameter affects practically all of them. A FWUAV executes translational motion along its body's x-axis (longitudinal axis) or y-axis (lateral axis). The UAV can produce forces and moments that allow it to move by altering the propulsion and control surfaces.

Adjusting the control surfaces, such as the ailerons for roll and the rudder for yaw, enables control over roll and yaw movements. These control inputs modify the aerodynamic forces and moments experienced by the UAV, leading to the necessary rotational movement and subsequent alteration in flight direction. It is important to recognize that the UAV's translational motion along the x and y axes can remain consistent even during roll and yaw maneuvers. Roll and yaw rotations primarily affect the UAV's orientation and heading as it progresses along its current trajectory within the body's reference frame.

To validate the model of FWUAV, simply apply the control surfaces $(\delta_t, \delta_a, \delta_e, \delta_r)$ and observe the effects of these control signals on the positions and attitudes of the FWUAV.The positions (x, y, z) are displayed on a single plot, while attitudes (ϕ, θ, ψ) are depicted together on another plot to facilitate comparison and observe variations in the system's states. Simulink block diagram for model validation is shown in appendix(B).

Responses

When the propeller of a FWUAV starts, it generates a thrust force that propels the aircraft forward at a high speed.The throttle control governs engine speed, which in turn affects propeller movement. In this case, let's assume a constant throttle deflection angle of $0.08rad$. As demonstrated by the FWUAV model, there is considerable interaction among the equations of motion in the model. The dynamics of an FWUAV are inherently interconnected, meaning that changing one parameter or input can have significant effects on multiple positions and orientations. This coupling arises due to the inter-dependencies between various forces and moments acting on the aircraft.

Adjusting control inputs like aileron deflection (δ_a), elevator deflection (δ_e), and rudder deflection (δ_r) influences the forces and moments experienced by the FWUAV. Modifications to these control inputs can result in changes to aerodynamic forces and moments, impacting the aircraft's motion across all axes. This is verified by the following results.

Case one: initially the three input control surface deflection angles are zero, the outputs still have non-zero characteristics. This is because the initial values and parameter settings in the model can contribute to these non-zero values as shown in figure 3.16 and figure 3.17. As shown from figure 3.16 , the FWUAV has traveled 392 meters in the forward direction (positive x-axis) and 533 meters in the vertical direction (positive z-axis) from its initial position. The y-axis, representing the lateral direction, remains unchanged at zero, suggesting that there is no sideways movement.

From figure 3.17,the roll angle and yaw angle of the FWUAV are both zero, indicating no roll

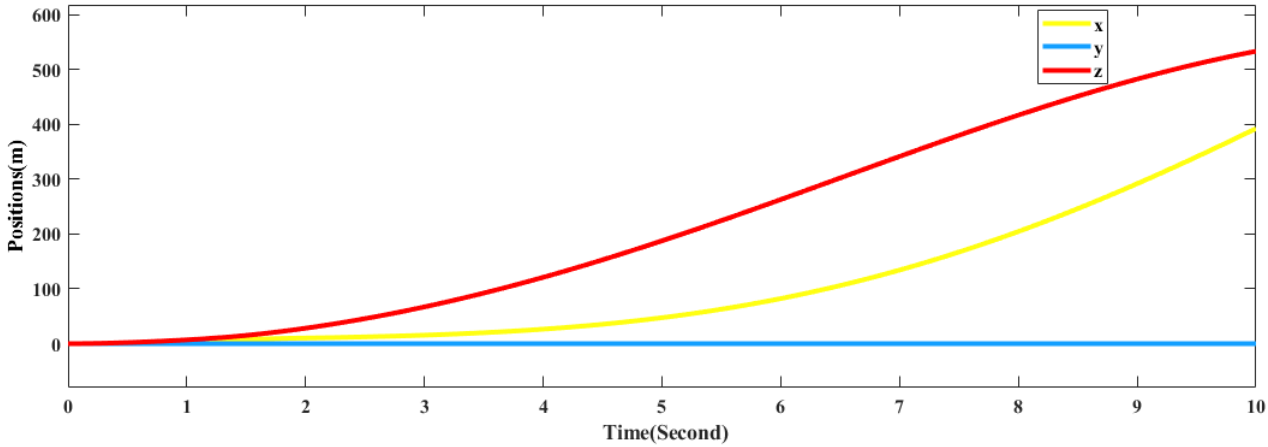

Figure 3.16: Responses of x,y,z Without Any Deflection of Control Surfaces

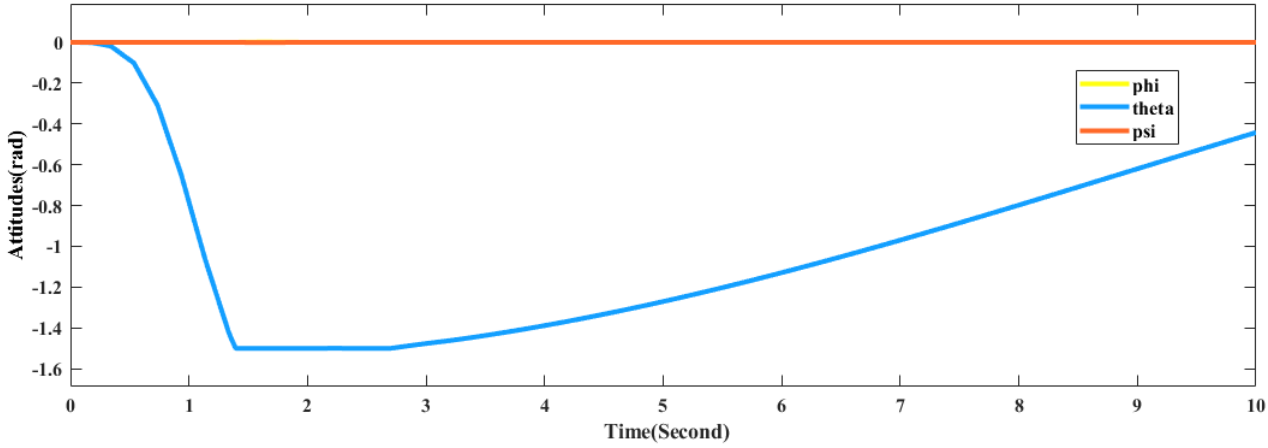

Figure 3.17: Responses of ϕ, θ, ψ Without Any Deflection of Control Surfaces

or yaw rotation. However, the pitch angle has a non-zero value that changes over time.At a certain time interval, the pitch angle is approximately -1.5 radians. This negative pitch angle suggests that the nose of the FWUAV is pointing downward relative to the horizontal plane. This corresponds to a pitch-down or descent motion. As time progresses, the pitch angle increases to approximately -0.45 radians. This indicates a reduction in the downward pitch, suggesting that the FWUAV starts to level off or pitch up slightly.

Case two: A constant elevator deflection of -0.2 radians was applied, with no deflection in the aileron and rudder. The response of the positions is depicted in figure 3.18.

The deflection of the elevator impacts the movement of the UAV along the x-axis (160m) and z-axis (36m), while the y-axis remains constant. This is attributed to the fact that the roll (ϕ) and yaw (ψ) angles remain at zero. The response of the attitude angles (orientation of FWUAV) in relation to the elevator deflection is depicted in figure 3.19. As indicated by the response, the roll and yaw angles remain at zero, while the pitch angle is altered. Based on the aforementioned findings, it can be inferred that the elevation or descent motion (pitch angle) as well as movement along the x-axis and z-axis of the FWUAV can be regulated by

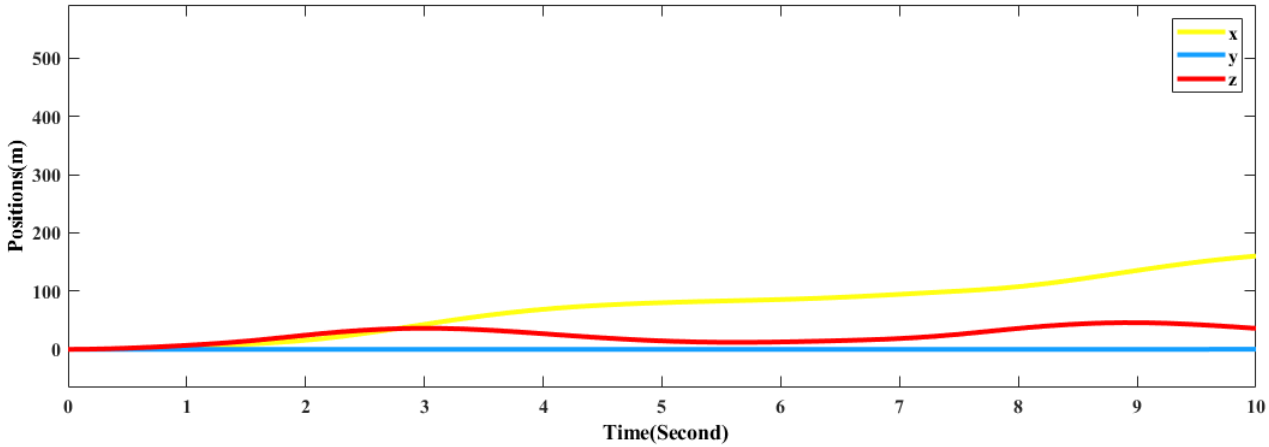

Figure 3.18: Responses of x,y,z with $\delta_e = -0.2ard$

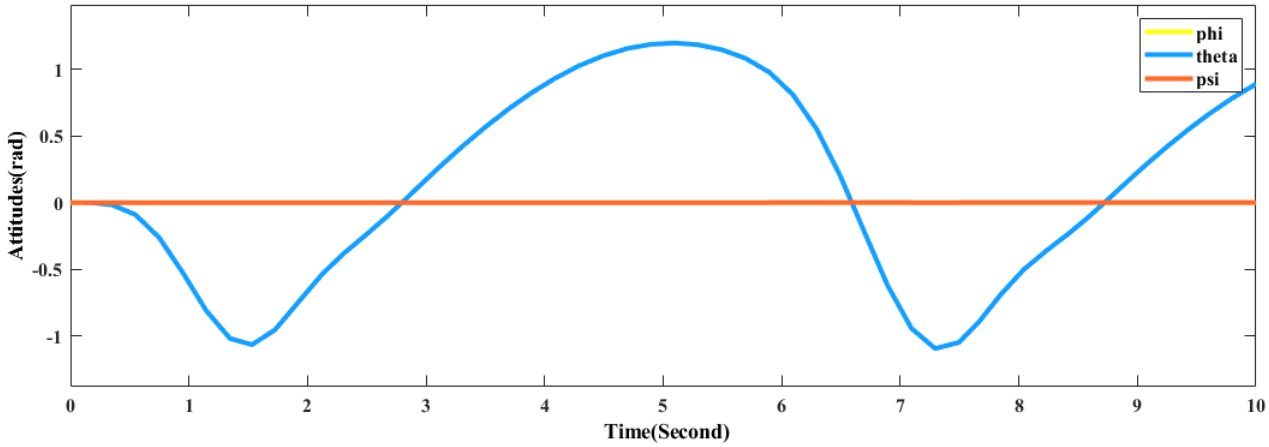

Figure 3.19: Responses of ϕ, θ, ψ with $\delta_e = -0.2ard$

employing the elevator control surface.

Case three: Deflecting the rudder control surface by 0.09 radians and the aileron control surface by 0.1 radians can lead to variations in the responses of the positions and orientations of the FWUAV. These responses are illustrated in figure 3.20 and figure 3.21 respectively.

As depicted in figure 3.20, the FWUAV moves along positive x-axis and z-axis(which are

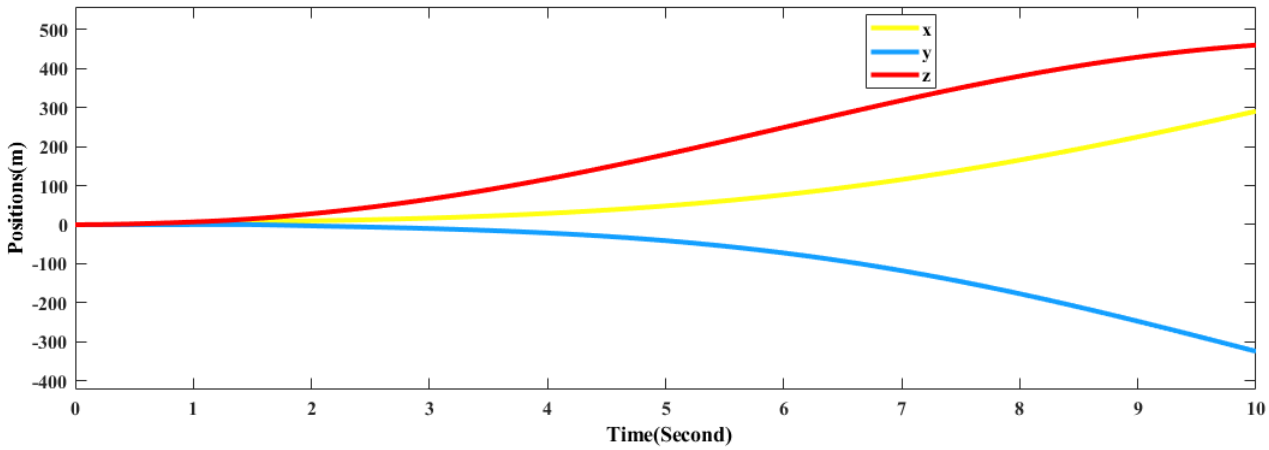

Figure 3.20: Responses of x,y,z with $\delta_a = 0.1rad$ and $\delta_r = 0.09rad$

almost similar to figure 3.17) and along negative y-axis, which is more affected by δ_a and

δ_r. This indicates that the movement of FWUAV along y-axis can be controlled by rudder and aileron control surfaces. From figure 3.21, it is shown that the pitch angle(θ) is similar

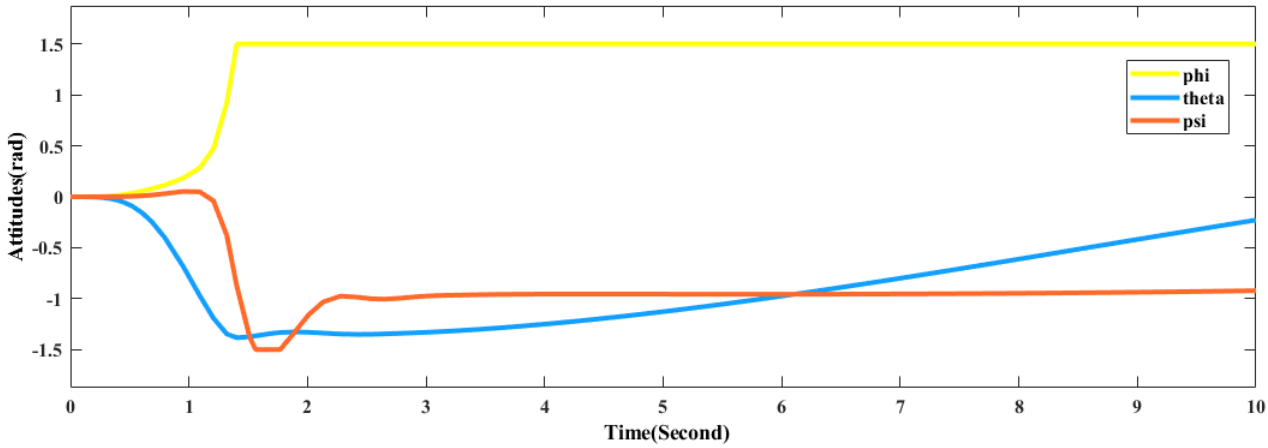

Figure 3.21: Responses of ϕ, θ, ψ with with $\delta_a = 0.1rad$ and $\delta_r = 0.09rad$

to θ in figure 3.18, but the roll an yaw angles are highly influenced by rudder and aileron control surface deflections. This suggests that the roll and yaw motions of the FWUAV can be regulated by the rudder and aileron control surfaces.

The three control surfaces of FWUAV controls the orientation of the UAV directly and its position indirectly.

Chapter 4

Controller Design

Based on mathematical models, this chapter discusses the controller design method for a FWUAV.The control systems theory employs deterministic control principles to manage the intricate dynamics of the FWUAV. FOSMC is considered a subset of variable structure systems theory. SMC represents a robust control methodology that aims to direct the system's state trajectory towards a predetermined manifold referred to as the sliding surface, thereby achieving the desired system behavior. It is well-known for its capacity to deal with system uncertainty as well as external disruptions. By introducing fractional calculus, FOSMC enhances the sliding mode control paradigm. Fractional calculus deals with non-integer order derivatives and integrals, allowing for greater flexibility in system modeling and control design. When compared to typical integer-order SMC, FOSMC can provide improved resilience, accuracy, and transient responsiveness by utilizing fractional-order differentiation and integration.

The third chapter presents the derivation of all kinematic and dynamic models for FWUAVs. These mathematical models are clearly still exceedingly sophisticated.Prior to constructing the controller, it is crucial to disentangle the mathematical models in order to streamline the control process. The Simulink block diagram containing FWUAV dynamics block, controller block and conversion block employed for analyzing the results of FWUAV presented in appendix(C).

4.1 Decoupled State Space Models of FWUAV

The objective of the decoupling process is to streamline the control of a standard FWUAV by concentrating on the primary state quantities and addressing the remaining degrees of freedom as uncertainties. Decoupling is undertaken to tackle the complexity associated with

simultaneously controlling and tracking all 12 degrees of freedom. Given that a FWUAV operates in a high-speed state, achieving precise control over all degrees of freedom might not be necessary or feasible. Thus, in this thesis, emphasis is placed on tracking and controlling six degrees of freedom. These six state variables consist of three attitude angles (ϕ, θ, ψ) and three positions (x, y, z). By selecting these six dominant state variables, the control system can prioritize and optimize the control efforts for these specific degrees of freedom. This approach simplifies the control process and allows for effective control and tracking of the UAV's key states and positions. [18]

The process of decoupling begins with the nonlinear mathematical model of the FWUAV, which is obtained from Chapter Three and can be represented by Equation 4.1.

$$\dot{x} = f(x, u) \tag{4.1}$$

Where

$x = (x, y, z, u, v, w, p, q, r, \phi, \theta, \psi)$

$u = (f_p, \delta_a, \delta_e, \delta_r) = (U_1, U_2, U_3, U_4)$

4.1.1 Decoupled State Space Model for Positions

To establish the state space representation of positions and develop a controller for the FWUAV, it is necessary to express the forces acting on the aircraft (including gravitational force, aerodynamic force, and propulsion force) in the inertial reference frame. Initially provided in Chapter 3 in the body reference frame, the equations for these forces require transformation into the inertial reference frame. This transformation entails considering the orientation of the aircraft, which is represented by the Euler angles (ϕ, θ, ψ), and applying appropriate rotations. Such representation facilitates the design and implementation of a controller capable of regulating the inertial position (x, y, z) and attitude (ϕ, θ, ψ) of the UAV. This controller accounts for uncertainties in aerodynamic forces and effectively utilizes controlled thrust force. The gravitational force in the inertial reference frame is expressed in equation (4.2).

$$f_g^v = \begin{bmatrix} 0 \\ 0 \\ mg \end{bmatrix} \tag{4.2}$$

The propulsion force can be expressed in inertial frame by multiplying equation (3.47) by

${R_b}^v$ as represented in equation (4.3)

$$f_p = \frac{1}{2}\rho S_p C_{prop} {R_b}^v \begin{bmatrix} (K_{motor}\delta_t)^2 - {V_a}^2 \\ 0 \\ 0 \end{bmatrix} \tag{4.3}$$

Letting the propulsion force in the x direction as U_1, that is:

$$f_p = {R_b}^v \begin{bmatrix} U_1 \\ 0 \\ 0 \end{bmatrix} = \begin{bmatrix} C_\theta C_\psi U_1 \\ C_\theta S_\psi U_1 \\ -S_\theta U_1 \end{bmatrix} \tag{4.4}$$

The aerodynamic forces are taken as a disturbance and can be expressed as

$$f_a = \begin{bmatrix} d_x \\ d_y \\ d_z \end{bmatrix} \tag{4.5}$$

Where, d_x, d_y, and d_z are aerodynamic forces in the x,y and z direction.

From Newton's second law of motion,

$$\Sigma F = ma \tag{4.6}$$

$$\begin{bmatrix} 0 \\ 0 \\ mg \end{bmatrix} + \begin{bmatrix} C_\theta C_\psi U_1 \\ C_\theta S_\psi U_1 \\ -S_\theta U_1 \end{bmatrix} + \begin{bmatrix} d_x \\ d_y \\ d_z \end{bmatrix} = m \begin{bmatrix} \ddot{x} \\ \ddot{y} \\ \ddot{z} \end{bmatrix} \tag{4.7}$$

Therefore, the state space representation of positions of FWUAV becomes:

$$\begin{aligned} \ddot{x} &= \frac{1}{m} C_\theta C_\psi U_1 + \frac{1}{m} d_x \\ \ddot{y} &= \frac{1}{m} C_\theta S_\psi U_1 + \frac{1}{m} d_y \\ \ddot{z} &= -\frac{1}{m} S_\theta U_1 + \frac{1}{m} d_z \end{aligned} \tag{4.8}$$

These equations can be written in terms of virtual control signals of positions as:

$$\begin{aligned} \ddot{x} &= \frac{1}{m}(U_x + d_x) \\ \ddot{y} &= \frac{1}{m}(U_y + d_y) \\ \ddot{z} &= \frac{1}{m}(U_z + d_z) \end{aligned} \tag{4.9}$$

Where, U_x ,U_y , U_z are virtual control signals for positions and can defined as:

$$\begin{aligned} U_x &= C_\theta C_\psi U_1 \\ U_y &= C_\theta S_\psi U_1 \\ U_z &= -S_\theta U_1 + mg \end{aligned} \tag{4.10}$$

4.1.2 Decoupled State Space Model for Attitude Angles

It is essential to derive the state-space relationships between these angles and the input signals. There are three input signals associated with the attitude angle: the aileron (U_2), the elevator command signal (U_3), and the rudder (U_4). To establish the necessary state-space functions, additional treatment of the kinematics and dynamics models is required.

4.1.2.1 Roll Angle (ϕ)

From equation (3.51), $\dot{\phi}$ is given by the equation:

$$\dot{\phi} = p + qsin\phi tan\theta + rcos\phi tan\theta$$

The parameter p predominantly influences variations in ϕ, hence other parameters can be regarded as uncertainties in the system.

$$\dot{\phi} = p + d_{\phi 1} \tag{4.11}$$

where

$$d_{\phi 1} = qsin\phi tan\theta + rcos\phi tan\theta \tag{4.12}$$

is the external disturbance of this system. Take the derivative of both sides of equation (4.11) with respect to t becomes:

$$\ddot{\phi} = \dot{p} + \dot{d}_{\phi 1} \tag{4.13}$$

Substituting $\dot{p}$ from equation (3.51) in toequation (4.13), and since $\dot{d}_{\phi 1}$ is a very small value, it is eliminated.

$$\ddot{\phi} = \Gamma_1 pq - \Gamma_2 qr + \frac{\rho V a^2 Sb}{2}[C_{P0} + C_{P\beta}\beta + C_{Pp}\frac{bp}{2Va} + C_{Pr}\frac{br}{2Va} + C_{P\delta_a}U_2 + C_{P\delta r}U_4] \quad (4.14)$$

Let d_ϕ is the total external disturbance and equation (4.14) can be rewritten as equation (4.15)

$$\ddot{\phi} = a_\phi \dot{\phi} + b_\phi U_2 + d_\phi \quad (4.15)$$

Where

$$\begin{aligned} a_\phi &= \frac{1}{4}\rho V_a S b^2 C_{Pp} \\ b_\phi &= \frac{1}{2}\rho V_a^2 S b C_{P\delta_a} = \frac{1}{2}\rho V_a^2 S b \Gamma_3 C_{l\delta_a} \\ d_\phi &= \Gamma_1 pq - \Gamma_2 qr + \frac{\rho V a^2 Sb}{2}[C_{P0} + C_{P\beta}\beta + C_{Pr}\frac{br}{2Va} + C_{P\delta r}U_4] \end{aligned} \quad (4.16)$$

4.1.2.2 Pitch Angle (θ)

From equation (3.51), $\dot{\theta}$ is given by the equation:

$$\dot{\theta} = qcos\phi - rsin\phi$$

Similarly, given that the angle ϕ has a small value, its effect on the system can be considered as an uncertainty. Meanwhile, the parameter q primarily induces changes in θ . Hence, the function of $\dot{\theta}$ can be reformulated as:

$$\dot{\theta} = q + (cos\phi - 1)q - r\sin\phi\ \dot{\theta} \quad = q + d_{\theta 1} \quad (4.17)$$

where $d_{\theta 1}$ represents the external disturbance of this system, defined as:

$$d_{\theta 1} = (cos\phi - 1)q - r\sin\phi \quad (4.18)$$

Taking the derivative of equation (4.17) on both sides with respect to t yields equation (4.19).

$$\ddot{\theta} = \dot{q} + \dot{d}_{\theta 1} \quad (4.19)$$

Substituting $\dot{q}$ from equation (3.51) in to equation (4.19) and since $\dot{d}_{\theta 1}$ is a very small value, it is eliminated.

$$\ddot{\theta} = \dot{q} = \Gamma_5 pr - \Gamma_6(p^2 - r^2) + \frac{\rho V a^2 Sc}{2J_y}[C_{m0} + C_{m\alpha}\alpha + C_{mq}\frac{cq}{2Va} + C_{m\delta_e}\delta_e] \tag{4.20}$$

Let d_θ is the total external disturbance and $\ddot{\theta}$ can be written as equation (4.21):

$$\ddot{\theta} = a_\theta \dot{\theta} + b_\theta U_3 + d_\theta \tag{4.21}$$

Where

$$\begin{aligned} a_\theta &= \frac{1}{4}\rho V_a S c^2 C_{mq} \\ b_\theta &= \frac{1}{2}\rho V_a^2 S c C_{m\delta_e} \\ d_\theta &= \Gamma_5 pr - \Gamma_6(p^2 - r^2) + \frac{\rho V a^2 Sc}{2J_y}[C_{m0} + C_{m\alpha}\alpha] \end{aligned} \tag{4.22}$$

4.1.2.3 Yaw Angle (ψ)

From equation (3.51), $\dot{\psi}$ is given by the equation:

$$\dot{\psi} = qsin\phi sec\theta + rcos\phi sec\theta \tag{4.23}$$

During drone flight, the angles ϕ and θ typically remain extremely small. The variation in angle ψ primarily correlates with r. Hence, when examining ψ, certain assumptions can be made: $sin\phi \approx 0$, $sec\theta \approx 1$, and $cos\phi \approx 1$. These assumptions represent inherent uncertainties within the system. Consequently, the equation can be reformulated as shown in equation (4.24).

$$\dot{\psi} = r + (cos\phi sec\theta - 1)r + qsin\phi sec\theta \tag{4.24}$$

Define $d_{\psi 1}$ is the external disturbance.

$$d_{\psi 1} = (cos\phi sec\theta - 1)r + qsin\phi sec\theta \tag{4.25}$$

Therefore,

$$\dot{\psi} = r + d_{\psi 1} \tag{4.26}$$

Differentiate both sides of equation (4.26) with respect to t:

$$\ddot{\psi} = \dot{r} + \dot{d}_{\psi 1} \tag{4.27}$$

Substituting $\dot{r}$ from equation (3.51) in to equation (4.27) and since $\dot{d}_{\psi 1}$ is a very small value, it is eliminated.

$$\ddot{\psi} = \Gamma_7 pq - \Gamma_1 qr + \frac{\rho V a^2 Sb}{2}[C_{r_0} + C_{r\beta}\beta + C_{r_p}\frac{bp}{2Va} + C_{r_r}\frac{br}{2Va} + C_{r_{\delta a}}\delta_a + C_{r_\delta r}\delta_r] \tag{4.28}$$

Let d_ψ is the total external disturbance and $\ddot{\psi}$ can be written as:

$$\ddot{\psi} = a_\psi \dot{\psi} + b_\psi U_4 + d_\psi \tag{4.29}$$

Where

$$\begin{aligned} a_\psi &= \frac{1}{4}\rho V_a Sb^2 C_{rr} = \frac{1}{4}\rho V_a Sb^2 \Gamma_8 C_{nr} \\ b_\psi &= \frac{1}{2}\rho V_a^2 Sb C_{r\delta_a} = \frac{1}{2}\rho V_a^2 Sb \Gamma_8 C_{n\delta_r} \\ d_\psi &= \Gamma_7 pq - \Gamma_1 qr + \frac{\rho V a^2 Sb}{2}[C_{r0} + C_{r\beta}\beta + C_{r_p}\frac{bp}{2Va} + C_{r_{\delta a}}U_2] \end{aligned} \tag{4.30}$$

Hence, the state-space representation for the control systems governing position and attitude angles can be expressed as follows:

$$\begin{aligned} \dot{x}_1 &= x_2 \\ \dot{x}_2 &= \frac{1}{m}(U_x + d_x) \\ \dot{x}_3 &= x_4 \\ \dot{x}_4 &= \frac{1}{m}(U_y + d_y) \\ \dot{x}_5 &= x_6 \\ \dot{x}_6 &= \frac{1}{m}(U_z + d_z) \\ \dot{x}_7 &= x_8 \\ \dot{x}_8 &= a_\phi\ x_8 + b_\phi U_2 + d_\phi \\ \dot{x}_9 &= x_{10} \\ \dot{x}_{10} &= a_\theta x_{10} + b_\theta U_3 + d_\theta \\ \dot{x}_{11} &= x_{12} \\ \dot{x}_{12} &= a_\psi x_{12} + b_\psi U_4 + d_\psi \end{aligned} \tag{4.31}$$

4.2 Introduction to Fractional Order Calculus(FOC)

Fractional calculus is indeed a branch of mathematical analysis that extends the concepts of integrals and derivatives to non-integer or fractional orders. It explores the possibilities of differentiating and integrating functions with arbitrary orders, allowing for a more comprehensive understanding of mathematical operations. In the context of control systems, fractional calculus has gained attention for its potential in improving controller performance and sensitivity. Fractional-order controllers (FOCs) utilize fractional differo-integral operators to achieve enhanced control capabilities. The fractional differo-integral operator ${}_{\alpha}D_t^{\beta} f(t)$ represents the fractional calculus operation applied to a function f(t). Here, α and β represent the order of differentiation and integration, respectively. The operator ${}_{\alpha}D_t^{\beta}$ combines both differentiation and integration of fractional orders, providing a more flexible and versatile tool for system analysis and design. By incorporating fractional calculus into control systems, FOCs can exhibit improved sensitivity, adaptability, and response characteristics compared to traditional integer-order controllers. The ability to adjust the differentiation and integration orders independently allows for fine-tuning the controller's behavior to meet specific control objectives. [19].The continuous differo-integral operator is given by the following:

$$ {}_{\alpha}D_t^{\beta} f(t) = \begin{cases} \frac{d^{\beta}}{dt^{\beta}} & R(\beta) > 0 \\ 1 & R(\beta) = 0 \\ \int_{\alpha}^{t} d\tau^{-\beta} & R(\beta) < 0 \end{cases} \tag{4.32} $$

Here, D stands for the fractional calculus operator, β signifies the fractional order, α and t represent the operational limits, and $R(\beta)$ denotes the real part of β. In the literature,there are different definitions of the fractional differ-integral operator. But the most commonly used definitions of fractional order derivatives are:

The Riemann-Liouville (RL) definition:

$$ {}_{\alpha}D_t^{\beta} f(t) = \frac{1}{\Gamma(m-\beta)} (\frac{d}{dt})^m \int_{\alpha}^{t} \frac{f(\tau)}{(t-\tau)^{\beta} - m + 1} d\tau \tag{4.33} $$

The Caputos definition:

$$ {}_{\alpha}D_t^{\beta} f(t) = \frac{1}{\Gamma(m-\beta)} \int_{\alpha}^{t} \frac{f(\tau)}{(t-\tau)^{\beta} - m + 1} d\tau \tag{4.34} $$

In the context of these fractional calculus expressions, the constraint, $m-1<\alpha<m$, holds, where m represents the smallest integer greater than α. The function (.) refers to Euler's gamma function, which is widely recognized and defined as follows:

$$\Gamma(x)=\int_0^\infty e^{-t}t^{x-1}dt, \qquad x>0 \tag{4.35}$$

In this thesis,the controller utilizes the sliding surface approach, and fractional-order modeling and control are implemented using the FOMCON toolbox. The FOMCON toolbox is a software package designed to facilitate the incorporation of fractional-order calculus tools into MATLAB, a widely used platform for numerical computation and simulation. By using the FOMCON toolbox, this thesis leverages the capabilities of fractional-order calculus for modeling and control purposes. The toolbox provides a set of functions and algorithms specifically tailored for fractional-order systems, allowing researchers and practitioners to work with fractional-order differential equations, fractional-order transfer functions.

4.3 FOSMC Design

FOSMC is indeed considered a subclass of variable structure system theory. It incorporates fractional order calculus into the sliding manifold, resulting in improved performance compared to conventional SMC in terms of tracking accuracy, speed of response, chattering, and disturbance rejection. One of the key advantages of FOSMC is its ability to ensure the system's states slide along the sliding surface.This characteristic splits the motion of the controlled system's states into two phases, as illustrated in figure 4.1: the reaching mode and the sliding mode. [20].

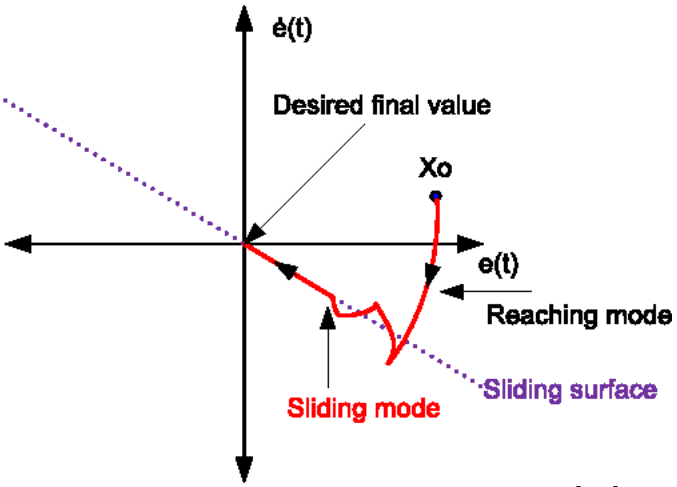

Figure 4.1: FOSMC's Sliding Surfaces[26]

The reaching Mode: It is also called the first phase of the surface.The system is moved from any beginning location to the sliding surface during this non-robust phase. This work is done by the discontinuous controller given by equation (4.36). The reaching phase can be decreased by increasing the FOSMC's discontinuous control gain k, although this results in significant chattering. A number of solutions have been proposed to deal with this problem, such as using a qausi function to approximate the signum function.

$$U_{dis}(t) = ksign(S(t)) \tag{4.36}$$

The sliding Mode: It is also called the second phase of the surface. In this phase, disturbances, parameter change, and unmodeled dynamics have no impact on the trajectories. Because of this characteristic, the FOSMC is a reliable control mechanism. When the initial value of a system is far from the sliding surface, it leads to prolonged reaching time. Consequently, control performance deteriorates significantly, and ensuring phase robustness becomes uncertain. This necessitates the introduction of a sliding phase. By setting the derivative of the sliding surface to zero ($\dot{S} = 0$), equivalent control rules can be derived and tasked with executing those operations. The combined action of the equivalent controller and the discontinuous controller constitutes the total control law.

$$U = U_{equ} + U_{dis} \tag{4.37}$$

4.3.1 Overall Block Diagram of the System

From the simulation results of the model verification it can be seen the influence of the control signals (deflection angles) on the positions and attitude angles of FWUAV. It can be deduced that the positions(x, y, z) and attitude angles(ϕ, θ, ψ) of FWUAV can be controlled by using the control signals. Virtual control signals which are derived using derived from the desired trajectory or position error are used as position control signals. There are two loops in the control strategy. The attitude angles such as roll angle, pitch angle, and yaw angle are all part of the inner control loop. The second loop is the outer control loop, responsible for managing position or displacement, encompassing movement in both higher and lower, front and back, as well as left and right directions. The control system inputs are the desired values of positions which are x_d, y_d, z_d and the desired roll angle ϕ_d, cause the relevant motions, and subsequently the associated displacements, to be made by the aircraft. The block diagram

of the whole control system is displayed in figure 4.2

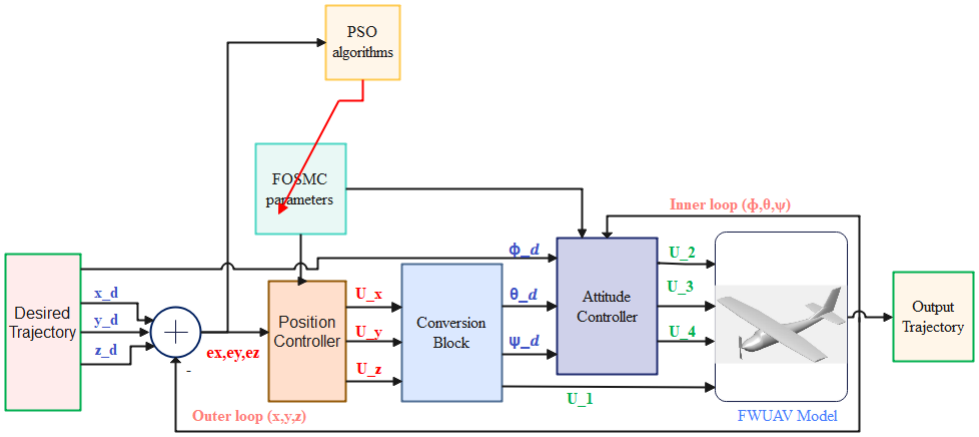

Figure 4.2: Overall Control System Block Diagram

4.3.2 Outer Control Loop FOSMC Design

In the case of an underactuated FWUAV, where it is not feasible to directly control all 6-DOF, an outer control loop is employed to indirectly control the position and altitude of the aircraft. This outer control loop generates virtual control signals, namely U_x, U_y, and U_z, which are used to calculate the desired pitch angle (θ_d), yaw angle (ψ_d) and total thrust force (U_1). The virtual control signals, U_x, U_y and U_z, represent the forces in the x, y, and z directions respectively. These signals are typically derived from a higher-level control system that aims to achieve specific position and altitude objectives for the FWUAV. The desired pitch angle (θ_d) and yaw angle (ψ_d) are then determined based on these virtual control signals. The specific relationship between the virtual control signals and the desired angles would depend on the aircraft's dynamics and control strategy employed. Once the desired pitch and yaw angles are obtained, they can be used in an inner control loop, along with other control inputs such as the aileron signal (U_2), elevator command signal (U_3), and rudder signal (U_4), to control the roll, pitch, and yaw motions of the FWUAV. Before starting the controller design, let's derive position error as:

$$\begin{bmatrix} e_x \\ e_y \\ e_z \end{bmatrix} = \begin{bmatrix} x_d - x \\ y_d - y \\ z_d - z \end{bmatrix}, \begin{bmatrix} \dot{e}_x \\ \dot{e}_y \\ \dot{e}_z \end{bmatrix} = \begin{bmatrix} \dot{x}_d - \dot{x} \\ \dot{y}_d - \dot{y} \\ \dot{z}_d - \dot{z} \end{bmatrix}, \begin{bmatrix} \ddot{e}_x \\ \ddot{e}_y \\ \ddot{e}_z \end{bmatrix} = \begin{bmatrix} \ddot{x}_d - \ddot{x} \\ \ddot{y}_d - \ddot{y} \\ \ddot{z}_d - \ddot{z} \end{bmatrix} \tag{4.38}$$

To apply FOSMC to FWUAV dynamics, sliding surfaces need to be specified for each of the x, y, and z directions. The sliding surfaces are critical in establishing stable and accurate control of the FWUAV. The sliding surfaces are typically defined as the desired states or

trajectories that the system's states should track. In the context of FOSMC, the sliding surfaces are designed to ensure that the system's states converge to and remain on these surfaces during the sliding mode. The control input or action is then designed to minimize the sliding surfaces and enforce the sliding mode dynamics. The sliding surfaces are defined as follows:

$$\begin{aligned} S_x &= c_x e_x + D^{\beta_x}\dot{e}_x = c_x e_x + D^{\beta_x+1}e_x \\ S_y &= c_y e_y + D^{\beta_y}\dot{e}_y = c_y e_y + D^{\beta_y+1}e_y \\ S_z &= c_z e_z + D^{\beta_z}\dot{e}_z = c_z e_z + D^{\beta_z+1}e_z \end{aligned} \tag{4.39}$$

Where, D^{β_x} is a fractional order derivative, which is found in FOMCON toolbox in matlab simulink. Control law can be computed after the sliding surface has been selected. The system must converge to the sliding surface according to this control law. It has to stay still once it hits the sliding surface. To facilitate position tracking, a FOSMC is formulated as follows:.

Designing a FOSMC U_x related to x position

Using Reaching Law, The equivalent controller can be determined by making, $\dot{S}_i = 0$ where, $i = x, y, z$

$$\begin{aligned} \dot{S}_x &= c_x\dot{e}_x + D^{\beta_x}\ddot{e}_x = 0 \\ &= c_x\dot{e}_x + D^{\beta_x+2}e_x = 0 \\ &= c_x\dot{e}_x + D^{\beta_x}(\ddot{x}_d - \ddot{x}) = 0 \end{aligned} \tag{4.40}$$

Substituting $\ddot{x}$ in equation (4.9) in to equation (4.40).

$$\begin{aligned} c_x\dot{e}_x + D^{\beta_x}(\ddot{x}_d - \frac{1}{m}(U_x + d_x)) = 0 \\ c_x\dot{e}_x + D^{\beta_x}\ddot{x}_d - \frac{D^{\beta_x}}{m}(U_x + d_x) = 0 \end{aligned} \tag{4.41}$$

Solving for U_x from equation (4.41) to get the equivalent controller.

$$\begin{aligned} U_{xeq} &= mc_x D^{-\beta_x}\dot{e}_x + m\ddot{x}_d - d_x \\ &= mc_x D^{-\beta_x+1}e_x + m\ddot{x}_d - d_x \end{aligned} \tag{4.42}$$

The combination of the continuous control signal described in equation (4.42) and the discontinuous control signal outlined in equation (4.36) constitutes the complete virtual controller

law along the x-axis, as presented in equation (4.43):

$$\begin{aligned} U_x &= U_{xeq} + U_{dis} \\ U_x &= mc_x D^{-\beta_x+1} e_x + m\ddot{x}_d - d_x + k_x sign(S(x)) \end{aligned} \tag{4.43}$$

Where, the equivalent and discontinuous control gains are denoted by c_x and k_x, respectively and β_x between 0 and 1 is the fractional order parameter.

Using Lyapunove for the condition of (k_x): The Lyapunov function, denoted as V_x and defined over the system state variables, is a positive scalar function, expressed as $V_x > 0$. It satisfies the condition that the time derivative $\dot{V}_x$ is negative, i.e., $\dot{V}_x < 0$. The selection of the Lyapunov function is based on the expression provided in equation (4.44)

$$V_x = \frac{1}{2} S_x^2 \tag{4.44}$$

To determine the minimum values of the discontinuous controller gains utilizing the signum function, we establish the proof outlined in equation (4.45)

$$\begin{aligned} \dot{V}_x &= S_x \dot{S}_x < 0 \\ &= S_x(C_x \dot{e}_x + D^{\beta_x}(\ddot{x}_d - \ddot{x})) < 0 \\ &= S_x(c_x \dot{e}_x + D^{\beta_x}(\ddot{x}_d - \frac{1}{m}(U_x + d_x))) < 0 \\ &= S_x(c_x \dot{e}_x + D^{\beta_x}\ddot{x}_d - \frac{D^{\beta_x}}{m} U_x - \frac{D^{\beta_x}}{m} d_x < 0 \\ &= S_x(c_x \dot{e}_x + D^{\beta_x}\ddot{x}_d - \frac{D^{\beta_x}}{m}(mC_x D^{-\beta_x}\dot{e}_x + m\ddot{x}_d - d_x + k_x sign(S(x)) - \\ &\qquad \frac{D^{\beta_x}}{m} d_x < 0 \\ &= S_x(-k_x sign(S(x))) < 0 \\ &= -k_x |(S(x))| < 0 \end{aligned} \tag{4.45}$$

k_x must be greater than zero for the Lyapunov function of equation (4.45)to be valid.

FOSMC design for y position virtual control variable U_y

Utilize a similar methodology on the x-axis to calculate the virtual controls along the y and z axes, aiming to minimize the error and bring it close to zero.

Using Reaching Law, The equivalent controller can be determined by making, $\dot{S}_y = 0$

$$\begin{aligned} \dot{S}_y &= c_y \dot{e}_y + D^{\beta_y} \ddot{e}_y = 0 \\ &= c_y \dot{e}_y + D^{\beta_y + 2} e_y = 0 \\ &= c_y \dot{e}_y + D^{\beta_y} (\ddot{y}_d - \ddot{y}) = 0 \end{aligned} \tag{4.46}$$

Substituting $\ddot{y}$ in equation (4.9) in to equation (4.46).

$$\begin{aligned} C_y \dot{e}_y + D^{\beta_y} (\ddot{y}_d - \frac{1}{m}(U_y + d_y)) = 0 \\ C_y \dot{e}_y + D^{\beta_y} \ddot{y}_d - \frac{D^{\beta_y}}{m}(U_y + d_y) = 0 \end{aligned} \tag{4.47}$$

Solving for U_y from equation (4.47) to get the equivalent controller.

$$\begin{aligned} U_{yeq} &= m c_y D^{-\beta_y} \dot{e}_y + m \ddot{y}_d - d_y \\ &= m c_y D^{-\beta_y + 1} e_y + m \ddot{y}_d - d_y \end{aligned} \tag{4.48}$$

The virtual controller along the y-axis results from the addition of the continuous and discontinuous control components.

$$\begin{aligned} U_y &= U_{yeq} + U_{dis} \\ U_y &= m c_y D^{-\beta_y + 1} e_y + m \ddot{y}_d - d_y + k_y sign(S(y)) \end{aligned} \tag{4.49}$$

Where, the equivalent and discontinuous control gains are denoted by c_y and k_y, respectively and β_y between 0 and 1 is the fractional order parameter.

Using Lyapunove for the condition of (k_y): The Lyapunov function, denoted as V_y, represents a positive scalar function dependent on the system state variables such that $V_y > 0$. Moreover, it fulfills the condition where the time derivative $\dot{V}_y$ is negative, expressed as $\dot{V}_y < 0$. The selection of the Lyapunov function is based on the equation provided as equation (4.50)

$$V_y = \frac{1}{2} S_y^2 \tag{4.50}$$

To obtain the minimum value of the discontinuous controller gains employing the signum function, we seek to provide a proof:

$$\begin{aligned}
\dot{V}_y &= S_y\dot{S}_y < 0 \\
&= S_y(c_y\dot{e}_y + D^{\beta_y}(\ddot{y}_d - \ddot{y})) < 0 \\
&= S_y(c_y\dot{e}_y + D^{\beta_y}(\ddot{y}_d - \frac{1}{m}(U_y + d_y))) < 0 \\
&= S_y(c_y\dot{e}_y + D^{\beta_y}\ddot{y}_d - \frac{D^{\beta_y}}{m}U_y - \frac{D^{\beta_y}}{m}d_y < 0 \\
&= S_y(c_y\dot{e}_y + D^{\beta_y}\ddot{y}_d - \frac{D^{\beta_y}}{m}(mc_yD^{-\beta_y}\dot{e}_y + m\ddot{y}_d - d_y + \\
&\qquad\qquad k_y sign(S(y)) - \frac{D^{\beta_y}}{m}d_y < 0 \\
&= S_y(-k_y sign(S(y))) < 0 \\
&= -k_y|(S(y))| < 0
\end{aligned} \tag{4.51}$$

k_y must be greater than zero for the Lyapunov function of equation (4.51) to be valid.

FOSMC design for z position virtual control variable U_z

Using Reaching Law, The equivalent controller can be determined by making, $\dot{S}_z = 0$

$$\begin{aligned}
\dot{S}_z &= c_z\dot{e}_z + D^{\beta_z}\ddot{e}_z = 0 \\
&= c_z\dot{e}_z + D^{\beta_z+2}e_z = 0 \\
&= c_z\dot{e}_z + D^{\beta_z}(\ddot{z}_d - \ddot{z}) = 0
\end{aligned} \tag{4.52}$$

Substituting $\ddot{z}$ from equation (4.9) in to equation (4.52).

$$\begin{aligned}
c_z\dot{e}_z + D^{\beta_z}(\ddot{z}_d - \frac{1}{m}(U_z + d_z)) = 0 \\
c_z\dot{e}_z + D^{\beta_z}\ddot{y}_z - \frac{D^{\beta_y}}{m}(U_z + d_z) = 0
\end{aligned} \tag{4.53}$$

Solving for U_z from equation (4.53) to get the equivalent controller.

$$\begin{aligned}
U_{zeq} &= mc_zD^{-\beta_z}\dot{e}_z + m\ddot{z}_d - d_z \\
U_{zeq} &= mc_zD^{-\beta_z+1}e_z + m\ddot{z}_d - d_z
\end{aligned} \tag{4.54}$$

The combination of the continuous control signal presented in equation (4.54) and the discontinuous control signal described in equation (4.36) constitutes the complete virtual controller

law along the z-axis, as specified in equation (4.55):

$$\begin{aligned} U_z &= U_{zeq} + U_{dis} \\ U_z &= mc_z D^{-\beta_z+1} e_z + m\ddot{z}_d - d_z + k_z sign(S(z)) \end{aligned} \tag{4.55}$$

Where, the equivalent and discontinuous control gains are denoted by c_z and k_z, respectively and β_z between 0 and 1 is the fractional order parameter.

Using Lyapunove for the condition of (k_z): The Lyapunov function, denoted as V_z, represents a positive scalar function dependent on the system state variables, ensuring that $V_z > 0$. Additionally, it satisfies the condition where the time derivative $\dot{V}_z$ is negative, indicated as $\dot{V}_z < 0$. The selection of the Lyapunov function is guided by the equation provided in equation (4.56)

$$V_z = \frac{1}{2} S_z^2 \tag{4.56}$$

To determine the minimum value of the discontinuous controller gains utilizing the signum function, let us provide a proof.

$$\begin{aligned} \dot{V}_z &= S_z \dot{S}_z < 0 \\ &= S_z(c_z \dot{e}_z + D^{\beta_z}(\ddot{z}_d - \ddot{z})) < 0 \\ &= S_z(c_z \dot{e}_z + D^{\beta_z}(\ddot{z}_d - \frac{1}{m}(U_z + d_z))) < 0 \\ &= S_z(c_z \dot{e}_z + D^{\beta_z}\ddot{z}_d - \frac{D^{\beta_z}}{m} U_z - \frac{D^{\beta_z}}{m} d_z < 0 \\ &= S_y(c_z \dot{e}_z + D^{\beta_z}\ddot{z}_d - \frac{D^{\beta_z}}{m}(mC_z D^{-\beta_z}\dot{e}_z + m\ddot{z}_d - d_z + \\ &\qquad\qquad k_z sign(S(z)) - \frac{D^{\beta_z}}{m} d_z < 0 \\ &= S_z(-k_z sign(S(z))) < 0 \\ &= -k_z |(S(z))| < 0 \end{aligned} \tag{4.57}$$

k_z must be greater than zero for the Lyapunov function of equation (4.57) to be valid.

To control the output of the underactuated component of the FWUAV individually, the variables θ, ψ, and U_1 can be utilized to establish three virtual control inputs. The virtual control inputs are applicable in the outer loop controller, particularly the position controller, for tracking a predetermined trajectory across the x, y, and z axes within three-dimensional space. The parameters θ and ψ denote the pitch and yaw angles of the FWUAV, respectively, serving as vital elements in governing the aircraft's orientation and heading.

Through adjustments to θ and θ, the FWUAV can effectively regulate its pitch and yaw movements to attain the intended trajectory.

The variable U_1 represents a virtual control input that can be used to control the overall thrust or vertical velocity of the FWUAV. By adjusting U_1, the FWUAV can control its altitude or vertical motion along the z-axis. These virtual control inputs, derived from the variables θ, ψ, and U_1, are then used as inputs to the position controller in the outer loop. The position controller generates the necessary control signals, such as U_x, U_y, and U_z, to indirectly control the position and altitude of the FWUAV along the x, y, and z axes. By establishing these virtual control inputs and incorporating them into the control system, the FWUAV can follow a specified trajectory and achieve precise control of its position and altitude, even with the underactuated nature of the system. These virtual control signals are given by equations 4.54

$$\begin{aligned} U_x &= mc_x D^{-\beta_x+1} e_x + m\ddot{x}_d - d_x + k_x sign(S(x)) \\ U_y &= mc_y D^{-\beta_y+1} e_y + m\ddot{y}_d - d_y + k_y sign(S(y)) \\ U_z &= mc_z D^{-\beta_z+1} e_z + m\ddot{z}_d - d_z + k_z sign(S(z)) \end{aligned} \tag{4.58}$$

The virtual control signals specified inequation (4.58) are employed to compute the desired pitch angle (θ_d), desired yaw angle (ψ_d), and U_1. With the FOSMC technique outlined above, it becomes possible to attain the sliding surface $S_x = 0$, $S_y = 0$, and $S_z = 0$, wherein the tracking errors e_x, e_y, and e_z tend towards zero exponentially as the angles θ and ψ are guided towards θ_d and ψ_d as promptly as feasible. FOSMC facilitates the adjustment of the three attitude angles (ϕ, θ, and ψ) to track their respective desired values (ϕ_d, θ_d, ψ_d) swiftly. The desired pitch angle, yaw angle and U_1 are calculated in equation (4.59): Recalling equation (4.10) and solving for θ, ψ as desired values and U_1 as the resultant thrust force.

$$\begin{aligned} \theta_d &= asin(\frac{mg - U_z}{U_1}) \\ \psi_d &= atan(\frac{U_y}{U_x}) \\ U_1 &= \sqrt{U_x^2 + U_y^2 + (mg - U_z)^2} \end{aligned} \tag{4.59}$$

4.3.3 Inner Control Loop FOSMC Design

Within the FWUAV system, the inner control loop manages the attitude control, focusing on stabilizing the roll, pitch, and yaw angles of the aircraft. While the desired pitch and yaw

angles originate from the outer control loop, the desired roll angle is specified independently. The primary objective of the inner control loop is to stabilize the tracking errors between the desired and actual roll, pitch, and yaw angles. FOSMC serves as a viable approach to formulate the control law and produce the input control signals (U_2, U_3, U_4) necessary for stabilizing the tracking errors within the attitude subsystem. We define the tracking errors and their derivatives for the inner loop's Euler angles as presented in equation (4.60)

$$\begin{bmatrix} e_\phi \\ e_\theta \\ e_\psi \end{bmatrix} = \begin{bmatrix} \phi_d - \phi \\ \theta_d - \theta \\ \psi_d - \psi \end{bmatrix}, \begin{bmatrix} \dot{e}_\phi \\ \dot{e}_\theta \\ \dot{e}_\psi \end{bmatrix} = \begin{bmatrix} \dot{\phi}_d - \dot{\phi} \\ \dot{\theta}_d - \dot{\theta} \\ \dot{\psi}_d - \dot{\psi} \end{bmatrix}, \begin{bmatrix} \ddot{e}_\phi \\ \ddot{e}_\theta \\ \ddot{e}_\psi \end{bmatrix} = \begin{bmatrix} \ddot{\phi}_d - \ddot{\phi} \\ \ddot{\theta}_d - \ddot{\theta} \\ \ddot{\psi}_d - \ddot{\psi} \end{bmatrix} \tag{4.60}$$

The expressions for the sliding surfaces pertaining to the ϕ, θ, and ψ angles are articulated in equationequation (4.61):

$$\begin{aligned} S_\phi &= c_\phi e_\phi + D^{\beta_\phi}\dot{e}_\phi = c_\phi e_\phi + D^{\beta_\phi+1}e_\phi \\ S_\theta &= c_\theta e_\theta + D^{\beta_\theta}\dot{e}_\theta = c_\theta e_\theta + D^{\beta_\theta+1}e_\theta \\ S_\psi &= c_\psi e_p si + D^{\beta_\psi}\dot{e}_\psi = c_\psi e_\psi + D^{\beta_\psi+1}e_\psi \end{aligned} \quad . \tag{4.61}$$

FOSMC design for the Roll moment control variable U_2

Using Reaching Law, The equivalent controller can be determined by making, $\dot{S}_\phi = 0$

$$\begin{aligned} \dot{S}_\phi &= c_\phi \dot{e}_\phi + D^{\beta_\phi}\ddot{e}_\phi = 0 \\ &= c_\phi \dot{e}_\phi + D^{\beta_\phi+2}e_\phi = 0 \\ &= c_\phi \dot{e}_\phi + D^{\beta_\phi}(\ddot{\phi}_d - \ddot{\phi}) = 0 \end{aligned} \tag{4.62}$$

Substituting $\ddot{\phi}$ from equation (4.15) in to equation (4.62).

$$\begin{aligned} c_\phi \dot{e}_\phi + D^{\beta_\phi}(\ddot{\phi}_d - a_\phi \dot{\phi} + b_\phi U_2 + d_\phi) = 0 \\ c_\phi \dot{e}_\phi + D^{\beta_\phi}\ddot{\phi}_d - D^{\beta_\phi} a_\phi \dot{\phi} - D^{\beta_\phi} b_\phi U_2 - D^{\beta_\phi} d_\phi) = 0 \end{aligned} \tag{4.63}$$

Solving for U_2 from equation (4.63) to get the equivalent roll moment control variable.

$$\begin{aligned} U_{2eq} &= \frac{c_\phi D^{-\beta_\phi}\dot{e}_\phi + \ddot{\phi}_d - a_\phi \dot{\phi} - d_\phi}{b_\phi} \\ &= \frac{c_\phi D^{-\beta_\phi+1} e_\phi + \ddot{\phi}_d - a_\phi \dot{\phi} - d_\phi}{b_\phi} \end{aligned} \tag{4.64}$$

The total roll moment control law is derived by combining the continuous and discontinuous control signals, as outlined in equation (4.65)

$$\begin{aligned} U_2 &= U_{2eq} + U_{2dis} \\ U_2 &= \frac{c_\phi D^{-\beta_\phi+1} e_\phi + \ddot{\phi}_d - a_\phi \dot{\phi} - d_\phi}{b_\phi} + k_\phi sign(S(\phi)) \end{aligned} \tag{4.65}$$

Where, the equivalent and discontinuous control gains are denoted by c_ϕ and k_ϕ, respectively and β_ϕ between 0 and 1 is the fractional order parameter.

Using Lyapunove for the condition of the switching gain (k_ϕ): Choosing the Lyapunov function as 4.66

$$V_\phi = \frac{1}{2} S_\phi^2 \tag{4.66}$$

To demonstrate the minimum value of the discontinuous controller gains using the signum function, we establish the proof outlined in equation (4.67)

$$\begin{aligned} \dot{V}_\phi &= S_\phi \dot{S}_\phi < 0 \\ &= S_\phi (c_\phi \dot{e}_\phi + D^{\beta_\phi}(\ddot{\phi}_d - \ddot{\phi})) < 0 \\ &= S_\phi (c_\phi \dot{e}_\phi + D^{\beta_\phi}(\ddot{\phi}_d - a_\phi \ \dot{\phi} - b_\phi U_2 - d_\phi) < 0 \\ &= S_\phi (c_\phi \dot{e}_\phi + D^{\beta_\phi}\ddot{\phi}_d - D^{\beta_\phi} a_\phi \ \dot{\phi} - D^{\beta_\phi} b_\phi U_2 - D^{\beta_\phi} d_\phi) < 0 \\ &= S_\phi (c_\phi \dot{e}_\phi + D^{\beta_\phi}\ddot{\phi}_d - D^{\beta_\phi} a_\phi \ \dot{\phi} - D^{\beta_\phi} b_\phi (\frac{c_\phi D^{-\beta_\phi+1} e_\phi + \ddot{\phi}_d - a_\phi \dot{\phi} - d_\phi}{b_\phi} + \\ &\qquad k_\phi sign(S(\phi)) - D^{\beta_\phi} d_\phi < 0 \\ &= S_\phi (-b_\phi k_\phi sign(S(\phi))) < 0 \\ &= -b_\phi k_\phi |(S(x))| < 0 \end{aligned} \tag{4.67}$$

Since b_ϕ is positive, k_ϕ must be greater than zero for the Lyapunov function of equation (4.67) to be valid.

FOSMC design for the Pitch moment control variable U_3

Using Reaching Law, The equivalent controller can be determined by making, $\dot{S}_\theta = 0$

$$\begin{aligned} \dot{S}_\theta &= c_\theta \dot{e}_\theta + D^{\beta_\theta} \ddot{e}_\theta = 0 \\ &= c_\theta \dot{e}_\theta + D^{\beta_\theta+2} e_\theta = 0 \\ &= c_\theta \dot{e}_\theta + D^{\beta_\theta} (\ddot{\theta}_d - \ddot{\theta}) = 0 \end{aligned} \tag{4.68}$$

Substituting $\ddot{\theta}$ from equation (4.21) in to equation (4.68).

$$\begin{aligned} c_\theta \dot{e}_\theta + D^{\beta_\theta}(\ddot{\theta}_d - a_\theta \ dot\theta + b_\theta U_3 + d_\theta) = 0 \\ c_\theta \dot{e}_\theta + D^{\beta_\theta}\ddot{\theta}_d - D^{\beta_\theta} a_\theta \ dot\theta - D^{\beta_\theta} b_\theta U_3 - D^{\beta_\theta} d_\theta) = 0 \end{aligned} \tag{4.69}$$

Solving for U_3 from equation (4.69) to get the equivalent roll moment control variable.

$$\begin{aligned} U_{3eq} &= \frac{c_\theta D^{-\beta_\theta}\dot{e}_\theta + \ddot{\theta}_d - a_\theta \dot{\theta} - d_\theta}{b_\theta} \\ &= \frac{c_\theta D^{-\beta_\theta + 1} e_\theta + \ddot{\theta}_d - a_\theta \dot{\theta} - d_\theta}{b_\theta} \end{aligned} \tag{4.70}$$

The total pitch moment control law is formed by combining the continuous and discontinuous control signals:

$$\begin{aligned} U_3 &= U_{3eq} + U_{3dis} \\ U_3 &= \frac{c_\theta D^{-\beta_\theta + 1} e_\theta + \ddot{\theta}_d - a_\theta \dot{\theta} - d_\theta}{b_\theta} + k_\theta sign(S(\theta)) \end{aligned} \tag{4.71}$$

Where, the equivalent and discontinuous control gains are denoted by c_θ and k_θ, respectively and β_θ between 0 and 1 is the fractional order parameter.

Using Lyapunove for the condition of the switching gain (k_θ): Choosing the Lyapunov function as equation (4.72)

$$V_\theta = \frac{1}{2} S_\theta^2 \tag{4.72}$$

To determine the minimum value of the discontinuous controller gains utilizing the signum function, we will establish the proof as presented in equation (4.73)

$$\begin{aligned} \dot{V}_\theta &= S_\theta \dot{S}_\theta < 0 \\ &= S_\theta(c_\theta \dot{e}_\theta + D^{\beta_\theta}(\ddot{\theta}_d - \ddot{\theta})) < 0 \\ &= S_\theta(c_\theta \dot{e}_\theta + D^{\beta_\theta}(\ddot{\theta}_d - a_\theta \ \dot{\theta} - b_\theta U_3 - d_\theta) < 0 \\ &= S_\theta(c_\theta \dot{e}_\theta + D^{\beta_\theta}\ddot{\theta}_d - D^{\beta_\theta} a_\theta \ \dot{\theta} - D^{\beta_\theta} b_\theta U_3 - D^{\beta_\theta} d_\phi) < 0 \\ &= S_\theta(c_\theta \dot{e}_\theta + D^{\beta_\theta}\ddot{\theta}_d - D^{\beta_\theta} a_\theta \ \dot{\theta} - D^{\beta_\theta} b_\theta(\frac{c_\theta D^{-\beta_\theta + 1} e_\theta + \ddot{\theta}_d - a_\theta \dot{\theta} - d_\theta}{b_\theta} + \\ &\qquad k_\theta sign(S(\theta)) - D^{\beta_\theta} d_\theta < 0 \\ &= S_\theta(-b_\theta k_\theta sign(S(\theta))) < 0 \\ &= -b_\theta k_\theta |(S(x))| < 0 \end{aligned} \tag{4.73}$$

Since b_θ is negative, k_θ must be less than zero for the Lyapunov function of 4.73 to be valid.

FOSMC design for the yaw moment control variable U_4

Using Reaching Law, The equivalent controller can be determined by making, $\dot{S}_\psi = 0$

$$\begin{aligned} \dot{S}_\psi &= c_\psi \dot{e}_\psi + D^{\beta_\psi} \ddot{e}_\psi = 0 \\ &= c_\psi \dot{e}_\psi + D^{\beta_\psi + 2} e_\psi = 0 \\ &= c_\psi \dot{e}_\psi + D^{\beta_\psi} (\ddot{\psi}_d - \ddot{\psi}) = 0 \end{aligned} \tag{4.74}$$

Substituting $\ddot{\psi}$ from equation (4.29) in to equation (4.74).

$$\begin{aligned} c_\psi \dot{e}_\psi + D^{\beta_\psi} (\ddot{\psi}_d - a_\psi \ dot\psi + b_\psi U_3 + d_\psi) = 0 \\ c_\psi \dot{e}_\psi + D^{\beta_\psi} \ddot{\psi}_d - D^{\beta_\psi} a_\psi \ dot\psi - D^{\beta_\psi} b_\psi U_4 - D^{\beta_\psi} d_\psi) = 0 \end{aligned} \tag{4.75}$$

Solving for U_4 from equation (4.75) to get the equivalent yaw moment control variable.

$$\begin{aligned} U_{4eq} &= \frac{c_\psi D^{-\beta_\psi} \dot{e}_\psi + \ddot{\psi}_d - a_\psi \dot{\psi} - d_\psi}{b_\psi} \\ &= \frac{c_\psi D^{-\beta_\psi + 1} e_\psi + \ddot{\psi}_d - a_\psi \dot{\psi} - d_\psi}{b_\psi} \end{aligned} \tag{4.76}$$

The entirety of the yaw moment control law is represented by the summation of the continuous and discontinuous control signals, as described in equation (4.77)

$$\begin{aligned} U_4 &= U_{4eq} + U_{4dis} \\ U_4 &= \frac{c_\psi D^{-\beta_\psi + 1} e_\psi + \ddot{\psi}_d - a_\psi \dot{\psi} - d_\psi}{b_\psi} + k_\psi sign(S(\psi)) \end{aligned} \tag{4.77}$$

Where, the equivalent and discontinuous control gains are denoted by c_ψ and k_ψ, respectively and β_ψ between 0 and 1 is the fractional order parameter.

Using Lyapunove for the condition of the switching gain (k_ψ) : Choosing the Lyapunov function as

$$V_\psi = \frac{1}{2} S_\psi^2 \tag{4.78}$$

To ascertain the minimum value of the discontinuous controller gains utilizing the signum

function, we will establish the proof as provided inequation (4.79)

$$\begin{aligned}
\dot{V}_\psi &= S_\psi \dot{S}_\psi < 0 \\
&= S_\psi(c_\psi \dot{e}_\psi + D^{\beta_\psi}(\ddot{\psi}_d - \ddot{\psi})) < 0 \\
&= S_\psi(c_\psi \dot{e}_\psi + D^{\beta_\psi}(\ddot{\psi}_d - a_\psi\ \dot{\psi} - b_\psi U_4 - d_\psi) < 0 \\
&= S_\psi(c_\psi \dot{e}_\psi + D^{\beta_\psi}\ddot{\psi}_d - D^{\beta_\psi} a_\psi\ \dot{\psi} - D^{\beta_\psi} b_\psi U_4 - D^{\beta_\psi} d_\psi) < 0 \\
&= S_\psi(c_\psi \dot{e}_\psi + D^{\beta_\psi}\ddot{\psi}_d - D^{\beta_\psi} a_\psi\ \dot{\psi} - D^{\beta_\psi} b_\psi(\frac{c_\psi D^{-\beta_\psi+1} e_\psi + \ddot{\psi}_d - a_\psi \dot{\psi} - d_\psi}{b_\psi} + \\
&\qquad\qquad k_\psi sign(S(\psi)) - D^{\beta_\psi} d_\psi < 0 \\
&= S_\psi(-b_\psi k_\psi sign(S(\psi))) < 0 \\
&= -b_\psi k_\psi |(S(x))| < 0
\end{aligned} \tag{4.79}$$

Since b_ψ is negative, k_ψ must be less than zero for the Lyapunov function of 4.79 to be valid. The controllers for position and attitude in FWUAV are outlined as follows:

$$\begin{aligned}
U_x &= mc_x D^{-\beta_x+1} e_x + m\ddot{x}_d - d_x + k_x sign(S(x)) \\
U_y &= mc_y D^{-\beta_y+1} e_y + m\ddot{y}_d - d_y + k_y sign(S(y)) \\
U_z &= mc_z D^{-\beta_z+1} e_z + m\ddot{z}_d - d_z + k_z sign(S(z)) \\
U_1 &= \sqrt{U_x^2 + U_y^2 + (mg - U_z)^2} \\
U_2 &= \frac{c_\phi D^{-\beta_\phi+1} e_\phi + \ddot{\phi}_d - a_\phi \dot{\phi} - d_\phi}{b_\phi} + k_\phi sign(S(\phi)) \\
U_3 &= \frac{c_\theta D^{-\beta_\theta+1} e_\theta + \ddot{\theta}_d - a_\theta \dot{\theta} - d_\theta}{b_\theta} + k_\theta sign(S(\theta)) \\
U_4 &= \frac{c_\psi D^{-\beta_\psi+1} e_\psi + \ddot{\psi}_d - a_\psi \dot{\psi} - d_\psi}{b_\psi} + k_\psi sign(S(\psi))
\end{aligned} \tag{4.80}$$

4.4 FOSMC Gain Tuning Using PSO

The FOSMC gains such as position control gains $(c_x, c_y, c_z, k_x, k_y, k_z, \beta_x, \beta_y, \beta_z)$ and attitude control gains $(c_\phi, c_\theta, c_\psi, k_\phi, k_\theta, k_\psi, \beta_\phi, \beta_\theta, \beta_\psi)$ in the FWUAV controllers of equation (4.80) are tuned using PSO. The Particle Swarm Optimization (PSO) algorithm, introduced by Eberhart and Kennedy in 1995 and later refined by Kennedy and Eberhart, is a stochastic optimization technique inspired by the behavior of swarms in nature. Mimicking the social dynamics observed in various animal groups such as insects, herds, birds, and fish, PSO enables cooperative exploration for tasks like food collection. Each member of the swarm

continually adjusts its search pattern based on its own experiences and the evolving interactions with other members. In this study, a Particle Swarm Optimization (PSO) technique is employed to automatically fine-tune the control gain parameters for both position and attitude of the Fixed-Wing Unmanned Aerial Vehicle (FWUAV) using Fractional Order Sliding Mode Control (FOSMC) controllers. The fitness function is constructed from several factors derived from the nonlinear, interconnected dynamics of the FWUAV as well as its trajectory tracking capabilities. Each particle's position corresponds to a specific configuration of the fractional order sliding mode controller, while its velocity reflects the degree of variation in this parameterization across simulations. The initial positions and velocities of particles and variables are randomly determined. Within the search space, particles continuously adjust their positions, and their performance is regularly evaluated[12][21].

The initialization matrix consists of N particles distributed throughout a D-dimensional search space, and PSO intelligently selects optimal parameters from these N particles. For effective functioning, PSO relies on a fitness function associated with the position of particles. Each particle i maintains its optimal position $P_{bi}(t+1)$ and also retains information about the optimal solution in its vicinity, denoted as $g_b(t+1)$, representing the location of the particle with the lowest fitness value within the swarm.

Three laws govern how each particle's displacement mechanism works. Initially, each particle tends to maintain its current velocity direction. Subsequently, it aims to approach its best-known position. Lastly, it also tends to gravitate towards the best position achieved by its neighboring particles.

4.4.1 PSO Algorithms

The PSO algorithm operates as a swarm-based search method where individuals, termed particles, represent potential solutions within a D-dimensional search space. These particles have the capacity to remember both their own optimal positions and those of the swarm, along with their velocities. Information from all particles is amalgamated in each generation to adjust the speed of movement in each dimension, subsequently determining the new position of each particle. Until reaching equilibrium, the optimal state, or the predefined termination conditions, particles continuously adjust their positions within the multidimensional search space. Through objective functions, a unique correlation among the dimensions of the problem space is established [22].

Let's imagine that the swarm size is N, and each particle's position vector in a D-dimensional

space is denoted by x_{ij}, while its velocity vector is represented by v_{ij}. The individual's optimal position, which is the best position the particle has encountered, is noted as p_{ij}, and the swarm's optimal position, the best position any individual within the swarm has encountered, is denoted as p_{gj}. This notation applies for $i = 1, 2, ...N$ and $j = 1, 2, ..., D$. The updated velocity matrix is denoted as v_{ij}, while the new position matrix of the particle is represented as x_{ij}, which is represented as:

$$v_{ij}(t+1) = wv_{ij}(t) + R_1C_1(p_{bij}(t) - x_{ij}(t)) + R_2C_2(g_{bij}(t) - x_{ij}(t)) \tag{4.81}$$

$$x_{ij}(t+1) = x_{ij}(t) + v_{ij}(t+1) \tag{4.82}$$

Evaluate the objective /fitness function f_i and update p_{besti} and g_{best}

$$\begin{cases} P_{besti} = X_i \\ f(p_{besti}) = f_i \end{cases} \quad if f_i < f(_{pbesti}) \tag{4.83}$$

$$\begin{cases} g_{best} = P_{besti} \\ f_{gbest} = f(_{pbesti}) \end{cases} \quad if f(_{pbesti}) < f(g_{best}) \tag{4.84}$$

Where, p_{besti} represents the best position discovered by particle i, while g_{best} signifies the best position discovered within the particle's neighborhood. The parameters w, C_1, and C_2 denote the inertial and acceleration coefficients, while R_1 and R_2 represent random variables drawn from a uniform distribution within the range [0, 1].

4.4.2 Fitness Function

A performance index is used in the suggested technique to quantify the optimization performance of the FWUAV's responses [23]. To minimize the disparities between the regulated output responses of the FWUAV and the desired output responses, a performance index, also referred to as the fitness function or objective function, is defined. This thesis aims to reduce FWUAV trajectory tracking error in both location and orientation. This fitness function, which is chosen by the field of control engineering, includes Integral Square Error (ISE), Integral Time Square Error (ITSE), Integral Absolute Error (IAE), and Integral Time

Absolute Error (ITAE) which are represented in the equation below.

$$\begin{aligned} ISE &= \int_0^\infty e^2(t)d_t \\ ITSE &= \int_0^\infty te^2(t)d_t \\ IAE &= \int_0^\infty |e(t)|d_t \\ ITAE &= \int_0^\infty t|e(t)|d_t \end{aligned} \tag{4.85}$$

Each fitness function in equation (4.85) has a different property. Small errors are not penalized at all, but large errors carry a heavy penalty under the ISE index. To achieve a system response characterized by rapidity and oscillatory behavior, a criterion is established that prioritizes the swift reduction of initial errors. Unlike IAE, which imposes substantial penalties for control errors, ITSE places emphasis on early deviations and imposes heavy penalties for errors occurring later in the transient response of the system. Systems optimized using ITAE tend to exhibit small overshoots and minimal damped oscillations. Mild penalties are applied for significant early errors, whereas errors occurring later in the response are heavily penalized under ITAE, resulting in prolonged settling times and increased control errors. This study adopts the ITAE performance index.

Chapter 5

Simulation Results and Discussion

5.1 Introduction

In this chapter, the simulation outcomes of employing FOSMC for closed-loop control of the system are illustrated using MATLAB/Simulink. Through these simulations, different facets of the system's performance can be examined and comprehended. The results are depicted graphically, offering visual comprehension of the system's dynamics and behavior. The controller's primary objective is to proficiently regulate the position and orientation of the flying system across various trajectories. To assess the dependability and efficacy of the proposed controller, two perturbed trajectories—helical and rectangular paths—are employed for evaluation.

5.2 Helical Trajectory Tracking of FWUAV

Figure 5.1 displays the 3D response of helical trajectory tracking. PSO approach with ITAE performance index is used to get optimal gains of FOSMC. The following tracking reference in space was used to generate the helical trajectory. The input trajectories along the x and y axes follow sinusoidal patterns with an amplitude of 12m and a frequency of 0.0318Hz, represented by the equations $x_d = 12 - 12\cos(0.2t)$ and $y_d = 12\sin(0.2t)$, respectively. The trajectory along the z-axis is linear, given by $z_d = t$, while the desired roll angle ϕ_d remains constant at 0.8 radians. The optimal control gains obtained by PSO for helical trajectory tracking are shown in table 5.1: To determine the tracking performance of the controller for the helical trajectory of the FWUAV, it is important to analyze how quickly the actual results align with the desired trajectory. As shown from the 3D plot, the desired trajectory

Table 5.1: gains tuned by PSO for helical trajectory

Gains	Values	Gains	Values	Gains	Values
c_x	3.7406	c_y	4.5265	c_z	3.3302
k_x	14.1772	k_y	9.6802	k_z	7.3255
β_x	0.4261	β_y	0.4585	β_z	0.2957
c_ϕ	1.8533	c_θ	2.5607	c_ψ	2.5131
k_ϕ	81.2472	k_θ	-56.3962	k_ψ	-93.5865
β_ϕ	0.1173	β_θ	0.1398	β_ψ	0.1619

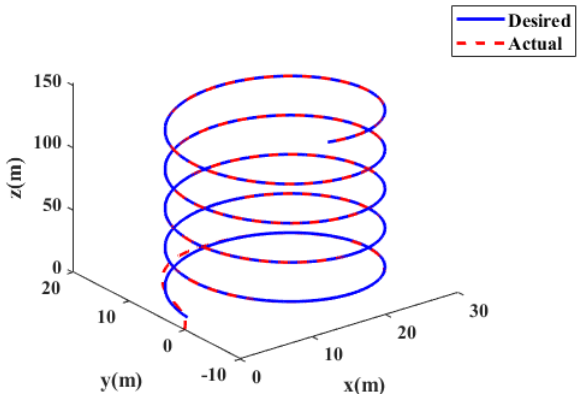

Figure 5.1: 3D Plot of Helical Trajectory Tracking

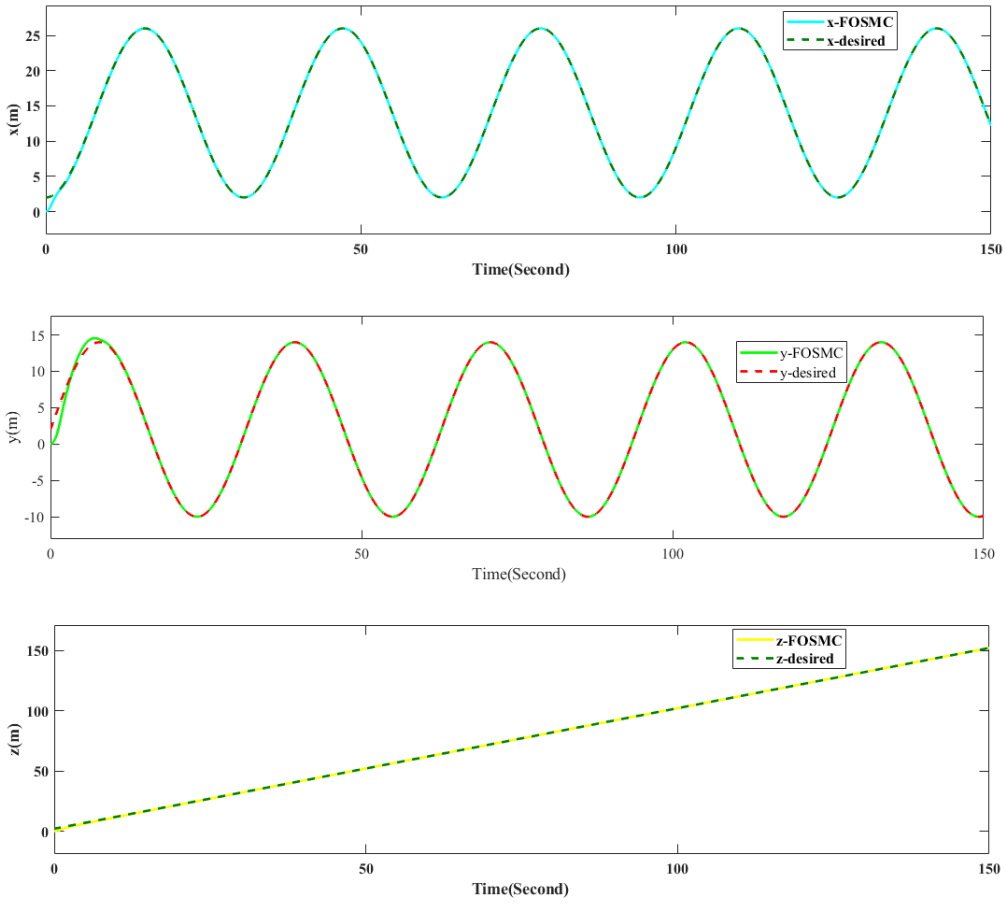

Figure 5.2: Helical Trajectory Tracking Positions

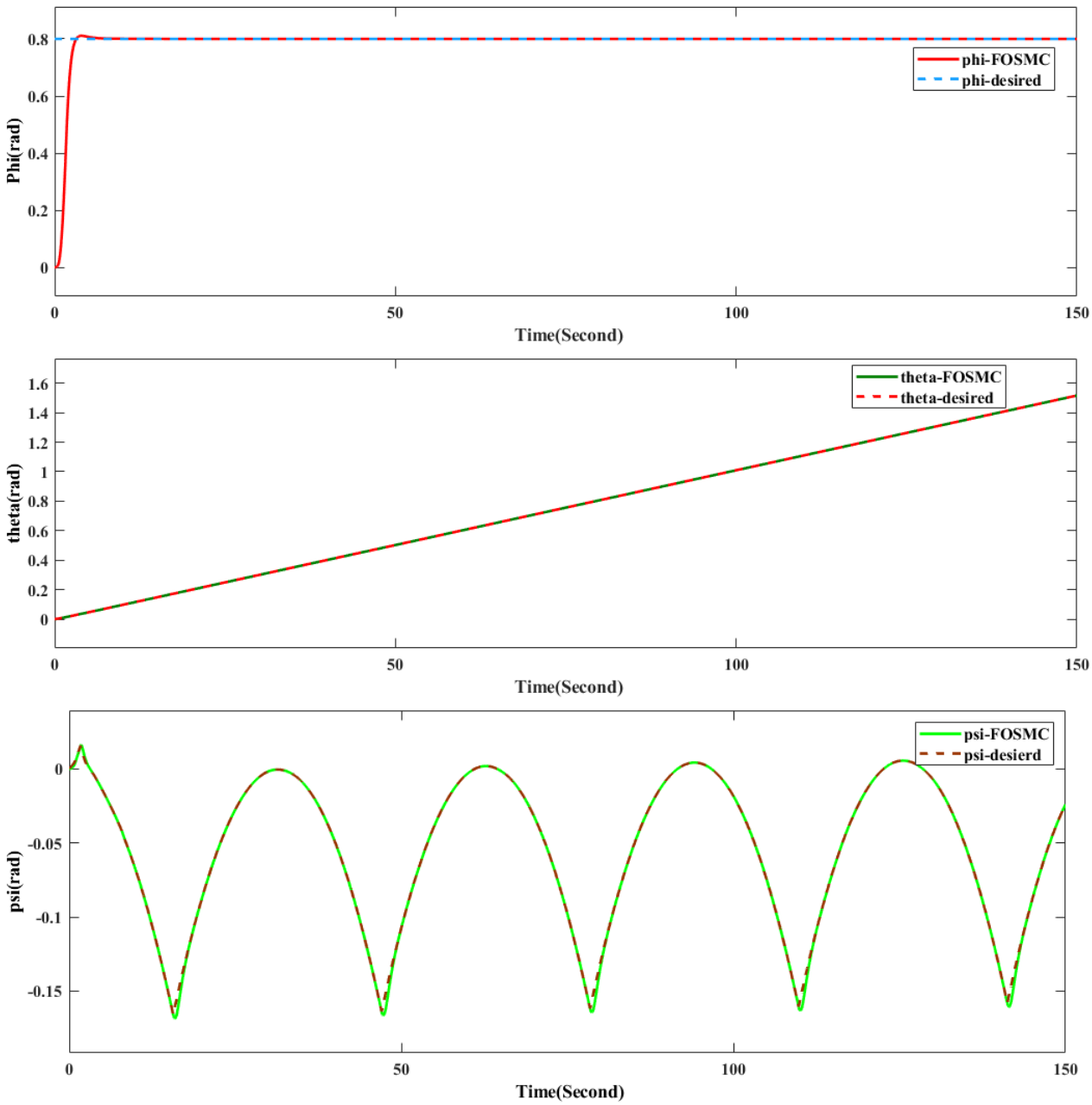

Figure 5.3: Helical Trajectory Tracking Angles

starts at (x_d, y_d, z_d)= $(2m, 0, 2m)$ to know the tracking performance(with in how much time the actual results follow the desired trajectory) of the controller.

Figure 5.2 illustrates the recorded positions along the x, y, and z axes corresponding to a helical trajectory of a FWUAV. The plot demonstrates the tracking performance of the FWUAV along the x-axis,y-axis and z-axis. It shows that the FWUAV successfully tracks the desired values along the x,y and z axes. The settling time for the x-axis is 2 seconds. This means that it takes approximately 2 seconds for the FWUAV's position along the x-axis to stabilize and align with the desired reference value. The settling time for the y-axis 8 seconds. Thus, it takes around 8 seconds for the FWUAV's position along the y-axis to settle and align with the desired reference value. The settling time for the z-axis is 11 seconds.

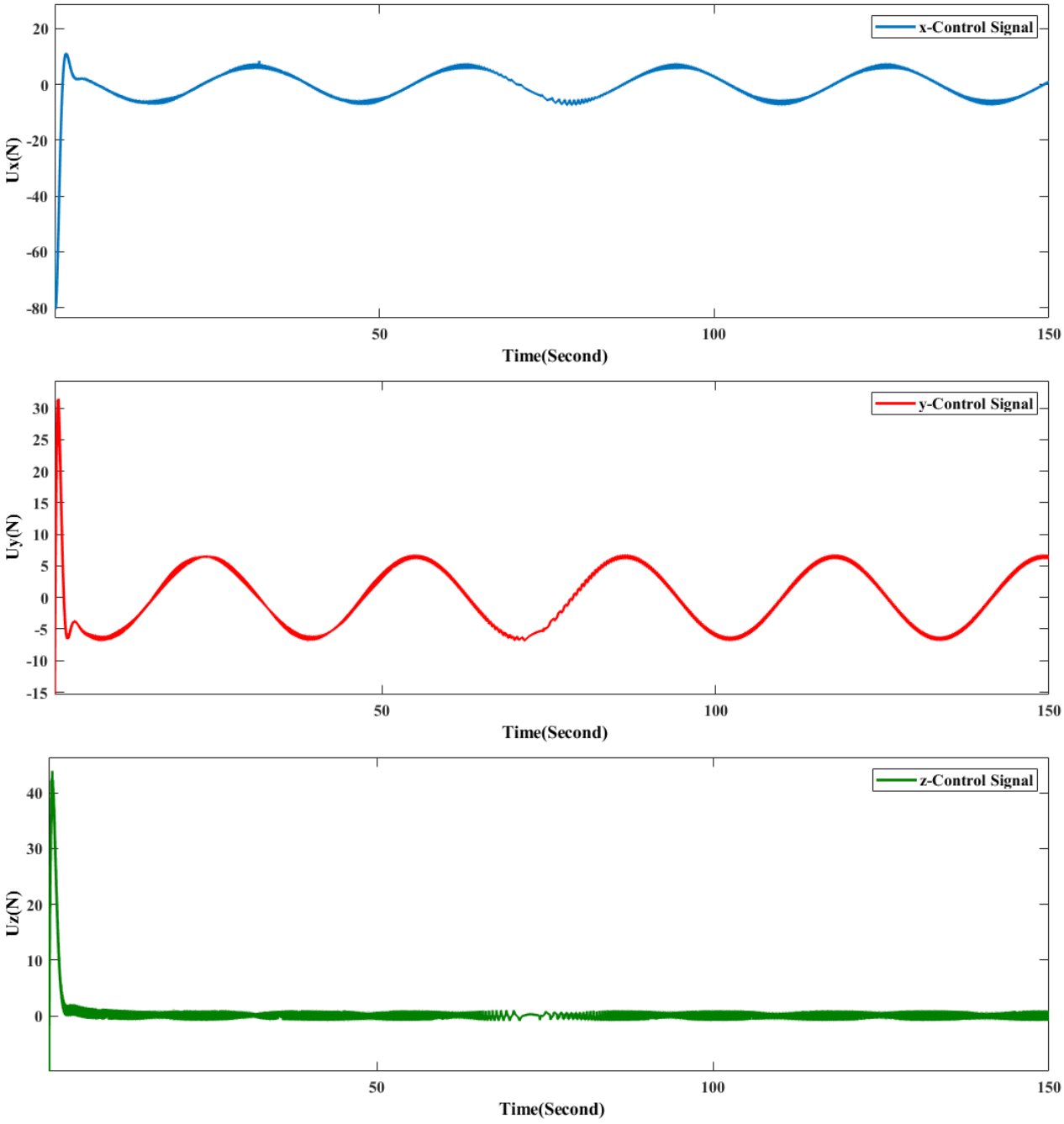

Figure 5.4: Control Efforts for x, y and z Positions respectively

This implies that it takes approximately 11 seconds for the FWUAV's position along the z-axis to stabilize and align with the desired reference value.

Figure 5.3 exhibits the generated reference signals for pitch and yaw angles derived from the outer loop, along with their respective output trajectories and the trajectory of the roll angle. From the results, it can be seen that the suggested FOSMC tailored PSO system can provide precise reference tracking. ϕ_d, θ_d and ψ_d are the desired trajectories of attitude angles and ϕ, θ and ψ are the actual or measured values. There is no overshoot on the results, this is because ITAE is used as a performance index, which minimizes overshoot and settling time.

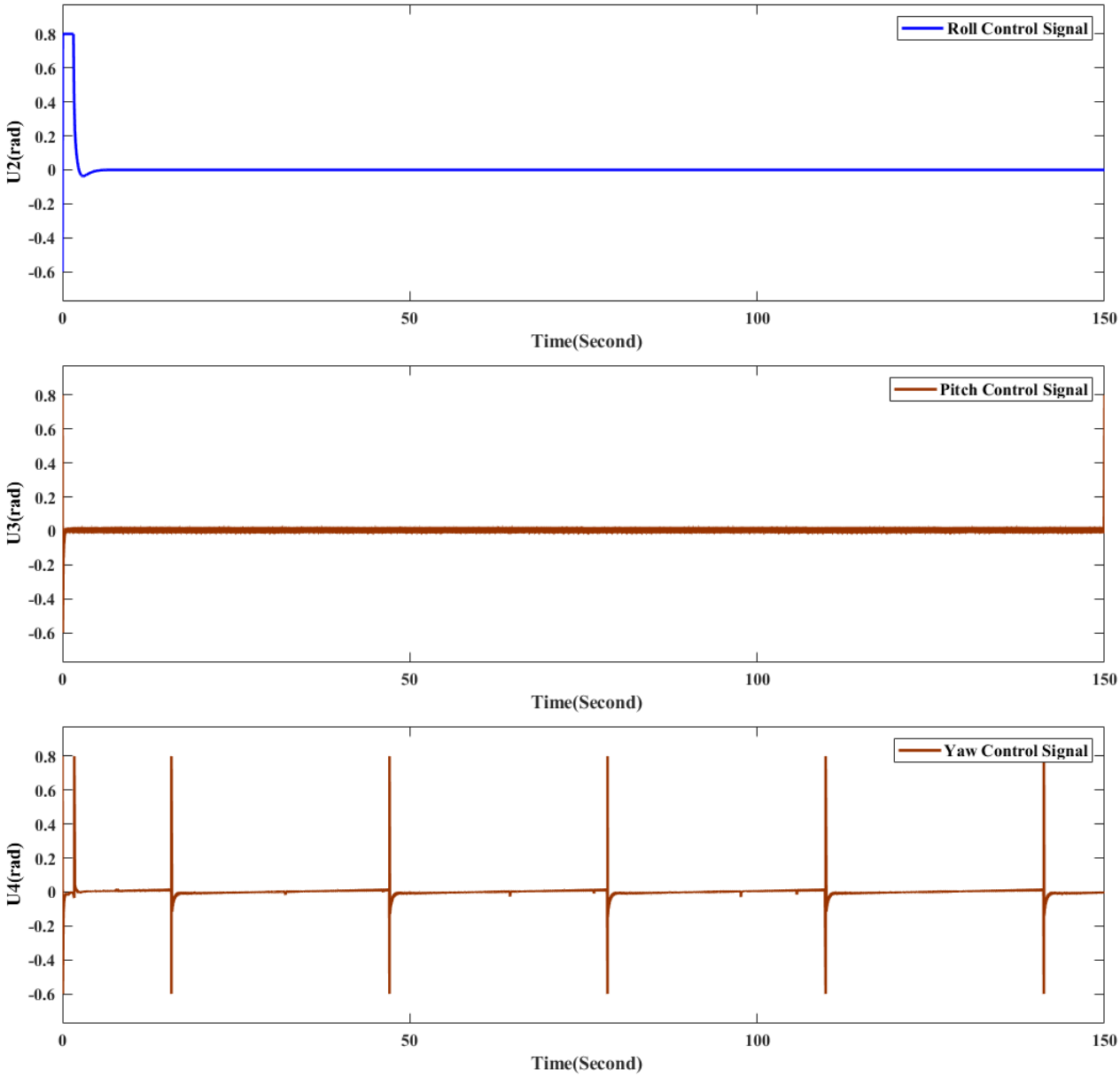

Figure 5.5: Control Efforts for Roll, Pitch and Yaw Angles respectively

Figure 5.4 displays the outer loop control or virtual controller signals U_x, U_y and U_z which are instrumental in determining θ_d, ψ_d, and thrust force (U_1). As shown from the figure, larger control signals are required at the beginning of the trajectory, and the amplitude of these control signals varies based on the specific input trajectory being followed.

Figure 5.5 represents the inner loop controller or attitude control signals for a FWUAV. Which are the roll angle control signal (U_2), pitch angle control signal (U_3), and yaw angle control signal (U_4). These signals are utilized to control the roll angle, pitch angle, and yaw angle, respectively, to maintain the desired angles and follow the given trajectory. At the curve of the trajectory, the FWUAV requires maximum control signals to ensure accurate tracking of the desired path.

5.3 Comparison of FOSMC with Conventional SMC

To track the desired values of helical trajectory , FOSMC have better performance in tracking accuracy and speed of response than conventional SMC. In contrast to the conventional SMC approach, the FOSMC method accelerates the convergence of all state variables towards their respective reference signals.

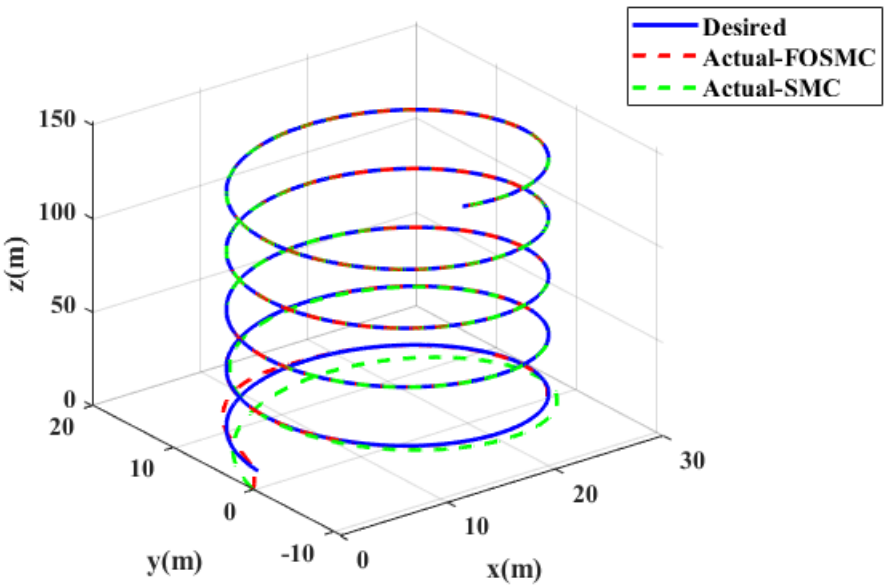

Figure 5.6: Comparison of Conventional SMC and FOSMC in Helical Trajectory

As shown from figure 5.6, a slow response is obtained from the conventional SMC (green color), while the FOSMC (red color) performs faster to converge to the desired value in the simulation.

In Figure 5.7, tracking locations in the x, y, and z axes are compared between traditional SMC and FOSMC in the same plane to evaluate controller performance. As shown from the result FOSMC is more accurate to track the desired value than conventional SMC.

Figure 5.8 illustrates the control efforts employed by SMC to achieve the desired helical trajectories for the positions of the FWUAV. It exhibits more chattering compared to figure 5.4, representing the control efforts utilized by FOSMC to track the given helical trajectory for the FWUAV.

In addition to the difference in the results of position tracking, the performance of FOSMC and conventional SMC can be analyzed using the performance index values of errors (ITAE) which is used for PSO tuning. Table 5.2 shows the performance index ITAE values for FOSMC and SMC of FWUAV an percentage of performance improvement of FOSMC over SMC can be calculated in equation (5.1). 76.5918% of performance is improved by FOSMC.

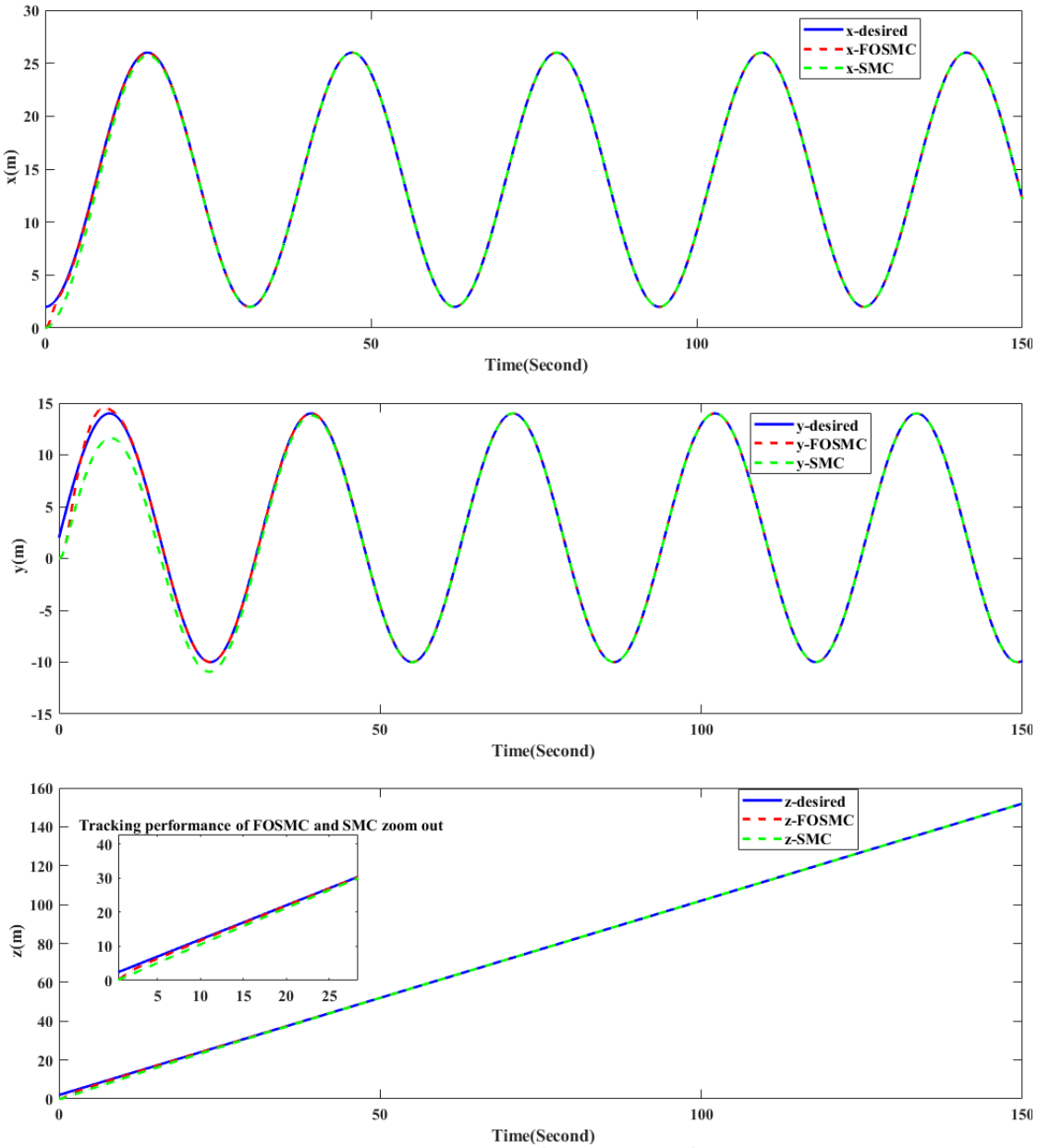

Figure 5.7: Positions along x,y and z axes

Let P be the improved performance and E be the sum of ITAEs:

$$
\begin{aligned}
E(SMC) &= 137.4 + 740.2 + 682.2 = 1559.8 \\
E(FOSMC) &= 56.72 + 185.7 + 122.7 = 365.12 \\
P &= \frac{E(SMC) - E(FOSMC)}{E(SMC)} * 100\% \\
&= 76.5918\%
\end{aligned} \tag{5.1}
$$

Where, E(SMC) sum of performance errors of SMC and E(FOSMC) sum of performance errors of FOSMC

The errors obtained by FOSMC and SMC are displayed in figure 5.9. It is concluded that

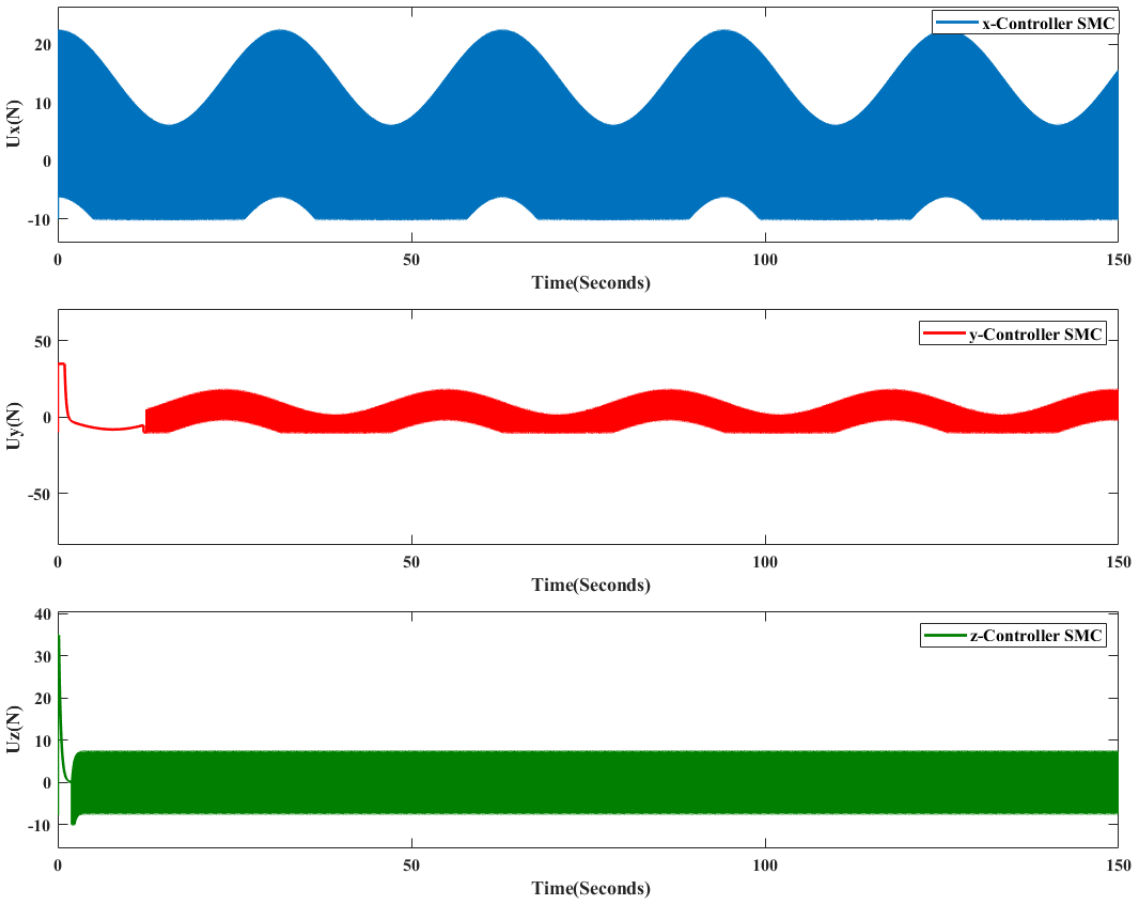

Figure 5.8: Control Efforts for x,y and z axes using SMC

Table 5.2: ITAE values for FOSMC and SMC

error	FOSMC	SMC
e_x	56.72	137.4
e_y	185.7	740.2
e_z	122.7	682.2

FOSMC is more accurate than SMC.

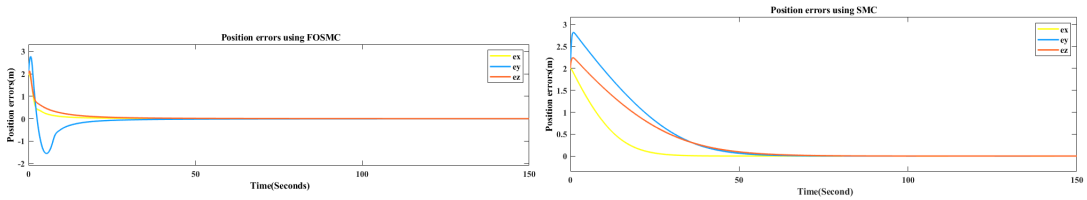

Figure 5.9: Position errors along x,y and z axes using FOSMC and SMC

5.4 Rectangular Trajectory Tracking of FWUAV

The third order polynomial input trajectory for this tracking is presented in appendix(D). In this thesis, it is assumed that UAV catapult launcher is used for takeoff and parachute is

used for recovery. The UAV catapult launcher is a device specifically designed to assist in the takeoff of FWUAVs. It has a device for accelerating the UAV to a minimal controllable airspeed in preparation for takeoff. The launcher typically consists of a rail or a track along which the UAV is propelled. By utilizing the catapult launcher, the UAV can achieve the necessary speed and lift to become airborne[25]. From the FWUAV parameters takeoff speed is 15m/s and flight path angle(γ) is 0.262 rad and the height of the catapult launcher is 2m [17]. Then,a third-order smooth trajectory is applied as a reference input after the catapult operation by taking initial and final way-points with the speed profile of the aircraft, and at the final point, a constant altitude which is linearly depends on x_d with a slop of $tan(\gamma)$ is maintained and navigation is started, the polynomials for takeoff is given as:

$$\begin{aligned} x_d &= a_0 + a_1 t + a_2 t^2 + a_3 t^3 \\ y_d &= 0 \\ z_d &= x_d tan(\gamma) + 2 \end{aligned} \tag{5.2}$$

After takeoff operation is performed, the UAV starts navigation or cruise in which the normal operation of the UAV is started. From the literature, the speed(cruise speed) of the FWUAV during this phase is constant and takes a value of 20m/s for this thesis ([17]). The speed in this scheme is constant until the operation is done. The flight path in this phase is a third-order smooth trajectory based on the slop continuity and the path continuity constraints, as well as the banking scheme. The equation of the trajectory for navigation and and banking scheme is given as:

$$\begin{aligned} x_d &= a_0 + a_1 t + a_2 t^2 + a_3 t^3 \\ y_d &= a_0 + a_1 t + a_2 t^2 + a_3 t^3 \\ z_d &= constant \end{aligned} \tag{5.3}$$

During the banking scheme, in order to remove sharp corners both x_d and y_d are used simultaneously for a certain amount of time (4 sec for this work).

On the other hand, for landing, a parachute is employed. The parachute is deployed to slow down and stabilize the descent of the UAV, allowing for a controlled and safe landing. This method is particularly useful when operating in areas where traditional landing approaches are not feasible or when landing in confined spaces.

The optimal control gains obtained by PSO for rectangular trajectory tracking are given in the table 5.4. The desired roll angle is given as: $\phi_d = 0.5rad$.

Figure 5.10 illustrates the system's response in three dimensions, as well as the tracking

Table 5.3: PSO tuned gains

Gain	Value	Gain	Value	Gain	Value
c_x	3.0023	c_y	3.5083	c_z	3.5369
k_x	49.2517	k_y	61.8626	k_z	110.3407
β_x	0.2994	β_y	0.2867	β_z	0.1266
c_ϕ	2.0023	c_θ	3.5194	c_ψ	3.1916
k_ϕ	90.324	k_θ	-170.0207	k_ψ	-150.8576
β_ϕ	0.0693	β_θ	0.0868	β_ψ	0.1997

response of each position corresponding to the respective inputs.. As shown from the 3D plot, the desired trajectory starts at (x_d, y_d, z_d)= $(0, 0, 2m)$, where $2m$ in the z-axis is the launcher height. Initially x_d is third order polynomial generated using initial time 0 and final time of $30sec$ and z_d is third order polynomial depends on x_d, flight path angle and launcher height.

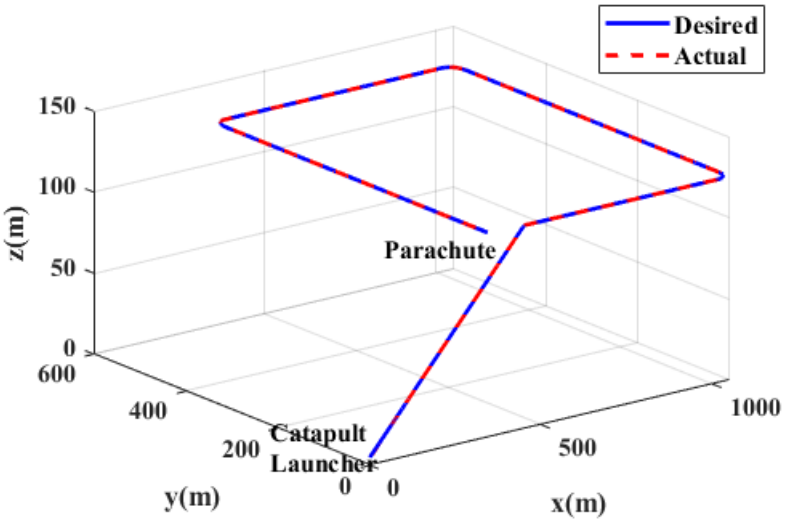

Figure 5.10: 3D Plot of Rectangular Trajectory Tracking

Figure 5.11 the tracking response of each position (x, y, z) along a rectangular trajectory, achieved through the utilization of FOSMC with PSO-tuned parameters. The figure depicts the tracking performance of the FWUAV in following a rectangular trajectory, and it highlights the effectiveness of the PSO auto-tuned FOSMC in achieving accurate position control. From the figure, it is evident that the FWUAV, controlled by the FOSMC with PSO-tuned parameters, exhibits minimal tracking errors for each position (x, y, z) along the rectangular trajectory. The good tracking performance indicated in the figure suggests that the control system, employing FOSMC with PSO-tuned parameters, effectively minimizes errors and

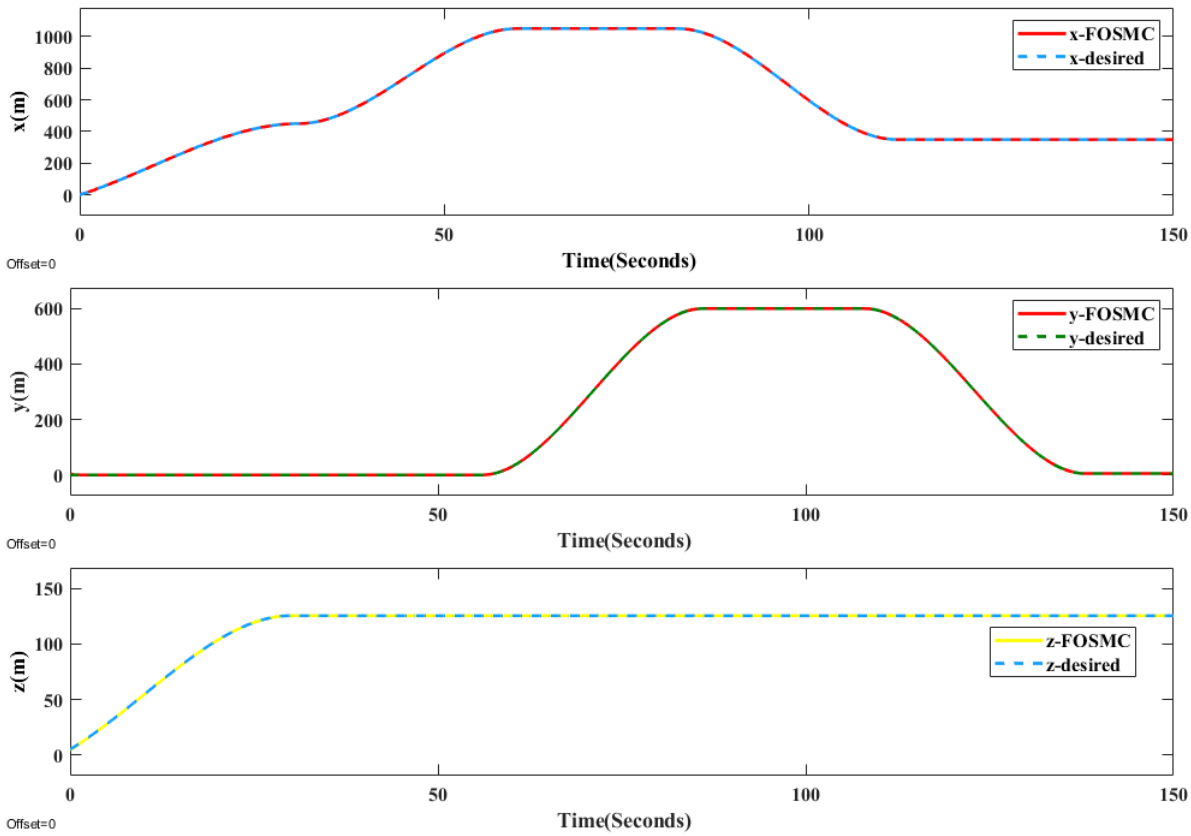

Figure 5.11: Rectangular Trajectory Tracking Positions

accurately tracks the desired trajectory. This demonstrates the successful application of the control strategy in achieving precise position control for the FWUAV.

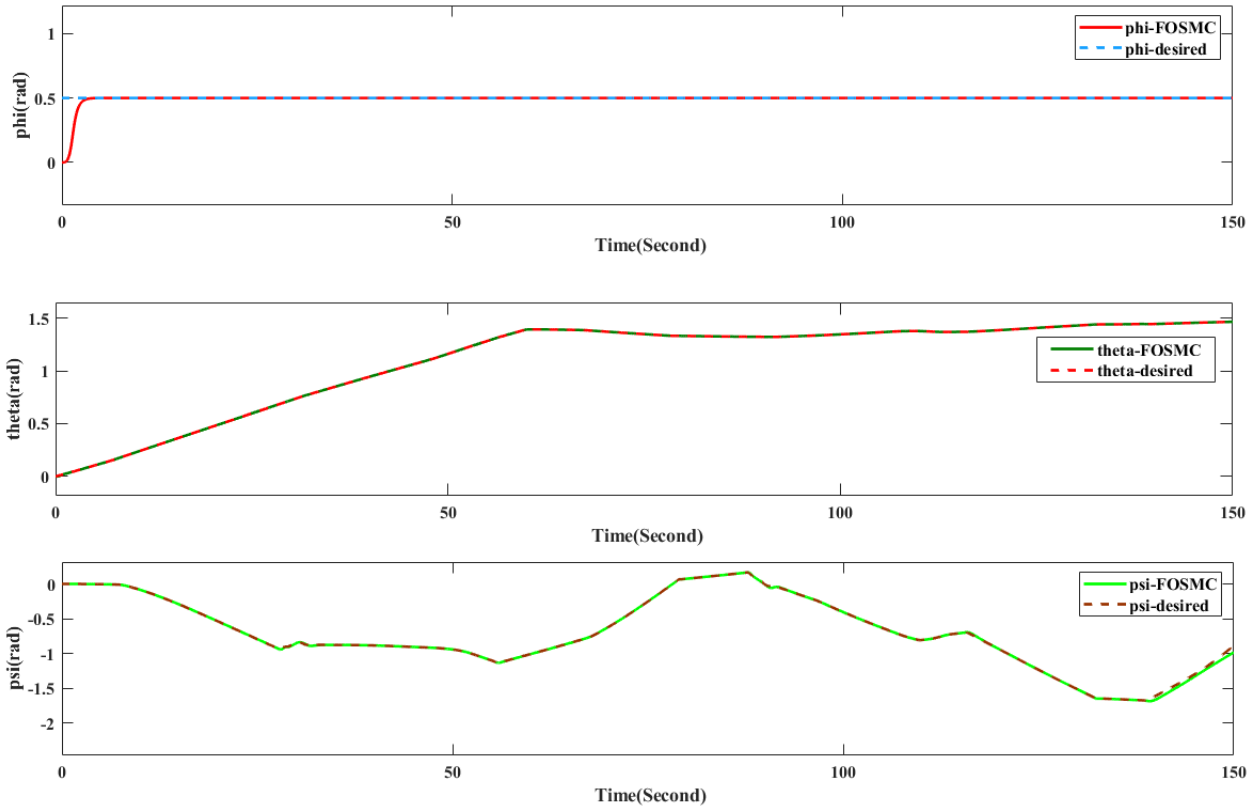

Figure 5.12: Tracking Angles for Rectangular Trajectories

Figure 5.12 depicts the responses of the desired and actual roll (ϕ), pitch (θ), and yaw (ψ) attitude angles. It illustrates how the measured angles align with the desired angles generated by the outer control loop of the control system. The figure indicates that the measured roll, pitch, and yaw angles closely track the desired values, indicating effective tracking of desired attitude angles for the FWUAV. Specifically, the roll angle accurately follows the reference roll angle, demonstrating successful maintenance of the desired roll motion. Similarly, the pitch and yaw angles closely align with the desired angles. The precise tracking of desired attitude angles by the measured angles underscores the effectiveness of the control system's inner loop, responsible for stabilizing and controlling the FWUAV's attitude. Through accurate tracking of desired angles, the control system ensures that the FWUAV maintains the intended orientation and direction during flight.

Figure 5.13 showcases the outer loop or virtual controller signals, namely U_x, U_y, and U_z. These signals play a crucial role in determining the desired pitch angle (θ_d) and yaw angle (ψ_d) for the FWUAV. Figure 5.14 in the thesis illustrates the inner loop controllers for the

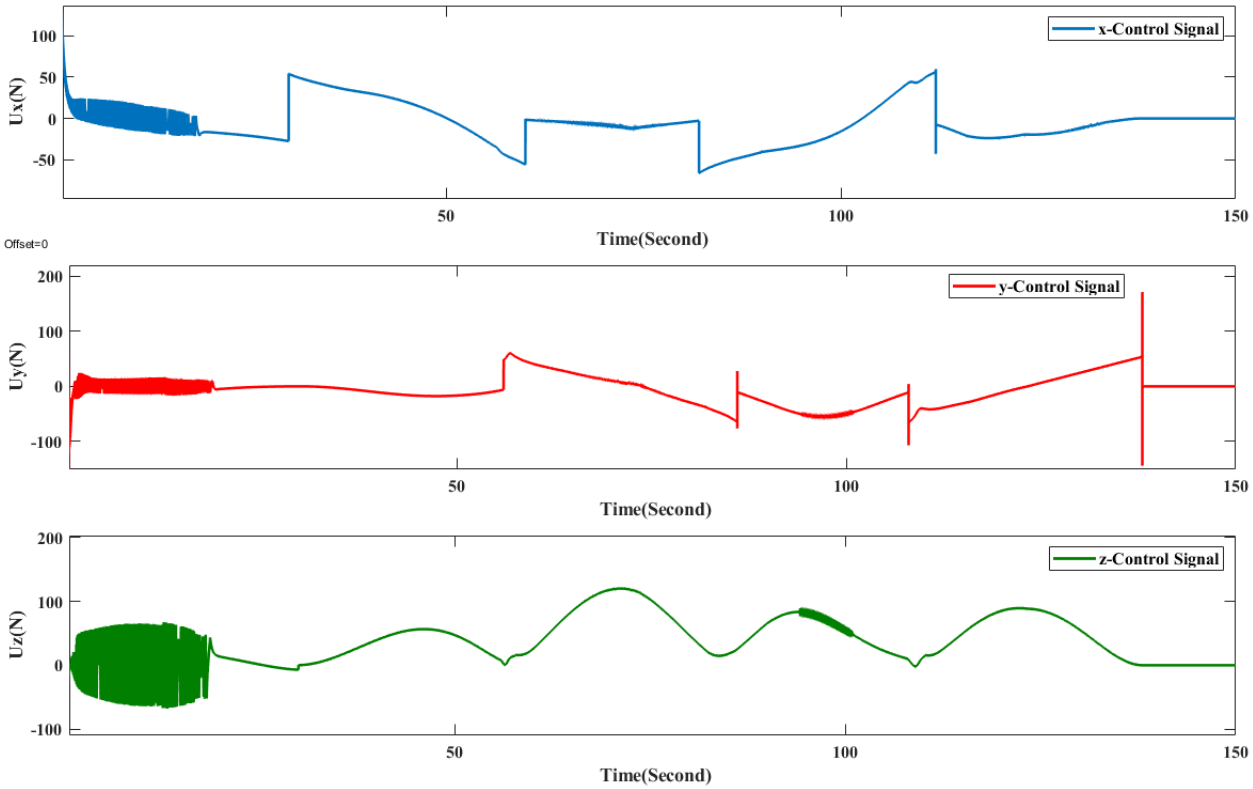

Figure 5.13: Virtual Control Efforts along x, y and z Positions respectively

FWUAV. It includes the roll angle controller (U_2), the attitude pitch angle controller (U_3), and the yaw angle controller (U_4). These controllers play a crucial role in stabilizing and controlling the FWUAV's attitude based on the desired angles and trajectories. These inner loop controllers work in conjunction with the outer loop controllers (as described earlier) to

ensure precise attitude control of the FWUAV. By regulating the roll, pitch, and yaw angles, the inner loop controllers contribute to achieving accurate and stable flight.

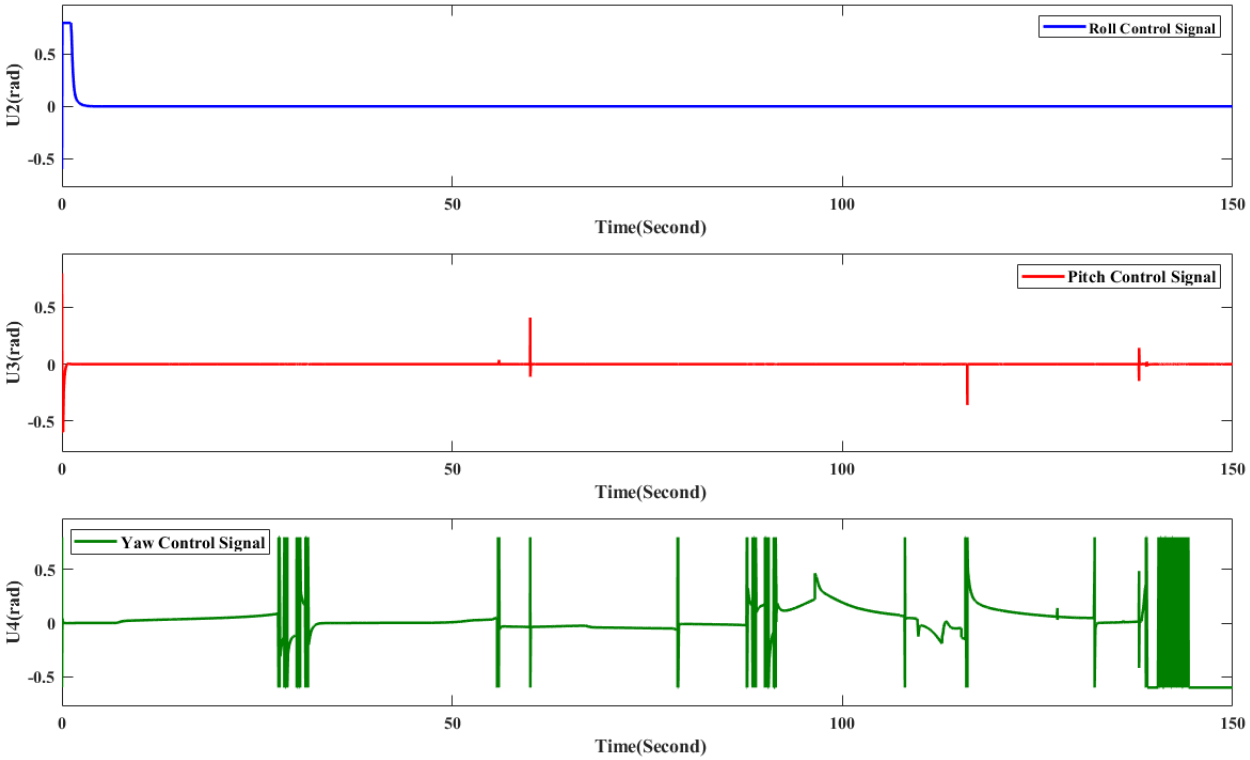

Figure 5.14: Attitude Control Efforts for Roll, Pitch and Yaw Angles respectively

5.5 Rectangular Path Trajectory Tracking Under Disturbance

5.5.1 Without Parameter Variation

To demonstrate the effectiveness of the FOSMC scheme in path tracking despite external disturbances, a simulation was conducted where a rectangular reference path was perturbed with external disturbances, without any variation in parameters. The simulation results indicate that the proposed controller exhibits improved performance in tracking the desired trajectory even in the presence of disturbances. The external disturbance introduced in this simulation is represented by a random signal with an amplitude of -1.5 N along the x, y, and z positions for 15-second intervals. These disturbances are visualized in figure 5.15.

Disturbances are introduced along the x-axis, y-axis, and z-axis at different time intervals and with 15 sec duration. Here are the details of the disturbance timings: Disturbance along x-axis: Start time: $t = 60$ seconds end time: $t = 75$ seconds Disturbance along y-axis: Start time: $t = 90$ seconds End time: $t = 105$ seconds Disturbance along z-axis: Start time:

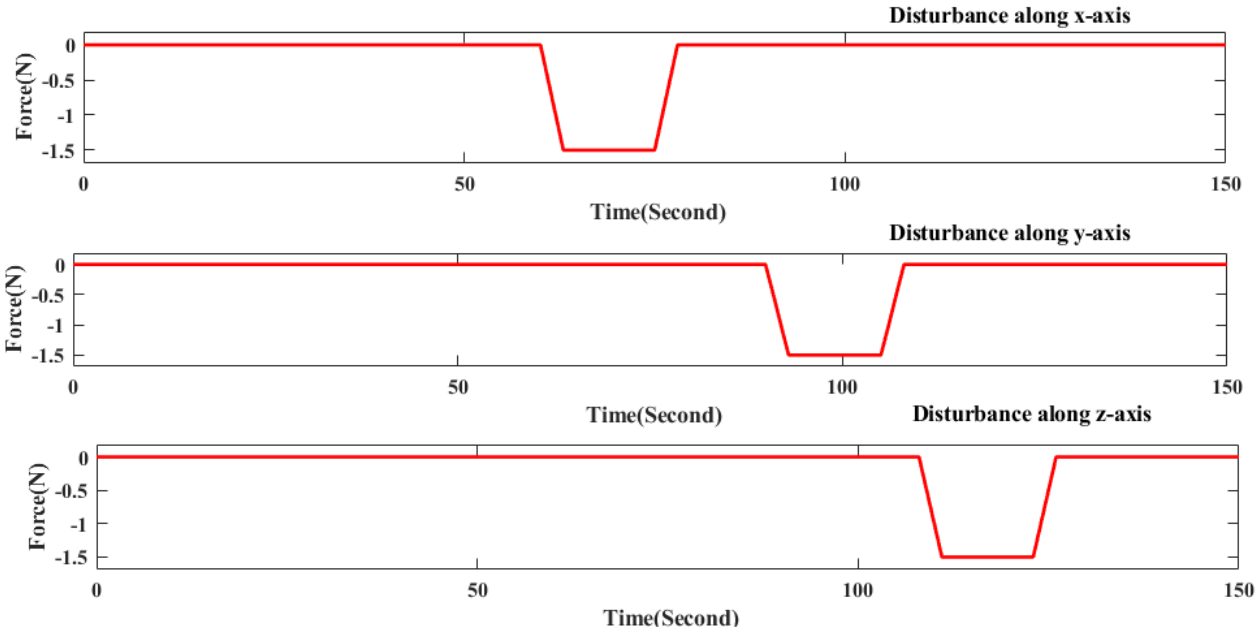

Figure 5.15: Applied Disturbance along x, y and z axes

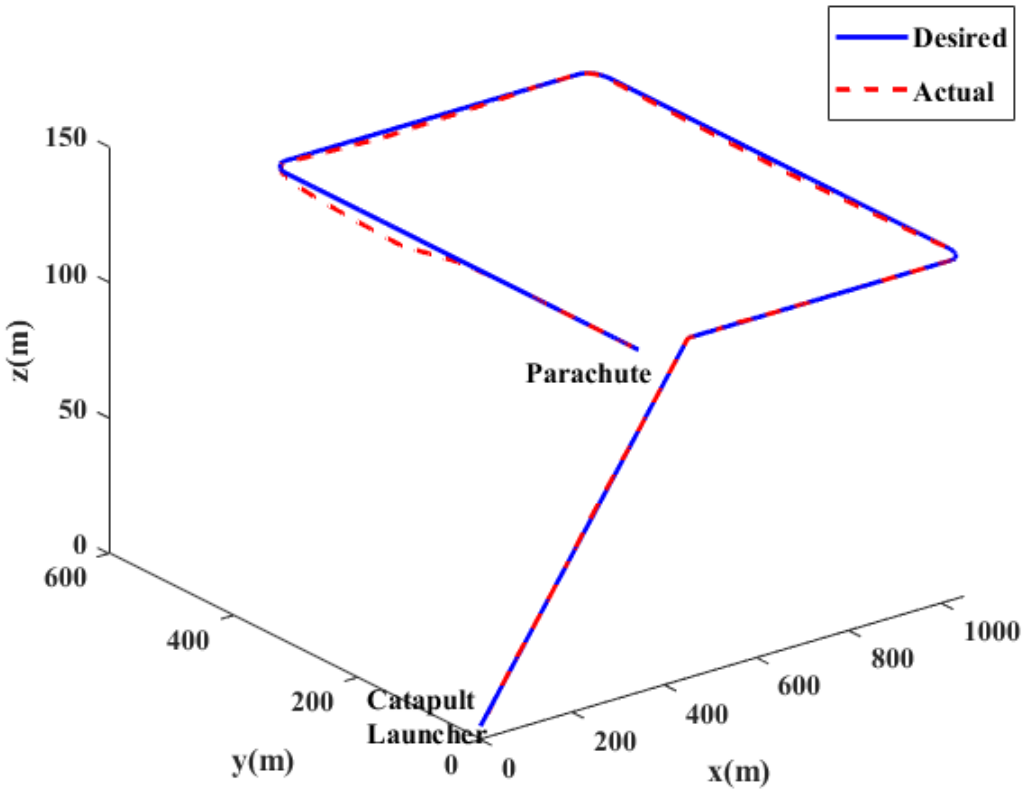

Figure 5.16: 3D Plot for Rectangular Trajectory Tracking Under Disturbance

$t = 110$ seconds End time: $t = 125$ seconds.

The response of the system under disturbances in three dimensions for the proposed controllers is illustrated infigure 5.16. This figure presents the behavior and performance of the control system when subjected to disturbances along the x-axis, y-axis, and z-axis simulta-

neously.

The effect of disturbances on the x, y, and z positions of a FWUAV having significant implications for its flight performance and control, and the ability of the controller to reject disturbances is shown in figure 5.17, figure 5.19 and figure 5.19 respectively. The depicted results indicate that the FOSMC effectively stabilizes the system and facilitates the convergence of positions to the desired values, even when subjected to disturbances. Despite the applied force as a disturbance being only 1.13% of the total weight of the FWUAV (calculated as 13.5 kg $\times$ 9.81 = 132.435 N) in magnitude, the FOSMC successfully rejects the disturbance, leading to errors converging to zero. Figure 5.20 represents the position errors and

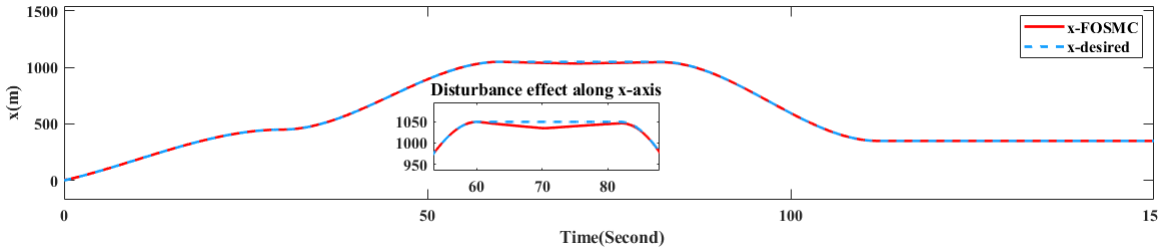

Figure 5.17: The Impact of Disturbance Along the x-axis

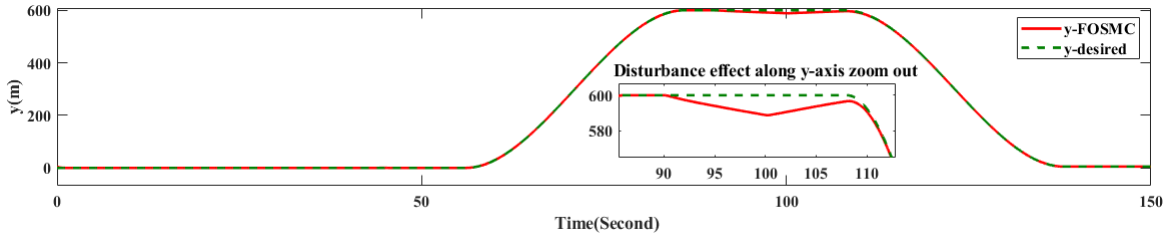

Figure 5.18: The Impact of Disturbance Along the y-axis

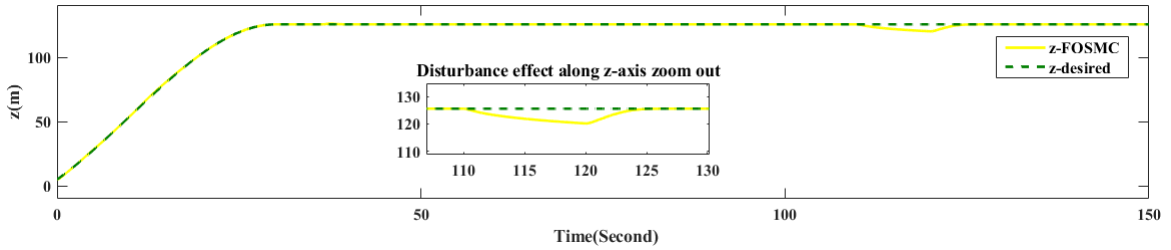

Figure 5.19: The Impact of Disturbance Along the z-axis

the effect of disturbances on the positions of the FWUAV. The figure demonstrates the performance of the FOSMC in rejecting external disturbances and minimizing position errors. The figure illustrates the behavior of position errors in the presence of applied disturbances.

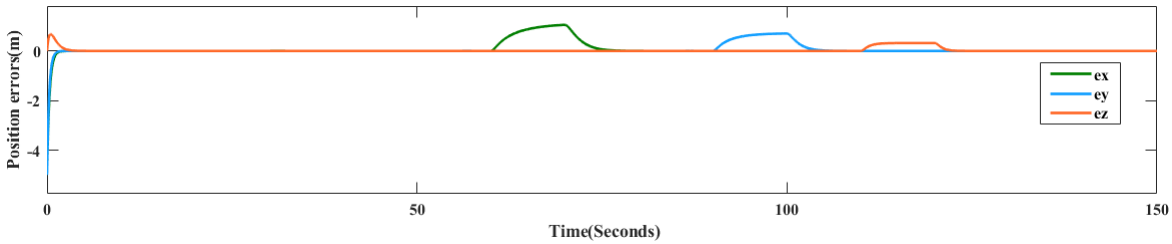

Figure 5.20: Errors on Effect of Disturbance along x,y,and z axes

5.5.2 With Parameter Variation

The same external disturbance (-1.5N) with the same time interval of 15sec is applied with mass and inertia values decreased by 25%. The response of FOSMC and SMC is plotted in figures below. The value of the decreased mass is 10.125kg and similarly, the inertia values used for this FWUAV is decreased by 25%.

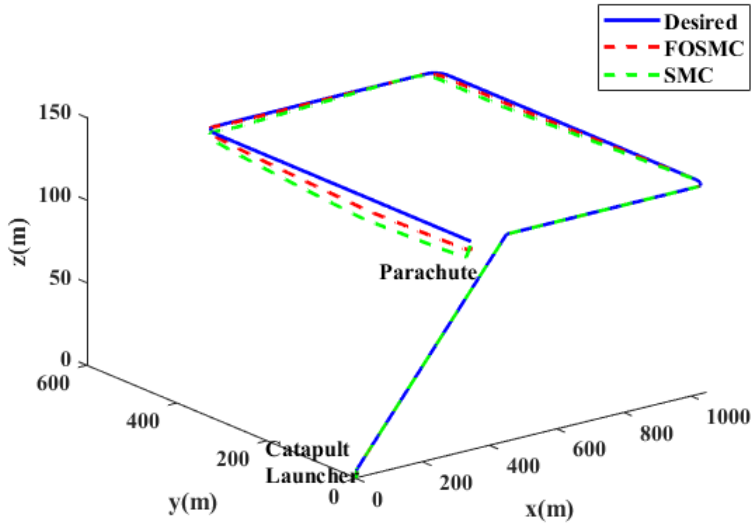

Figure 5.21: 3D Response

Figure 5.21 displays the 3D response and by comparing the 3D response plots between FOSMC and SMC, it is seen that the performance of both controllers under the influence of external disturbances and varied mass and inertia parameters. The FOSMC has improved disturbance rejection and robustness to parameter variations, leading to more accurate and stable trajectory tracking compared to traditional SMC.

Figure 5.22 and Figure 5.24 display the x, y, z positions of a system controlled by FOSMC and SMC. According to the visual representation, FOSMC demonstrates a quicker ability to follow the specified trajectories compared to SMC. Additionally, the control efforts for both controllers are showcased in figure 5.23 and figure 5.25. Notably, the control efforts of SMC exhibit chattering, characterized by rapid and erratic changes, and the utilization of

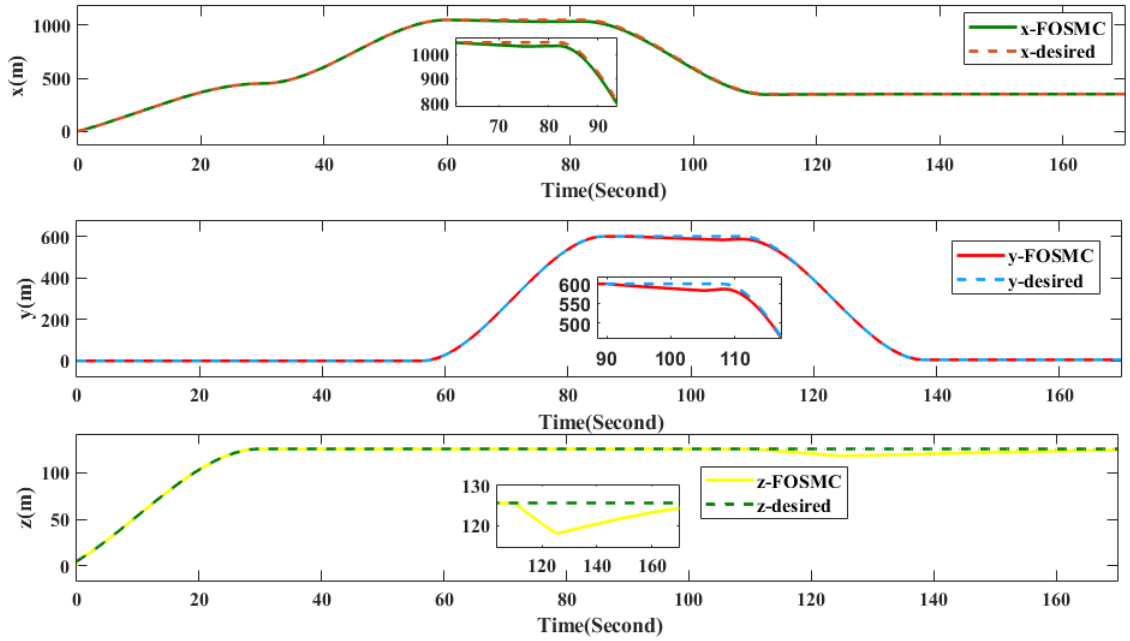

Figure 5.22: Positions of FOSMC

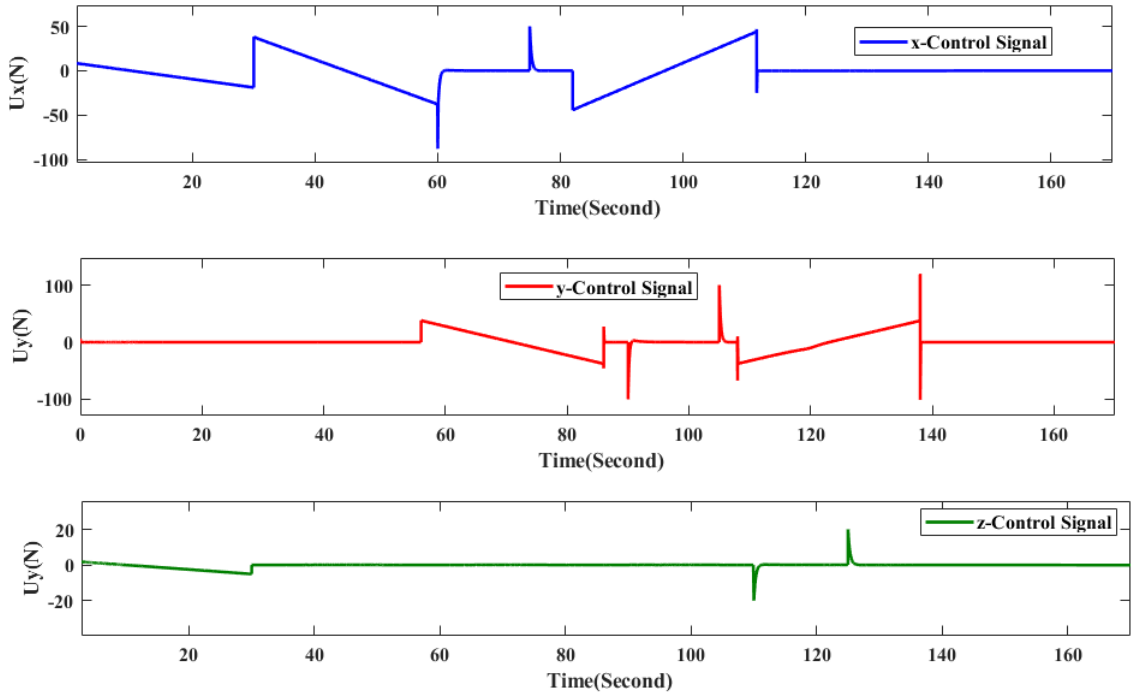

Figure 5.23: Control Efforts for Positions of FOSMC

FOSMC results in a reduction of chattering in the control efforts. FOSMC exhibits smoother control efforts with reduced oscillations or chattering compared to SMC, it indicates that FOSMC is more effective in reducing chattering in the presence of parameter variations and disturbances

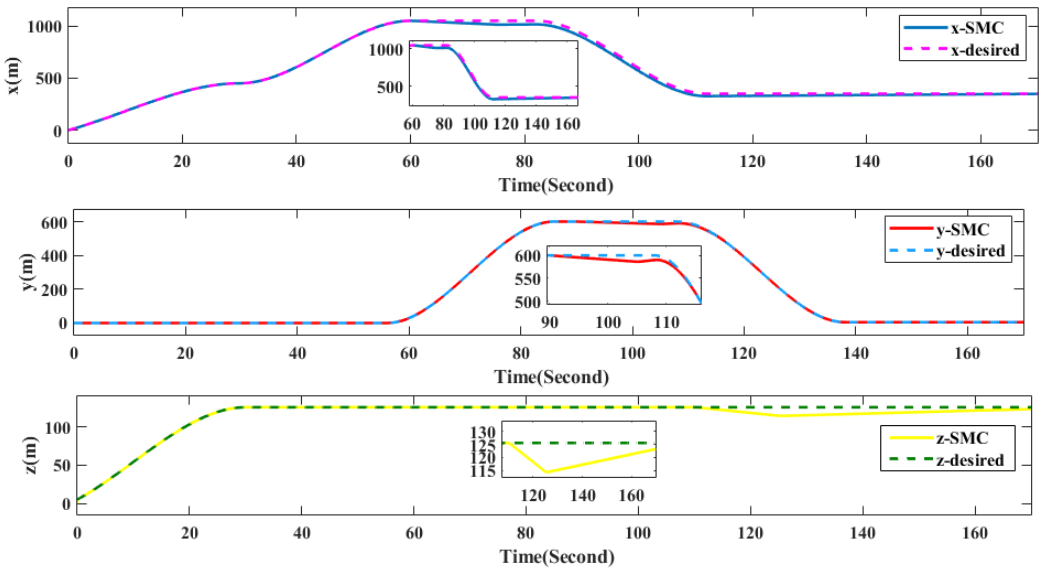

Figure 5.24: Positions of SMC

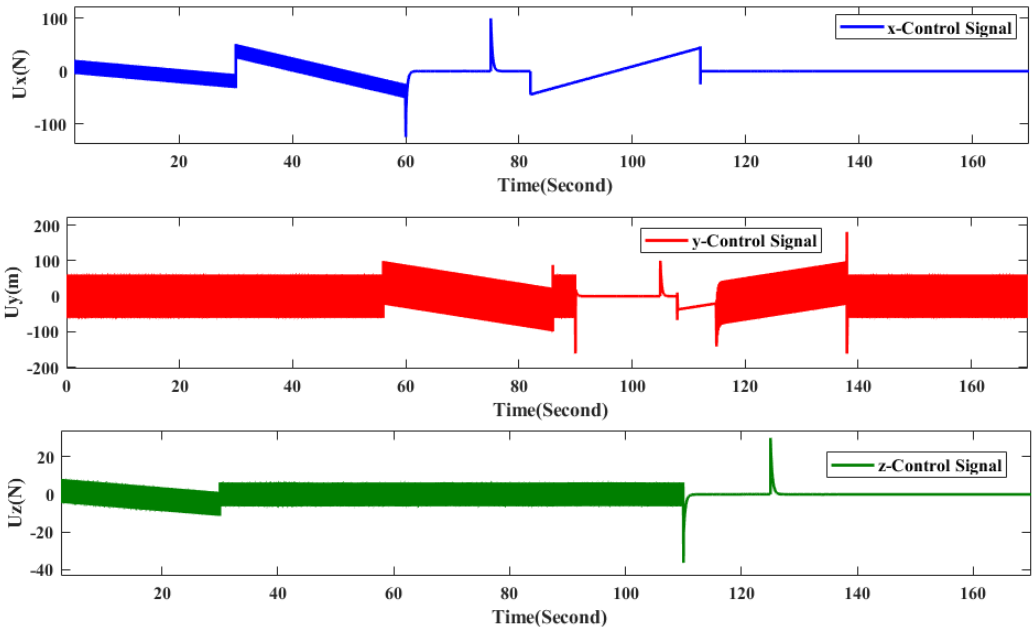

Figure 5.25: Control Efforts for Positions of SMC

5.6 Comparison of LQR,FOPID, SMC and FOSMC Using Longitudinal Flight Dynamics of FWUAV

The longitudinal flight dynamics of FWUAV consists of forward and vertical velocities (u and w), pitch rate (q) and pitch angle (θ). The 6-DOF equation of motion of FWUAV is given in equation (3.50) and equation (3.51) and from these equations $\dot{u}, \dot{w}, \dot{q}$, and $\dot{\theta}$, are the nonlinear longitudinal equation of motion of FWUAV.

$$x_{lon} = (u, w, q, \theta) \tag{5.4}$$

The control signal is elevator control surface deflection (δ_e), which is U_3 in this case. Before employing optimal control techniques such as LQR to the nonlinear dynamic model of the fixed-wing UAV, it is necessary to linearize the model around a trim condition. When a FWUAV maintains a constant altitude, wings-level, and steady flight, certain aspects of its states reach equilibrium. This includes the altitude, denoted as $h = -pd$; the velocities in the body frame, namely u, v, w; the Euler angles, represented by ϕ, θ, ψ; and the angular rates, which are p, q, and r. In aerodynamics terminology, an aircraft is considered to be in trim when it is in such equilibrium. To specifically control the pitch of a fixed-wing UAV, only the longitudinal equations of motion are considered. Consequently, the resulting linear model for the FWUAV comprises decoupled longitudinal dynamics. The linearized model of these longitudinal dynamics is derived under the assumption that the lateral states are zero ($\phi = p = r = \beta = v = 0$). With these assumptions, substituting equation (5.5)

$$\begin{aligned} V_a &= \sqrt{u^2 + w^2} \\ \alpha &= tan^{-1}(w/u) \end{aligned} \tag{5.5}$$

into the longitudinal dynamics and using the Jacobians of equations of states and control inputs, the linearized model of the longitudinal flight dynamics in state space is given as:

$$\begin{bmatrix} \dot{u} \\ \dot{w} \\ \dot{q} \\ \dot{\theta} \end{bmatrix} = \begin{bmatrix} X_u & X_w & X_q & -gcos\theta & 0 \\ Z_u & Z_w & Z_q & -gsin\theta & 0 \\ M_u & M_w & M_q & 0 & 0 \\ 0 & 0 & 1 & 0 & 0 \end{bmatrix} \begin{bmatrix} u \\ w \\ q \\ \theta \end{bmatrix} + \begin{bmatrix} X_{\delta_e} \\ Z_{\delta_e} \\ M_{\delta_e} \\ 0 \end{bmatrix} \delta_e \tag{5.6}$$

The coefficients are given in appendix(E). Equation (5.6) have the form of

$$\begin{aligned} \dot{x} &= Ax + Bu \\ y &= Cx + Du \end{aligned} \tag{5.7}$$

A is system matrix, B is input matrix and C is the output matrix and D is the feed forward matrix which is zero.

5.6.1 LQR Controller Design

LQR is an optimum control strategy that maximizes performance based on certain metrics [27]. The LQR technique relies on reducing criteria through feedback

$$u(t) = -Kx(t) \tag{5.8}$$

The LQR approach creates a linear state feedback rule, as indicated in equation (5.9), for a controlled LTI system with a state-space model equation (5.8).

$$\begin{aligned} \dot{x}(t) &= Ax(t) + Bu(t) \\ \dot{y}(t) &= Cx(t) + Du(t) \end{aligned} \tag{5.9}$$

x(t) and y(t) represent the n-dimensional state and r-dimensional output vectors, respectively, whereas u(t) represents the m-dimensional control vector. The control law in equation (5.8) reduces the quadratic performance index J (cost function) indicated in equation (5.10). The performance index for reducing control effort and states can be expressed as:

$$J = \int_0^\infty (x^T Q x + U^T R U)\, dt \tag{5.10}$$

The weight matrices are denoted by Q and R. Q is an n-dimensional symmetric positive semi-definite state weighting matrix ($Q >= 0$), whereas R is an m dimensional symmetric positive definite control weighting matrix ($R > 0$). In equation (5.8) K represents the control gain matrix from equation (5.11).

$$K = R^{-1} B^T P \tag{5.11}$$

Where, P is the only symmetric, positive semi-definite solution to the Algebraic Riccati Equation (ARE), as proven in equation (5.12).

$$PA + A^T P + Q - PBR^{-1}B^T P = 0 \tag{5.12}$$

In this thesis MATLAB/Simulink is designed for LQR controller to control the pitch angle of the aircraft with the defined values of Q and R in equation (5.13) whose optimal values are obtained by trial and error method and using A and B matrices in the system dynamics which are derived using constant aerodynamic coefficients of the system in table 3.2 and

table 3.3.

$$A = \begin{bmatrix} -0.38 & 0.60 & -0.36 & -9.80; \\ -0.98 & -7.81 & 15.32 & -0.21 \\ 0.18 & -8.31 & -35.21 & 0 \\ 0 & 0 & 1 & 0 \end{bmatrix}, B = \begin{bmatrix} -0.36 \\ -3.62 \\ -106.32 \\ 0 \end{bmatrix} \tag{5.13}$$

$$C = \begin{bmatrix} 0 & 0 & 0 & 1 \end{bmatrix}, \qquad D = 0 \tag{5.14}$$

$$Q = \begin{bmatrix} 0.5 & 0 & 0 & 0 \\ 0 & 0.1 & 0 & 0 \\ 0 & 0 & 0 & 0 \\ 0 & 0 & 0 & 100 \end{bmatrix}, \quad R = 10 \tag{5.15}$$

The block diagram of LQR controller is give in figure below:

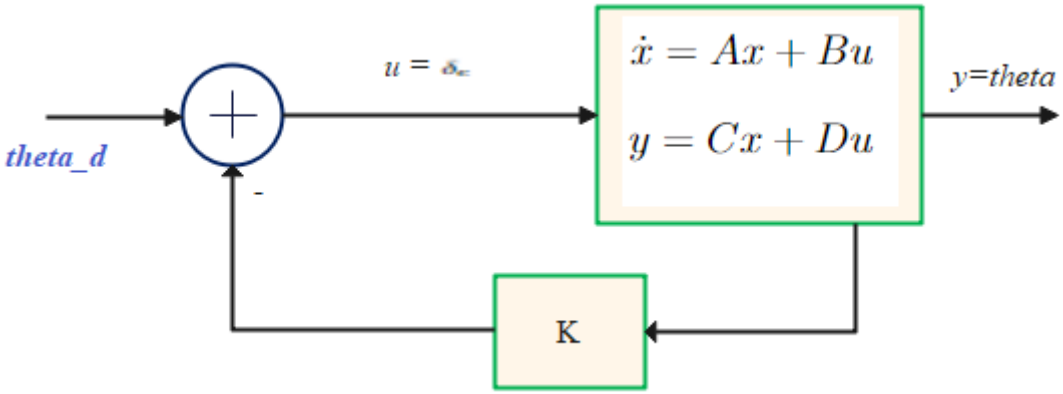

Figure 5.26: Block Diagram for LQR controller

5.6.2 FOPID Controller Design

The effectiveness of fractional-order controllers is widely acknowledged, largely attributed to the development of efficient techniques for differentiating and integrating equations with non-integer orders [28].

FOPID uses the transfer function of a system, here the transfer function of pitch angle is derived as follows: We start by establishing a simplified connection between the elevator deflection δ_e and the pitch angle θ. From equation (3.51), there is the equation:

$$\begin{aligned} \dot{\theta} &= qcos\phi - rsin\phi \\ &= q + (cos\phi - 1)q - r\sin\phi \qquad (5.16) \\ &= q + d_{\theta 1} \qquad (5.17) \end{aligned}$$

where $d_{\theta 1}$ is small for small roll angles ϕ. Differentiating both sides defined as:

$$\ddot{\theta} = \Gamma_5 pr - \Gamma_6(p^2 - r^2) + \frac{\rho V a^2 Sc}{2J_y} \times [C_{m0} + C_{m\alpha}\alpha + C_{mq}\frac{cq}{2Va} + C_{m\delta_e}\delta_e] + \dot{d}_{\theta 1} \tag{5.18}$$

$$\ddot{\theta} = \Gamma_5 pr - \Gamma_6(p^2 - r^2) + \frac{\rho V a^2 Sc}{2J_y} \times [C_{m0} + C_{m\alpha}(\theta - \gamma) + C_{mq}\frac{c}{2Va}(\dot{\theta} - d_{\theta 1}) + C_{m\delta_e}\delta_e] + \dot{d}_{\theta 1} \tag{5.19}$$

$$\ddot{\theta} = (\frac{\rho V a^2 Sc}{2J_y}C_{mq}\frac{c}{2Va})\dot{\theta} + (\frac{\rho V a^2 Sc}{2J_y}C_{m\alpha})\theta + (\frac{\rho V a^2 Sc}{2J_y}C_{m\delta_e})\delta_e + (\Gamma_5 pr - \Gamma_6(p^2 - r^2) + \frac{\rho V a^2 Sc}{2J_y}[C_{m0} - C_{m\alpha}\gamma - C_{mq}\frac{c}{2Va}d_{\theta 1}] + \dot{d}_{\theta 1}) \tag{5.20}$$

$$\ddot{\theta} = -a_\theta\dot{\theta} - b_\theta\theta + c_\theta\delta_e + d_{\theta_2} \tag{5.21}$$

Where

$$\begin{aligned} a_\theta &= \frac{\rho V_a Sc^2}{4J_y}C_{mq} \\ b_\theta &= \frac{\rho V_a^2 Sc}{2J_y}C_{m\alpha} \\ c_\theta &= \frac{\rho V_a^2 Sc}{2J_y}C_{m\delta_e} \\ d_{\theta_2} &= \Gamma_5 pr - \Gamma_6(p^2 - r^2) + \frac{\rho V a^2 Sc}{2J_y}[C_{m0} - C_{m\alpha}\gamma - C_{mq}\frac{c}{2Va}d_{\theta 1}] + \dot{d}_{\theta 1} \end{aligned} \tag{5.22}$$

The linearized model for the pitch angle's evolution is subjected to Laplace transform to obtain its transformed representation:

$$\theta(s) = (\frac{c_\theta}{s^2 + a_\theta s + b_\theta})(\delta_e(s) + \frac{1}{c_\theta}d_{\theta_2}(s)) \tag{5.23}$$

During straight and level flight conditions, $r = p = \phi = \gamma = 0$. Moreover, air frames are commonly engineered such that the coefficient $C_{m0} = 0$, thereby implying $d_{\theta_2} = 0$. With the understanding that $\dot{\theta} = q + d_{\theta 1}$, the transfer function for pitch angle can be rewritten as:

$$\begin{aligned} \theta(s) &= \frac{c_\theta}{s^2 + a_\theta s + b_\theta}\delta_e(s) \\ \frac{\theta(s)}{\delta_e(s)} &= \frac{c_\theta}{s^2 + a_\theta s + b_\theta} \end{aligned} \tag{5.24}$$

By using the values in table 3.2 and table 3.3 and constant airspeed Va of 20 m/s, the

transfer function becomes:

$$\frac{\theta(s)}{\delta_e(s)} = \frac{3.8632}{s^2 + 0.2340s + 34.9527} \tag{5.25}$$

The transfer function of FOPID controller is defined as:

$$G_c(s) = K_p + K_i s^{-\lambda} + s^{\mu} K_d \tag{5.26}$$

Where, λ represents order of integration and μ represents order of derivative. The value of both parameters is between 0 and 1. The gains are optimized by tuning and the optimized values are $Kp = 127.684054515561, Ki = 346.136495372955, Kd = 10.4308579680231, \lambda = 0.756, \mu = 0.876$. The block diagram of FOPID is given in the following figure:

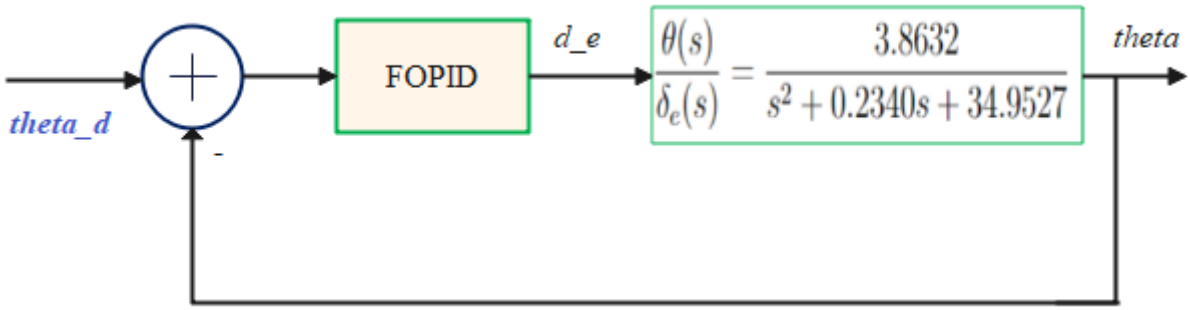

Figure 5.27: Block Diagram for FOPID controller

Simulation for linear controllers (LQR and FOPID) is done using MATLAB/Simulink and comparison is done with nonlinear controllers (SMC and FOSMC) for pitch angle. The result is shown in figure below:

As shown from the figure 5.28, LQR and FOPID controllers experiences some overshoot

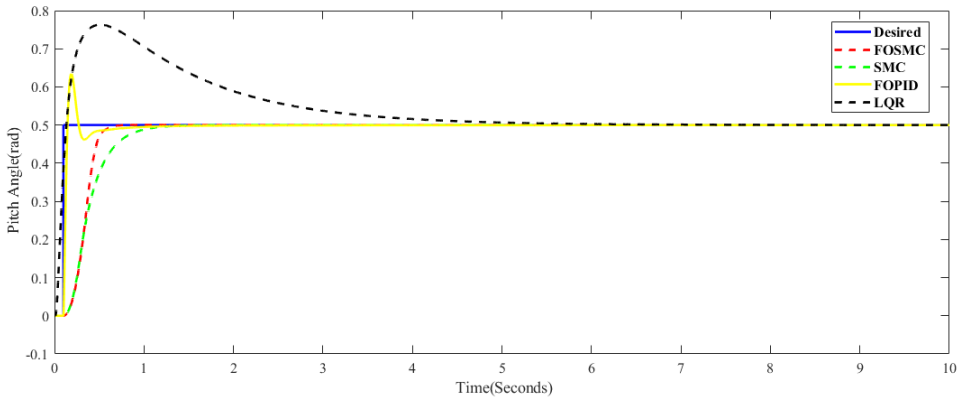

Figure 5.28: Simulation result for comparison

(52.566% for LQR and 26.57% for FOPID) and have large settling time compared to others.

The performance of controllers with settling time is summarized in the table below:

Figure 5.29 shows the result of the controllers with applied external disturbance. This

Table 5.4: Comparison of Controllers Using settling time

Controller	Settling Time(Sec)
LQR	5.4098
FOPID	4.8573
SMC	2.724
FOSM	0.835

disturbance a retarding force generated by wind and the value of this force is around 7% of the weight of the aircraft and inertia and mass are decreased by 25%. As shown from the figure, FOSMC and FOPID have better performance in disturbance rejection and parameter variation than SMC and SMC is better than LQR.

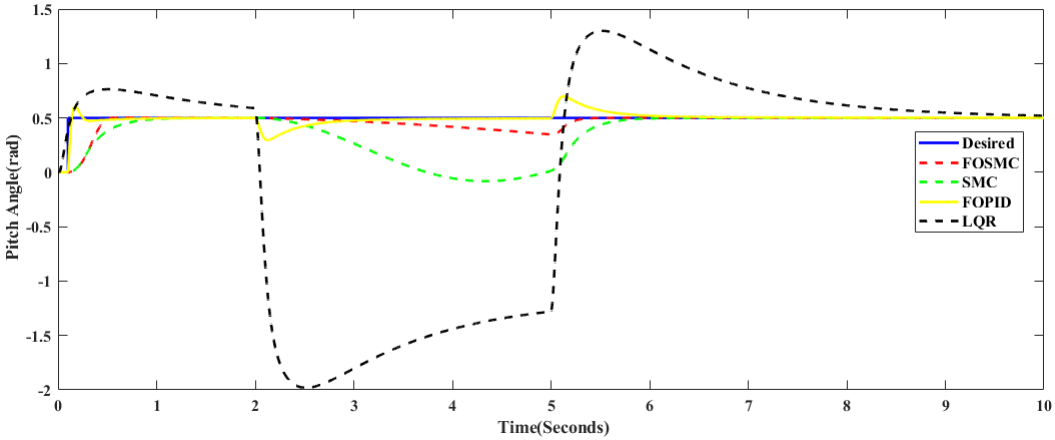

Figure 5.29: Simulation result with disturbance

Chapter 6

Conclusions and Future Works

6.1 Conclusion

This research investigates trajectory tracking for fixed-wing UAVs using a fractional order sliding mode controller (FOSMC). It encompasses modeling, control design, and performance assessment. The FOSMC controller adeptly regulates the UAV's position and attitude across all six degrees of freedom. Parameters of the FOSMC controller are fine-tuned using Particle Swarm Optimization (PSO). Simulation outcomes indicate that the FOSMC controller surpasses the conventional sliding mode controller in trajectory tracking, disturbance rejection, and parameter variation management. It demonstrates quicker convergence, diminished tracking errors, and improved maintenance of the desired trajectory. The PSO-tuned FOSMC controller exhibits robust performance, accurately tracking trajectories, and effectively handling external disturbances and parameter variations. Additionally, a Linear Quadratic Regulator (LQR) and Fractional Order PID controllers are designed by linearizing the longitudinal flight dynamics of the system, and the performance of LQR, FOPID, SMC, and FOSMC controllers are evaluated through step input for pitch attitude control.

6.2 Future Works

This thesis concentrates solely on examining the performance of the FWUAV, assessing the robustness and efficacy of the controller in minimizing errors to track desired trajectories, and exploring automatic controller gain tuning methods through various paths. The study primarily focuses on trajectory tracking of positions and attitude angles of the FWUAV. However, it is possible to design controllers without decoupling the dynamics of FWUAV.

The author suggests that interested researchers delve into the design and analysis of such controllers:

- Linear controllers can be extended to lateral dynamics of the FWUAV
- **Integration of Advanced Control Techniques:** Investigate the integration of other advanced control techniques, such as model predictive control (MPC), reinforcement learning, or neural network-based controllers, in combination with FOSMC. This hybrid approach may provide improved robustness and adaptability Integration of Sensor Fusion Techniques
- The integration of wind estimation algorithms or adaptive control mechanisms.
- Hardware Implementation

Bibliography

[1] Bao, Changchun, Yufei Guo, Leru Luo, and Guanqun Su. "Design of a Fixed-Wing UAV controller based on adaptive backstepping sliding mode control method." IEEE Access 9 (2021): 157825-157841.

[2] Espinoza, Tadeo, A. E. Dzul, Rogelio Lozano, and Pavel Parada. "Backstepping-sliding mode controllers applied to a fixed-wing UAV." Journal of Intelligent and Robotic Systems 73 (2014): 67-79.

[3] Guo, Yufei, Leru Luo, and Changchun Bao. "Design of a fixed-wing UAV controller combined fuzzy adaptive method and sliding mode control." Mathematical Problems in Engineering 2022 (2022).

[4] FARI, STEFANO. "Guidance and control for a fixed-wing UAV." (2017).

[5] Ashari, Ahmad, Andi Dharmawan, Hafizna Arsyil Fadhli, and Ariesta Martiningtyas Handayani. "Flight Trajectory Control System on Fixed Wing UAV using Linear Quadratic Regulator." International Journal of Engineering Research and (2019).

[6] Albaker, B. M., and N. A. Rahim. "Flight path PID controller for propeller-driven fixed-wing unmanned aerial vehicles." International Journal of the Physical Sciences 6, no. 8 (2011): 1947-1964.

[7] Sarhan, Amr, and Shiyin Qin. "Adaptive PID control of UAV altitude dynamics based on parameter optimization with fuzzy inference." International Journal of Modeling and Optimization 6, no. 4 (2016): 246.

[8] Kayacan, Erdal, Mojtaba Ahmadieh Khanesar, Jaime Rubio-Hervas, and Mahmut Reyhanoglu. "Learning control of fixed-wing unmanned aerial vehicles using fuzzy neural networks." International Journal of Aerospace Engineering 2017 (2017).

[9] Castañeda, Herman, Oscar S. Salas-Peña, and Jesús de León-Morales. "Extended observer based on adaptive second order sliding mode control for a fixed wing UAV." ISA transactions 66 (2017): 226-232.

[10] Hernandez, Jorge L., Iván González-Hernández, and Rogelio Lozano. "Attitude and altitude control for a fixed wing UAV applied to photogrammetry." In 2019 International Conference on Unmanned Aircraft Systems (ICUAS), pp. 498-502. IEEE, 2019.

[11] Low, Chang Boon. "A trajectory tracking control design for fixed-wing unmanned aerial vehicles." In 2010 IEEE International Conference on Control Applications, pp. 2118-2123. IEEE, 2010.

[12] Nobahari, Hadi, and Alireza Sharifi. "Wind compensation in trajectory tracking of a fixed wing uav using a nonlinear model predictive controller based on the particle swarm optimization." In 2019 7th International Conference on Robotics and Mechatronics (ICRoM), pp. 138-143. IEEE, 2019.

[13] Liu, Cunjia, Owen McAree, and Wen-Hua Chen. "Path-following control for small fixed-wing unmanned aerial vehicles under wind disturbances." International Journal of Robust and Nonlinear Control 23, no. 15 (2013): 1682-1698.

[14] Yu, Ziquan, Hamed Badihi, Youmin Zhang, Yajie Ma, Bin Jiang, and Chun-Yi Su. "Fractional-order sliding-mode fault-tolerant neural adaptive control of fixed-wing UAV with prescribed tracking performance." In 2020 2nd International Conference on Industrial Artificial Intelligence (IAI), pp. 1-6. IEEE, 2020.

[15] Andre, N., B. Samir, and S. Roland. "Dynamic Modeling of Fixed-Wing UAVs." Aircraft and Spacecraft Systems Design Lecture Notes, Autonomous Systems Lab, ETH Zürich, Switzerland (2006).

[16] Beard, Randal. "UAV Coordinate Frames and Rigid Body Dynamics." (2004).

[17] Khan, Mahmud Safat. Modelling and Simulation of Small Scale Fixed-Wing Autonomous Aerial Vehicles. Sheffield Hallam University (United Kingdom), 2021.

[18] Beard, Randal W., and Timothy W. McLain. Small unmanned aircraft: Theory and practice. Princeton university press, 2012.

[19] Han, Yang, Peng Li, and Zhiqiang Zheng. "A non-decoupled backstepping control for fixed-wing UAVs with multivariable fixed-time sliding mode disturbance observer." Transactions of the Institute of Measurement and Control 41, no. 4 (2019): 963-974.

[20] Matušů, Radek. "Application of fractional order calculus to control theory." International journal of mathematical models and methods in applied sciences 5, no. 7 (2011): 1162-1169.

[21] Bouarroudj, Noureddine, Djamel Boukhetala, and Fares Boudjema. "Sliding-mode controller based on fractional order calculus for a class of nonlinear systems." International Journal of Electrical and Computer Engineering 6, no. 5 (2016): 2239-2250.

[22] El Gmili, Nada, Mostafa Mjahed, Abdeljalil El Kari, and Hassan Ayad. "Particle swarm optimization based proportional-derivative parameters for unmanned tilt-rotor flight control and trajectory tracking." Automatika 61, no. 2 (2020): 189-206.

[23] Wang, Dongshu, Dapei Tan, and Lei Liu. "Particle swarm optimization algorithm: an overview." Soft computing 22 (2018): 387-408.

[24] Xiao, Ayang, Benli Wang, Chaoli Sun, Shijie Zhang, and Zhenguo Yang. "Fitness estimation based particle swarm optimization algorithm for layout design of truss structures." Mathematical Problems in Engineering 2014 (2014).

[25] Zhen, Ziyang, Ju Jiang, Xinhua Wang, and Kangwei Li. "Modeling, control design, and influence analysis of catapult-assisted take-off process for carrier-based aircrafts." Proceedings of the Institution of Mechanical Engineers, Part G: Journal of Aerospace Engineering 232, no. 13 (2018): 2527-2540.

[26] Ahmad, Irfan, Muwaida Liaquat, Fahad Mumtaz Malik, Hameed Ullah, and Usman Ali. "Variants of the sliding mode control in presence of external disturbance for quadrotor." IEEE Access 8 (2020): 227810-227824.

[27] Ingabire, Aline, and Andrey A. Sklyarov. "Control of longitudinal flight dynamics of a fixedwing UAV using LQR, LQG and nonlinear control." In E3S Web of Conferences, vol. 104, p. 02001. EDP Sciences, 2019.

[28] Kaur, Amrit, and Ranjit Kaur. "Comparison of Simulink Based Fopid and Pid Controller." Research Cell: An International Journal of Engineering Sciences (2016): 97-111.

Appendices

Appendix A

Rotation Matrices and inertia J

Examine the two coordinate frames illustrated in the figure below. The vector $\boldsymbol{p}$ can be represented in both the f^0 frame and the f^1 frame.

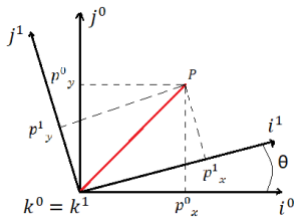

Figure 6.1: Rotation in 2D

The association between these unit basis vectors ($\boldsymbol{i}^0, \boldsymbol{j}^0, \boldsymbol{k}^0, \boldsymbol{i}^1, \boldsymbol{j}^1$, and $\boldsymbol{k}^1$) can be expressed using rotation matrices in the following manner:

$$\boldsymbol{p}^1 = R_0^1 \boldsymbol{p}^0$$

Describing the geometry depicted in the above figure, a right-handed rotation by an angle θ about the $\boldsymbol{k}^0$ axis is defined as.

$$R_0^1 = \begin{bmatrix} cos\theta & sin\theta & 0 \\ -sin\theta & cos\theta & 0 \\ 0 & 0 & 1 \end{bmatrix}$$

Using a similar approach, the right-handed rotations about the $\boldsymbol{j}^0$ axis and $\boldsymbol{i}^0$ axis can be represented by the equations below.

$$R_0^1 = \begin{bmatrix} cos\theta & 0 & -sin\theta \\ 0 & 1 & 0 \\ sin\theta & 0 & cos\theta \end{bmatrix}$$

$$R_0^1 = \begin{bmatrix} 1 & 0 & 0 \\ 0 & cos\theta & sin\theta \\ 0 & -sin\theta & cos\theta \end{bmatrix}$$

The inertia matrix used in the derivation of dynamic equation of FWUAV is given by:

$$J = \begin{bmatrix} J_x & -J_{xy} & -J_{xz} \\ -J_{xy} & J_y & -J_{yz} \\ -J_{xz} & -J_{yz} & J_z \end{bmatrix}$$

Where

$J_x = \int (y^2 + z^2) dm \qquad J_y = \int (x^2 + z^2) dm \qquad J_z = \int (x^2 + y^2) dm$

$J_{xy} = \int (xy) dm \qquad J_{xz} = \int (xz) dm \qquad J_{yz} = \int (yz) dm$

Γ_1.....Γ_8 are constants and given by:

$\Gamma_1 = \frac{J_{xz}(J_x - J_y + J_z)}{\Gamma} \qquad \Gamma_2 = \frac{J_z(J_z - J_y) + J_{xz}^2}{\Gamma}$

$\Gamma_3 = \frac{J_z}{\Gamma} \qquad \Gamma_4 = \frac{J_{xz}}{\Gamma}$

$\Gamma_5 = \frac{J_z - J_x}{J_y} \qquad \Gamma_6 = \frac{J_{xy}}{J_y}$

$\Gamma_7 = \frac{(J_x - J_y)J_x + J_{xy}^2}{\Gamma} \qquad \Gamma_8 = \frac{J_x}{\Gamma}$

and $\Gamma = J_x J_z - J_{xz}^2$

Appendix B

Simulink block of the FWUAV mathematical model

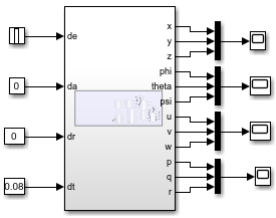

Figure 6.2: Simulink Block Diagram for Model Verification

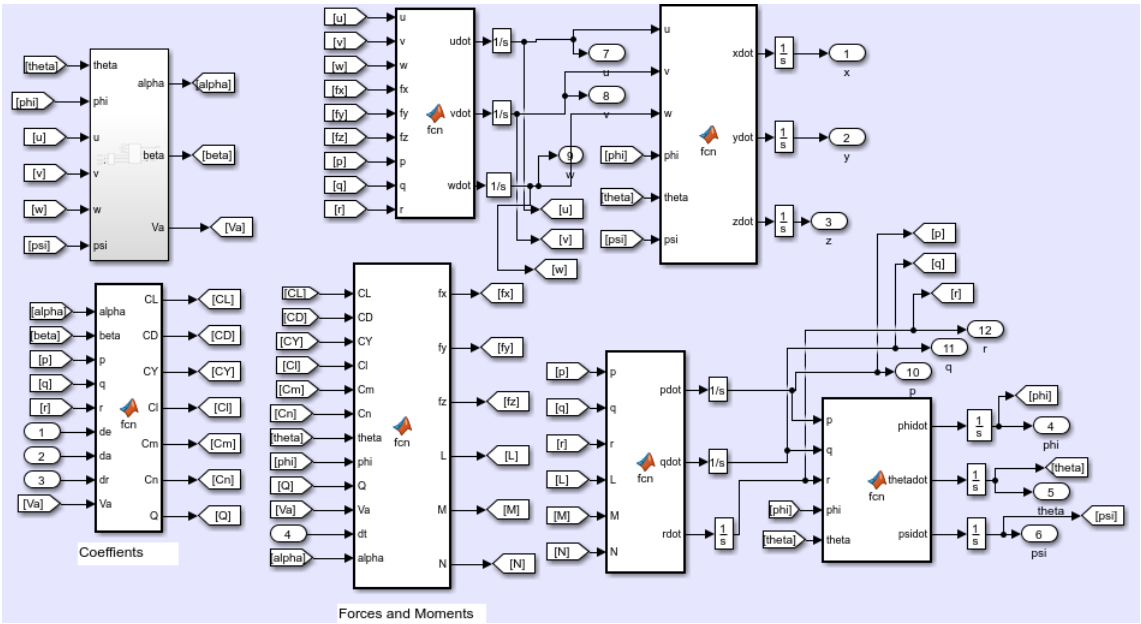

Figure 6.3: Inside the Simulink Block

Appendix C

Simulink Model for controller design of FWUAV

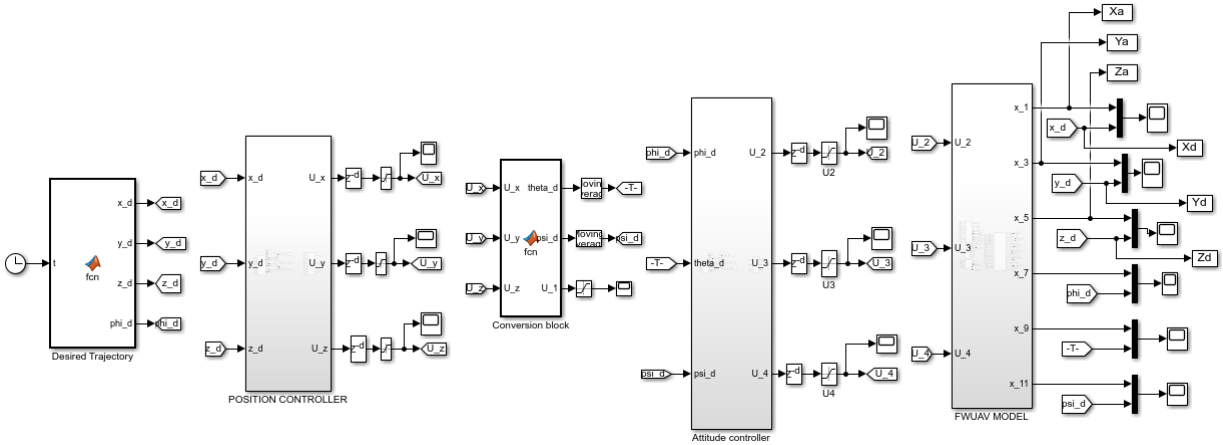

Figure 6.4: Simulink Block Diagram of Overall System

Appendix D

Matlab Code for Rectangular Trajectory Generation

```
function [x_d,y_d,z_d,phi_d]=fcn(t)
g=(15/180)*pi;%Flight Path Angle
if t<=30
    x_d=15*t+0.5*t^2-0.016666666666667*t^3;
     y_d=0;
     z_d=tan(g)*x_d+5;% 2 louncher height
elseif (t>30) && (t<=56)
     x_d=3450-240*t+6*t^2-0.044444444444000*t^3;
     z_d=1.255771365940028e+02;
     y_d=0;
elseif (t>56) && (t<=60)
     x_d=3.450000*10^3-0.2400000*10^3*t+0.00600000*10^3*t^2-
     0.000044444444444*10^3*t^3;
     z_d=1.255771365940028e+02;
     y_d=1.407715555555557*10^4-(0.064213333333333*10^4)*t+
     (0.000946666666667*10^4)*t^2-(0.000004444444444*10^4)*t^3;
elseif (t>60) && (t<=82)
     x_d=1050;
    z_d=1.255771365940028e+02;
     y_d=1.407715555555557*10^4-(0.064213333333333*10^4)*t+
     (0.000946666666667*10^4)*t^2-(0.000004444444444*10^4)*t^3;
     elseif (t>82) && (t<=86)
 x_d=(-4.322878518518527*10^4+(0.142862222222222*10^4)*t-
 (0.001508888888889*10^4)*t^2+(0.000005185185185*10^4)*t^3);
    z_d=1.255771365940028e+02;
```

```
y_d=1.407715555555557*10^4
-0.064213333333333*10^4*t+0.000946666666667*10^4*t^2-
0.000004444444444*10^4*t^3;
    elseif (t>86) && (t<=108)
  x_d=(-4.322878518518527*10^4+(0.142862222222222*10^4)*t-
  (0.001508888888889*10^4)*t^2+(0.000005185185185*10^4)*t^3);
     z_d=1.255771365940028e+02;
    y_d=600;
        elseif (t>108) && (t<=112)
    x_d=(-4.322878518518527*10^4+(0.142862222222222*10^4)*t-
    (0.001508888888889*10^4)*t^2+(0.000005185185185*10^4)*t^3);
  z_d=1.255771365940028e+02;
    y_d=-7.805424000000016*10^4+0.197064000000000*10^4*t-
    0.001626333333333*10^4*t^2+0.000004407407407*10^4*t^3;
        elseif (t>112) && (t<=138)
            x_d=350;
           z_d=1.255771365940028e+02;
       y_d=-7.805424000000016*10^4+(0.197064000000000*10^4)*t-
       (0.001626333333333*10^4)*t^2+(0.000004407407407*10^4)*t^3;
   else
            x_d=350;
           z_d=1.255771365940028e+02;
            y_d=5;
end
phi_d=0.5;
```

Appendix E

Coefficient Values For Linearized Longitudinal Dynamics of FWUAV

$$
\begin{aligned}
X_u &= \frac{\rho u S}{m}(C_{X_0} + C_{X_\alpha}\alpha + C_{X_{\delta_e}}\delta_e) - \frac{\rho S w C_{X_\alpha}}{2m} + \frac{\rho S c C_{X_q} u q}{4 m V_a} \\
X_w &= -q + \frac{\rho w S}{m}(C_{X_0} + C_{X_\alpha}\alpha + C_{X_{\delta_e}}\delta_e) + \frac{\rho S u C_{X_\alpha}}{2m} + \frac{\rho S c C_{X_q} w q}{4 m V_a} \\
X_q &= -w + \frac{\rho S c C_{X_q} q}{4m} \\
X_{\delta_e} &= \frac{\rho V_a^2 S C_{X_{\delta_e}}}{2m} \\
Z_u &= q + \frac{\rho u S}{m}(C_{Z_0} + C_{Z_\alpha}\alpha + C_{Z_{\delta_e}}\delta_e) - \frac{\rho S w C_{Z_\alpha}}{2m} + \frac{\rho S c C_{Z_q} u q}{4 m V_a} \\
Z_w &= \frac{\rho w S}{m}(C_{Z_0} + C_{Z_\alpha}\alpha + C_{Z_{\delta_e}}\delta_e) + \frac{\rho S u C_{Z_\alpha}}{2m} + \frac{\rho S c C_{Z_q} w q}{4 m V_a} \\
Z_q &= u + \frac{\rho S c C_{Z_q} q}{4m} \\
Z_{\delta_e} &= \frac{\rho V_a^2 S C_{Z_{\delta_e}}}{2m} \\
M_u &= \frac{\rho u S c}{J_y}(C_{m_0} + C_{m_\alpha}\alpha + C_{m_{\delta_e}}\delta_e) - \frac{\rho S w C_{m_\alpha}}{2 J_y} + \frac{\rho S c^2 C_{m_q} u q}{4 J_y V_a} \\
M_w &= \frac{\rho w S c}{J_y}(C_{m_0} + C_{m_\alpha}\alpha + C_{m_{\delta_e}}\delta_e) + \frac{\rho S u c C_{m_\alpha}}{2 J_y} + \frac{\rho S c^2 C_{m_q} w q}{4 J_y V_a} \\
M_q &= \frac{\rho S c^2 V_a C_{m_q} q}{4 J_y} \\
M_{\delta_e} &= \frac{\rho V_a^2 S c C_{m_{\delta_e}}}{2 J_y}
\end{aligned}
\tag{6.1}
$$